

# CRHyME (Climatic Rainfall Hydrogeological Modelling Experiment): a new model for geo-hydrological hazard assessment at the basin scale

Andrea Abbate<sup>1</sup>, Leonardo Mancusi<sup>1</sup>, Francesco Apadula<sup>1</sup>, Antonella Frigerio<sup>1</sup>, Monica Papini<sup>2</sup>, Laura Longoni<sup>2</sup>

<sup>1</sup>RSE, Ricerca Sistema Energetico, Via Rubattino 54, Milano

5 <sup>2</sup>Politecnico di Milano, Piazza Leonardo da Vinci 32, Milano

Correspondence to: Andrea Abbate (andrea.abbate@rse-web.it)

**Abstract.** This work presents the new model CRHyME (Climatic Rainfall Hydrogeological Modelling Experiment), a tool for ~~the~~ geo-hydrological hazard evaluation. CRHyME is a physically based and spatially distributed model written in Python language ~~that and~~ represents an extension of the classic hydrological models working ~~that simulate inflows outflows~~ at the  
10 basin scale. ~~CRHyME's main focus consists of A series of routines have been integrated to describe the simulating rainfall-induced phenomena of~~ geo-hydrological instabilities such as shallow landslides, ~~as well as~~ debris flows, catchment erosion, and sediment transport into the river. These phenomena are ~~generally conventionally~~ decoupled ~~with respect to from~~ ~~at the~~ ~~continuous~~ hydrological ~~simulation routine~~ while in CRHyME they are ~~quantitatively and~~ simultaneously ~~and quantitatively~~ evaluated ~~within the same code~~ through a multi-hazard approach.

15 CRHyME has been tested on some case studies ~~in across Northern Italian basins Italy~~. ~~Among these, The Caldane catchment, a well-monitored basin of 27 km<sup>2</sup> located near Lecco city (Lombardy), was considered for the calibration of solid transport routine testing also the~~ spatial ~~scale dependence related to digital terrain resolution~~. CRHyME was applied across larger basins of the Valtellina (Alps) and Emilia's (Apennines) areas (~~~2600 km<sup>2</sup>~~) which have experienced severe geo-hydrological episodes triggered by heavy precipitation in the recent past. ~~were considered for the calibration and validation procedures of the model~~  
20 ~~thanks also to the availability of literature data concerning past occurred geo hydrological instability phenomena. CRHyME's Calibration and validation of the model conducted on presented case studies have~~ been assessed ~~through through some~~ hydrological indexes NSE (Nash–Sutcliffe Efficiency) and RMSE (Root Mean Square Error) ~~hydrological error metrics~~ while for landslides ~~phenomena~~ the ROC (Receiver Operating Characteristic) methodology was applied. CRHyME has been able to: ~~1)~~ reconstruct the ~~surface runoff river discharge~~ at the reference hydrometric stations located at the outlets of the basins,  
25 ~~2) to~~ estimate the ~~solid transportsediment yield~~ at some hydropower reservoirs ~~compared to the chosen as a reference data~~, and ~~to 3) evaluate individuate the location and the~~ triggering conditions of shallow landslides and debris flows ~~occurred, compared to those recorded in the literature~~. The ~~good performance ranking of CRHyME has shown a rather good performance of the model in terms of~~ was reached assuring the stability of the code, a rather fast computation, and maintaining the ~~numerical conservativity of water and sediment balances. CRHyME has revealed therefore has been revealed as~~ a suitable tool for the  
30 ~~quantification of the geo-hydrological process, answering the recent needs of their numerical simulation not only for back analysis studies but also useful for Civil Protection multi-hazard assessment.~~  
~~revealing suitable not only for back analysis studies but also as an efficient tool for Civil Protection multi hazard assessment.~~

## 1 Introduction

35 ~~Natural disasters are a critical issue in terms of economic losses and casualties (ISPRA, 2018). Only in 2020, the worldwide losses related to geohazard were quantified as 210 billion dollars and 8'200 victims (Munich Re, 2021). Among the natural disasters, the events linked to geo-hydrological phenomena, such as floods and landslides, certainly play a significant role. Landslides, Floods— and landslides floods, and debris flows represent serious geo-hydrological hazards in mountain environments (Gariano and Guzzetti, 2016). Among them, shallow landslide, debris flow failures and soil erosion are controlled by rainfall-triggering events of varying intensity and duration (Abbate et al., 2021a) while sediment transport is a~~



Milledge et al., 2014; Montrasio, 2008; Takahashi, 2009) ~~where strong that hypothesis and simplification for the hydrological parameterization are adopted.~~

85 ~~Geo-hydrological phenomena have been historically decoupled and investigated separately. To fill this gap and make them more integrated within a numerical model, some take into account some aspect of the hydrological cycle but they are generally not fully integrated into a rainfall-runoff routine. Moreover, several models have limiting spectra of application mainly due to other limitations such as input data requirements, the scale of simulation and the data resolution (Devia et al., 2015; Moges et al., 2021).~~

90 ~~Fortunately, some advances attempts in this direction have been made were recently proposed in very recent years.~~ In this regard, CHASM (Combined Hydrology and Stability Model) (Bozzolan et al., 2020) and Landlab (Strauch et al., 2018) represent the two latest modelling frameworks that have addressed the need to start evaluating the geo-hydrological hazard and risks ~~considering jointly with also~~ hydrological and ~~climatical-climatic~~ aspects. The new methodological approaches shown by CHASM and Landlab models have been assessed thanks to the progressively ~~increasing increase of the data availability for~~ GIS (Geographical Information Systems) data availability on a worldwide scale and thanks to the recent improvements in computer programming for environmental systems modelling. Indeed, the creation of efficient and open-source built-in functions for different language programs, such as Matlab, C++ or Python, has sped up and facilitated the implementation of self-made ~~earthland--~~surface models. These functions have been already successfully implemented by PCR-GLOBWB-2 (Sutanudjaja et al., 2018)- and WFLOW (Schellekens et al., 2020) models, as well as in the European hydrological model LISFLOOD (Van Der Knijff et al., 2010) and OPENLISEM (Roo et al., 1996).

~~In this paramount~~ Among the of currently available software solutions and modelling approaches and software solutions, a comprehensive multi-hazard model specifically designed for evaluating geo-hydrological threats is still needed. Geo-hydrological processes are many and ~~generally happen~~ happen simultaneously at a watershed scale. They ~~need-require~~ to be modelled together to better know their mutual influences and feedback, trying to overcome the theoretical subdivisions existing in the literature's methodologies ~~currently adopted~~. Moreover, diversified input data formats, their spatial and temporal resolution, and the scale dependency of geo-hydrological simulation (Devia et al., 2015; Moges et al., 2021) represent real challenges to be carefully addressed to not undermine the applicability of these integrated models. -Starting from this point Under these premises, ~~Starting from these considerations and taking inspiration from these models, the first version of~~

110 ~~CRHyME was developed-~~ the main motivations aimed at the construction of the new CRHyME code are here presented:

- Build an integrated but versatile model for simulating rainfall-induced geo-hydrological processes (flood, erosion, sediment transport and shallow landslide triggering);
- Allow fast and efficient calculations within a spatially distributed model, designed to operate at catchment scale without constraints on spatial and temporal input data resolution;
- 115 ▪ Implementation of a code inside a robust framework, using Opens Source Python libraries which enable fast coding and easy sub-module modifications/integrations;
- Address code compatibility for assimilating input data from Opens Source datasets available at a worldwide scale, permitting a simulation reproducibly in any worldwide catchments.;

Starting from these considerations and taking inspiration from these analogue models cited before, CRHyME (Fig. 1) was developed to try to improve overall geo-hydrological modelling, filling fill the existing gaps and issues, ~~improving overall geo-hydrological modelling~~. This paper presents the main features key features and applications of the ~~CRHyME model code~~. Structure and constitutive equations are reported in the Material and Method section. Then ~~the-some~~ case studies developed across Italian territory waere re taken into account considered for the calibration and validation of the new model. In the Result sections ~~the main outcomes of CRHyME applications are reported and they are extensively commented on within the~~ Discussion and Conclusions section they are extensively commented on within the Discussion and Conclusions sections.

## 2 Material and Methods

In this paragraph, the CRHyME model's ~~peculiarities are illustrated~~ main features, the sub-module structure and their constitutive equations, the input dataset required for its initialization, and a presentation of calibration and validation case studies are illustrated ~~study~~. (Figure 1), created for a correct quantification of the hazard deriving from floods and landslides at basin scale.

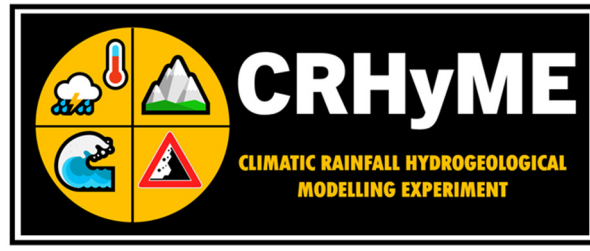


Figure 1: The CRHyME model logo.

**2.1 Key mModel main features** CRHyME's engine is based on PCRaster libraries (Karssenberget al., 2010; Pebesma et al., 2007) which is a collection of open source software targeted at the development and deployment of spatio-temporal environmental models. These functions can include a rich set of model building blocks and analytical functions for manipulating raster GIS maps, a framework for the construction of stochastic spatio-temporal models and a tool for interactive visualisation of spatio-temporal data. They are mainly applied in environmental modelling such as rainfall runoff models and slope stability models and can deal with spatially distributed earth surface data that are discretized considering the single cell of terrain domain as the reference element where model calculations are carried out. Using PCRaster libraries, **4 different processes that describe quantitatively the geo-hydrological hazards that may occur at the catchment scale have been implemented:**

- **River flow discharge and volume;**
- **River erosion and sediment transport discharge and volume;**
- **Shallow landslide triggering condition;**
- **Debris flow triggering condition.**

The most innovative part of the code CRHyME aims to model together rainfall-induced hydrological and geological processes occurring at the catchment scale, e.g. floods and landslides. In CRHyME these processes are evaluated simultaneously within hydrological routine: ~~are strongly connected and they usual~~ includes the physical relations that describe how the hydrological assessment can influence and potentially trigger the geo-hydrological hazards occurring at the basin scale:

the ~~bed-load~~ sediment transport, ~~in terms of the bed-load process~~ has been described considering the Erosion Potential Method (EPM) for simulating erosion ~~processes sources~~ (Longoni et al., 2016; Brambilla et al., 2020; Milanesi et al., 2015; Ivanov et al., 2020a) and the stream power laws ~~available in the literature~~ for defining the transport capacity of the rivers (Vetsch et al., 2018); the ~~sFor what concerns~~ shallow landslide failure assessment, ~~slope stability models commonly adopted in engineering geology have been implemented to evaluate the stability conditions of natural slopes~~ was carried out considering 4 infinite-slope stability models by (Iverson (-2000), Montrasio (-2008), Harp et al. (-2006) and; Milledge et al. (-2014); ~~T the selection of the stability model depends on the number and type of landslides (e.g., deep-seated, shallow), the type and amount of information available to characterize the slope or landslide, and the extent of the study area (e.g., a single slope or landslide, a catchment, a large geographical region).~~ In CRHyME, we were interested mainly in the simulation of the shallow landslide. the debris flows ~~behave intermediately among floods and landslides~~ was and their stability assessment was evaluated through the theory proposed by (Takahashi, (2009), Theule (2012) and Jakob and Jordan (2001) since, according to Theule, 2012, Jakob and Jordan, 2001,, defining a rigid boundary between flood, solid transport, debris flow and shallow landslide processes

is not always possible. they phenomena reside in the middle so defining a unique criterion for analysing their instability cannot be assessed straightforwardly since they can behave intermediately among floods and landslides.

165

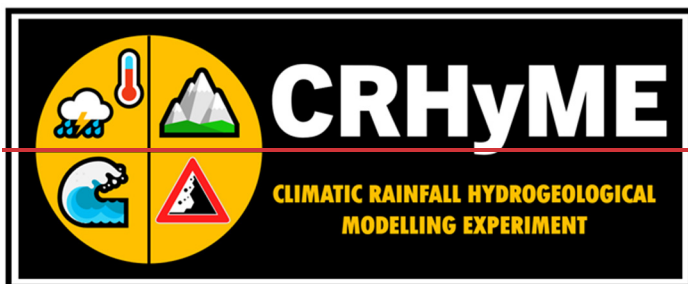
The aim was to merge the potentiality of the reference models cited before : including a well-organized model framework, already adapted to work with meteorological reanalysis and climate scenarios data (PCR-GLOBWB-2), predicting and quantifying some geo-hydrological processes (Landlab and CHASM), and extending the event based simulation (OPENLISEM) to a continuous simulation over a longer period. The CRHyME's code architecture is partially inherited by the PCR-GLOBWB-2 model (Sutanudjaja et al., 2018). This model is characterized by a well-organized model framework that could guarantee the robustness and the stability of the code, fast modelling and reduced time consumption thanks to embedded function parallelization, and no constraints on the spatial and temporal resolution of the input data. The PCR-GLOBWB-2 engine is based on PCRaster libraries (Karssenberget al., 2010; Pebesma et al., 2007). The PCRaster Python libraries offer a series of standard functions prepared for hydrological processing on calculation grids which can be easily "called" via Python scripts to perform individual operations. CRHyME's framework is organized within a modular structure which enables easier single-model updating and to introduce facilitating new features introduction. Python programming language is open-source, and its flexibility permits to fast management of of largemeteorological and climatic-GIS databases which are essential for computing extending the event based simulation (OPENLISEM) to a continuous simulation over a longer period geo-hydrological hazard simulations over large domains. ,reworkedside, CRHyME's engine is based on PCRaster libraries (Karssenberget al., 2010; Pebesma et al., 2007) which is a collection of open source software targeted at the development and deployment of spatio-temporal environmental models. These functions can include a rich set of model building blocks and analytical functions for manipulating raster GIS maps, a framework for the construction of stochastic spatio-temporal models and a tool for interactive visualisation of spatio-temporal data. They are mainly applied in environmental modelling such as rainfall-runoff models and slope stability models and can deal with spatially distributed earth surface data that are discretized considering the single cell of terrain domain as the reference element where model calculations are carried out. Using PCRaster libraries.

170

175

180

185



190 Figure 1: CRHyME logo.

## 2.2 Model Structure

195

The CRHyME model is composed of a series of modules that run successively in a time-loop as represented in Figure 2. The simulations are initialized from a pre-compiled ".INI" file (see the Appendix A) where all the settings and input data paths are specified (see the Appendix B). The first 6 modules evaluate the hydrological cycle and constitute the "hydrological module". The CRHyME's novelty is the "landslide module" where slope instability conditions and sediment transport

dynamics are simulated considering the computed soil moisture and the runoff respectively. The modules included in the code are:

In the .INI file are essentially reported the simulation time settings (e.g. starting date and ending date), the spatially distributed input data and the meteorological and climatological data series, the settings of each computational module and the name of the output files. The .INI file is read by the “deterministic\_runner.py” file that starts the CRHyME model and its internal routines. Except for “pre\_processing.py”, “reporting.py” and “plot.py” modules, where variables are respectively defined, saved, and plotted following the formats and standards of the PCRaster libraries (Sutanudjaja et al., 2018; Karssenberget al., 2010), other modules contain the physical equations that aim to simulate the geo-hydrological cycle.

2-1. CLIMA: elaborates precipitation and temperature data from reanalysis and climate datasets, using the “NetCDF” (Network Common Data Form, “.netcdf”) format (Bonanno et al., 2019; Sutanudjaja et al., 2018);

3-2. METEO: elaborates precipitation and temperature data from ground-based weather stations using the PCRaster standard format “.tss” (Karssenberget al., 2010) for data series and calculates the evapotranspiration;

4-3. INTERCEPTION: excludes from the net precipitation the canopy interception and computes the snow dynamic;

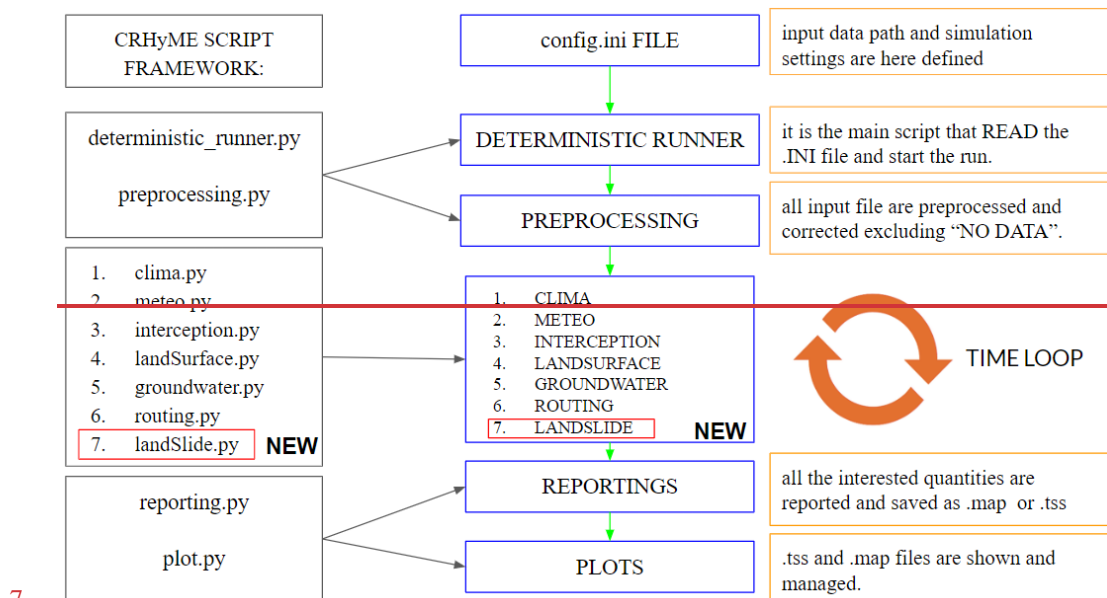
5-4. LANDSURFACE: evaluates the water balance in the superficial soil giving information about runoff, soil moisture and percolation losses;

6-5. GROUNDWATER: evaluates the water balance in the groundwater layer;

7-6. ROUTING: calculates the runoff routing across the watershed;

8.—LANDSLIDE: identifies the triggering conditions for landslides and debris flows, and flows, and calculates erosion and bed-load sediment transport in rivers.

The first 6 modules constitute the “hydrological module” and are intended to evaluate the hydrological cycle while the “landslide module” is the CRHyME’s novelty where slope instability conditions and sediment transport dynamics are simulated considering the computed soil moisture and the runoff respectively.



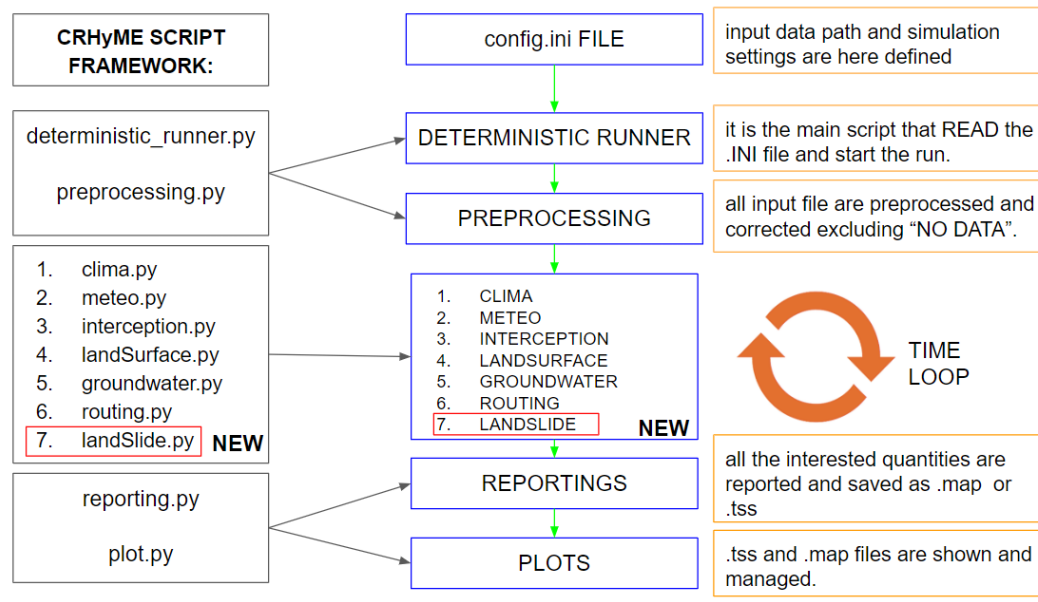


Figure 2: Framework of the `_model` CRHyME. Main Python scripts are listed, explaining their functionality and their link with the other parts of the code. For further details see Appendix A and B.

The PCRaster libraries implemented in CRHyME have the advantage of being fully parallelized to work with multicore processors (Karssenberget al., 2010). This is an important aspect of our code that permits us to decrease sharply the time-consuming of each simulation. The intrinsic parallelization of the PCRaster libraries simplifies and facilitates code maintenance and updating, without any further parallelization optimizations. In Table 1 the operating time calculation ranked for the model CRHyME is reported for different numbers of core processors (worker thread).

CPU cores	PCRaster N° Worker Thread	Single-Operation on LANDSURFACE Module with a large file (10'000 cells)	Single-Cycle (1° to 7° Module) of Model Iteration with a large file (10'000 cells)
2-cores	2	4.07 s	Around 20—25 s
4-cores	4	1.48 s	Around 8—10 s
8-cores	8	1.05 s	Around 5—6 s

Table 1: Performances of CRHyME model working on different CPU core sets. It can be noticed that by increasing the number of cores available, the computation time for a particular operation can drop significantly.

### 2.2.1 Model initialization

A fundamental starting point for CRHyME's code initialization consists of the choice of a suitable digital terrain elevation model (DTMDEM) used in CRHyME as a starting point for the computations. From DEM all the essential data listed in the ".INI" file are derived all the essential data listed at the beginning of the .INI file required for hydrological operations using PCRaster libraries: the "clone.map", a 0-1 mask that defines the computational domain, and the "ldd.map", the local drain direction map (Karssenberget al., 2010; Pebesma et al., 2007). In CRHyME, the is provided by HydroSHEDS DEM (Hydrological data and maps based on Shuttle Elevation Derivatives at multiple Scales, <https://www.hydrosheds.org>) (Lehner et al., 2008) was taken as a reference. The is provided by HydroSHEDS DEM is designed specifically for hydrological models and has been already pre-processed to guarantee the flow connectivity of the river network (hydrologically conditioned). Its spatial resolution is about 3-sec degree, which corresponds approximately to about 90 m at the equator, and it was retained sufficiently accurately for medium-scale catchment analysis. Using the built-in PCRaster functions, the 'flow accumulation', the 'slope', the 'curvature' and the 'slope-aspect' data were reconstructed immediately from HydroSHEDS DTMDEM. In addition to these morphological data, other informative layers are required in CRHyME for geo-hydrological assessment for the geo-hydrological assessment are:

- 250 ▪ the Corine Land Cover data (<https://land.copernicus.eu>) (Girard et al., 2018) is the European inventory of landcover that was considered for defining vegetation interception and soil infiltration coefficients, spatial evapotranspiration flux and root cohesion for landslide stability;
- 255 ▪ the Soil Grids data at 250 m resolution from the world database ISRIC (International Soil Reference and Information Centre) — World Soil Information (<https://maps.isric.org/>) (Hengl et al., 2017), were considered for assessing soil physical properties such as depth and soil composition which are implemented inside infiltration, percolation, erosion and landslide stability routines;
- the hydraulic properties of soils, such as the permeability and porosity, from the European Soil Data Centre (ESDAC) database (<https://esdac.jrc.ec.europa.eu/>) and other worldwide repositories (Tóth et al., 2017; Ross et al., 2018; Huscroft et al., 2018), were considered for assessing superficial and groundwater hydrological balance.

260 ~~The datasets here described are freely available freely for the entire European area, but analogous can be found for other continents. Since they are provided with an open source licence they can be implemented without restrictions. This choice aims to extend and generalise as much as possible the reproducibility of CRHyME's simulations in any worldwide catchments without any constraint on territorial input data. Moreover, (Web Feature Service () Web Coverage Service() them, speeding up~~

265 ~~required by simulations gathered from (Rete Monitoraggio ARPA Lombardia; Rete Monitoraggio ARPA Emilia)reanalysis (Bonanno et al., 2019)built calculate the distribution (Daly et al., 1997; Chow et al., 1988) (Daly et al., 1997; Chow et al., 1988; Abbate et al., 2021b; Terzago et al., 2018)required internal (Figure 2) wa.~~



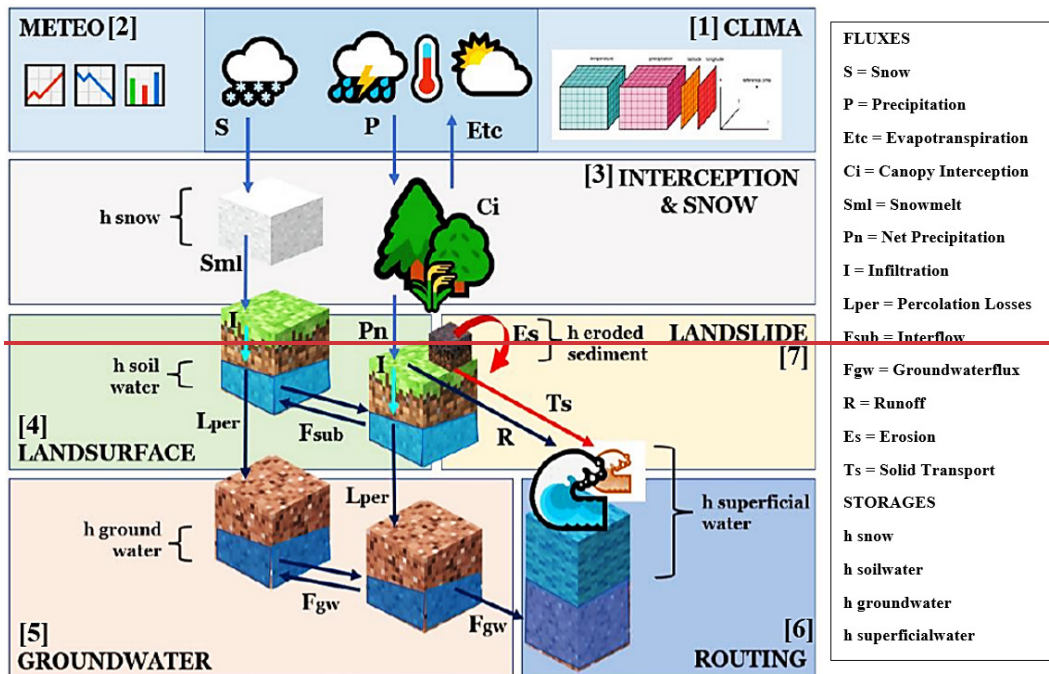
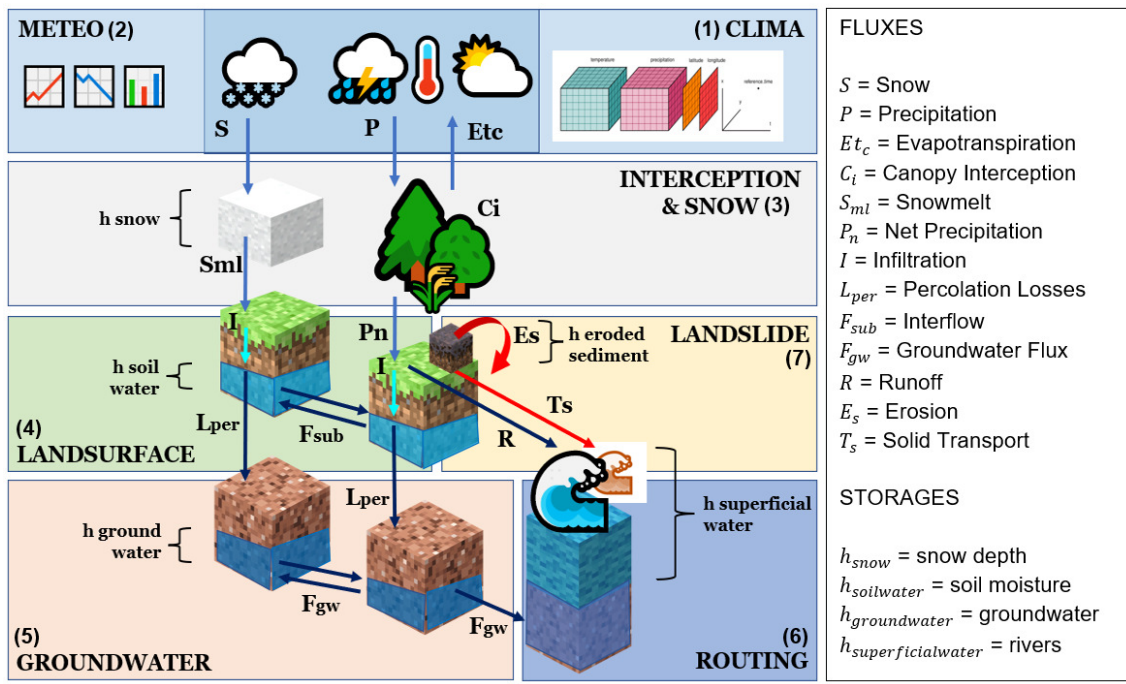


Figure 3: Scheme of the soil water and sediment balances and related mass-fluxes implemented in CRHyME. Fluxes and Storage variables constituting the model are listed.

270

The datasets here described are freely available for the entire European area, but analogous could be found for other continents. Since they are provided with an open-source licence they have been implemented without restrictions. This choice aims to extend and generalise as much as possible the reproducibility of CRHyME's simulations in any worldwide catchments avoiding any constraint on territorial input data. Moreover, these databases provide free Web Feature Service (WFS) and Web Coverage Service (WCS) services, allowing to download them more easily and speeding up CRHyME initialization.

275

Temperature and rainfall data required by simulations were gathered from ground-based meteorological stations (Rete Monitoraggio ARPA Lombardia; Rete Monitoraggio ARPA Emilia) and locally available reanalysis databases (Bonanno et al., 2019). Temperature fields were built by combining the data series at each timestep, estimating the regression coefficient with respect to the station elevation and then using the DEM information to calculate the temperature distribution (Daly et al.,

280

1997; Chow et al., 1988). For rain gauge precipitation, a simple IDW (Inverse Weight Distance) interpolator was implemented with a distance exponent equal to 2 while for rainfall data coming reanalysis data, a simple nearest-neighbour algorithm has

been adopted to downscale the precipitation field at DEM resolution (Daly et al., 1997; Chow et al., 1988; Abbate et al., 2021b; Terzago et al., 2018). CRHyME's timestep required for completing a single loop of all internal modules (Fig. 2) was assumed to be equal to the meteorological forcings timestep and could vary from a minimum of 5 min up to a maximum of 1 day. In this current work, the timestep selected for CRHyME's computations is 1 day.

(Jacob et al., 2014; Sutanudjaja et al., 2018)

### 2.2.2\_Hydrological modules and equations

The hydrological modules (Fig. 2 and 3, from 1 to 6) evaluate the processes of transformation inflows-outflows using input maps of weather forcings consisting of precipitation  $P$  [mm timestep<sup>-1</sup>] and average, maximum, and minimum temperature  $T$  [C°]. In CRHyME, the model also calculates evapotranspiration losses  $ET_c(t)$  according to two formulations chosen by the user: Hargreaves and Penman-Monteith, both taken from FAO guidelines (Raziei and Pereira, 2013; Allan et al., 1998). Although during intense precipitation events the evapotranspiration portion can often be neglected (Chow et al., 1988), its calculation is essential for continuous long-term hydrological simulations. Moreover, this is important also for short-term simulations because may influence the initial conditions of the soil moisture  $S_m(t)$  (Abbate et al., 2019; Lazzari et al., 2018; Mostbauer et al., 2018). Each cell of the terrain domain is considered like a tank that communicates in cascade to the others following the downstream river network (Brambilla et al., 2020; Roo et al., 1996; Sutanudjaja et al., 2018). Hydrological balance is schematized considering 4 imaginary layers where water can be temporarily stored:

1. Snow Storage, Eq. (1) where the snow balance is assessed by the quantity  $h_{snow}(t)$  variable, [mm];
2. Superficial Soil Storage, Eq. (2) and (3) where soil infiltration is computed and the superficial soil balance is assessed by the variable  $h_{soilwater}(t)$  variable, [mm];
3. Groundwater Soil Storage, Eq. (5) where the groundwater balance is assessed by the quantity  $h_{groundwater}(t)$  variable, [mm];
4. Runoff Storage, Eq. (6) where the runoff generated by an excess of infiltration and exfiltration is routed across the catchment and described by the variable  $h_{runoff}(t)$ , [mm].

3. The superficial soil storage is the core of hydrological balance assessment where all the water mass fluxes, in [mm timestep<sup>-1</sup>], are exchanged between atmosphere and terrain. Balances are schematized by Eq.(1), Eq. (2) and Eq. (3) and the fluxes in this layer are evaluated [mm timestep<sup>-1</sup>]. Canopy Interceptions  $C_i(t)$ :

• Infiltration  $I(t)$ : that is the part of the volume that enters the soil using two of the most common infiltration models Horton and SCS-CN (Chow et al., 1988; Chen and Young, 2006; Mishra et al., 2003; Morbidelli et al., 2018; Ravi et al., 1998; Smith and Parlange, 1978; Ross et al., 2018); Canopy Interceptions  $C_i(t)$ : that is the part of the rainfall intercepted by trees leaves;

• Snowmelt  $S_{ml}(t)$  and Snow  $S(t)$ : the melted snow coming from the snowpack;

• Infiltration  $I(t)$ : that is the part of the volume that enters the soil using two of the most common infiltration models Horton and SCS-CN (Chow et al., 1988; Chen and Young, 2006; Mishra et al., 2003; Morbidelli et al., 2018; Ravi et al., 1998; Smith and Parlange, 1978; Ross et al., 2018);

- Infiltration balance in Eq. (2) establishes the net water volume  $I(t)$  that enters the soil. From precipitation  $P(t)$  the net precipitation arriving at the soil interface  $P_n(t)$  is evaluated by subtracting the rainfall intercepted by tree leaves, e.g. Canopy Interceptions  $C_i(t)$  (Li et al., 2017; Nazari et al., 2019). When the temperature  $T$  is  $< 0^\circ\text{C}$ , all the precipitation is stored as snowpack  $h_{snow}(t)$  Eq. (1) and released afterward as snowmelt contribute  $S_{ml}(t)$  when temperature increases above  $0^\circ\text{C}$  following a degree-day approach (Chow et al., 1988; Cazorzi and Dalla Fontana, 1996).  $I(t)$  is estimated directly using the common infiltration methods proposed by Horton and SCS-CN (Chow et

al., 1988; Chen and Young, 2006; Mishra et al., 2003; Morbidelli et al., 2018; Ravi et al., 1998; Smith and Parlange, 1978; Ross et al., 2018) and the runoff generated by an excess of precipitation at the surface  $R(t)$ , is obtained by the difference of  $P_n(t) - I(t)$ ;

Superficial soil moisture balance in Eq. (3) permits to evaluate the quantity  $S_m(t)$  which is expressed dimensionless as a ratio between  $h_{soilwater}(t)$  [mm] and the product of terrain porosity  $n$  and the superficial soil depth ( $depth_{soil}$ ). Porosity and superficial soil depth are determined respectively from Tóth et al. (2017), Ross et al. (2018), Huscroft et al. (2018) and Hengl et al. (2017) databases. The other terms of the water balance are:

- $ETc(t)$  evapotranspiration losses according to Hargreaves and Penman-Montheit formulations suggested by FAO guidelines (Raziei and Pereira, 2013; Allan et al., 1998);
- $L_{per}(t)$  percolation losses are the part of the volume that goes to the deepest groundwater layer, evaluated as a function of the soil water balance in unsaturated conditions using Van Genuchten's functions and parameters (Jie et al., 2016; Van Genuchten, 1980; Daly et al., 2017; Groenendyk et al., 2015; Vitvar et al., 2002; Jackson et al., 2014; Klaus and Jackson, 2018);
- Exfiltration  $Ex(t)$  and  $Ex_{GW}(t)$  is the leakage of water on the surface that occurs after the complete saturation of the superficial soil storage (ponding);
- $F_{sub}(t)$ , expressed in  $[m^3 s^{-1}]$ , is the sub-surface lateral fluxes generated inside the superficial soil layer through the Dupuit approximation of the Darcy law for water filtration in soils. Here is a correction of the saturated permeability  $K_s$   $[m s^{-1}]$  considering the relative permeability  $K_r$  [-] caused by the partial saturation conditions has been included in the formula (Van Genuchten, 1980).  $\Delta x$  and  $\Delta y$  represent the cell dimensions in [m].

(groundwater) following the complete saturation of the soil (aquifer) column.

$F_{sub}(t)$  and  $F_{GW}(t)$ : lateral fluxes generated inside superficial soil layer and groundwater layer, following the Dupuit law for unsaturated saturated soils.

$F_{kin-dyn}(t)$ : runoff fluxes computed using the kinematic or dynamic flow routing PCRaster functions.

All the fluxes related to water mass balance are converted to the standard international units such as  $[m^3 s^{-1}]$  for discharges while storage quantities  $\Delta h_{snow}(t)$ ,  $\Delta h_{soilwater}(t)$ ,  $\Delta h_{groundwater}(t)$  and  $\Delta h_{runoff}(t)$  are converted into  $[m^3]$  for volumes.  $S_m(t)$  is expressed in [mm] and converted to adimensional quantity [-] if divided by product of the terrain porosity  $n$  and height.

$\frac{dh_{snow}(t)}{dt} \cong \frac{\Delta h_{snow}(t)}{\Delta t} = S(t) - S_{ml}(t)$	(1)
$I(t) = (P(t) - C_I(t) - S_{ml}(t)) - R(t) = P_n(t) - R(t)$	(2)
$\frac{d(S_m(t) * depth_{soil} * n)}{dt} S_m(t) = \frac{dh_{soilwater}(t)}{dt} \cong \frac{\Delta h_{soilwater}(t)}{\Delta t} \pm \frac{F_{sub}(t)}{\Delta x * \Delta y}$ $= I(t) - ETc(t) - Ex(t) - L_{per}(t)$	(3)

The groundwater reservoir depth ( $depth_{GW}$ ) has been modelled considering a spatial distribution described in Eq. (4) (Fan et al., 2007; de Graaf et al., 2015; Pelletier et al., 2016). According to these studies, as the superficial slope increases, the aquifer depth is reduced until it reaches the minimum value of 0 m, e.g., corresponding to the condition of complete absence.

$depth_{GW} = a / (1 + b * slope)$	(4)
------------------------------------	-----

In Eq. (4) the slope is expressed as a tangent to the angle of inclination of the surface while  $a$  and  $b$  represent coefficients that are distinguished according to the depths of interest: where the depth of the bedrock is supposed to be low ( $< 10$  m, superficial bedrock), the suggested parameters are  $a = 20$  and  $b = 125$ , while if the bedrock depth is significative ( $> 10$  m, deep regolith)  $a = 120$  and  $b = 150$ . In CRHyME an intermediate condition has been adopted between superficial bedrock and deep regolith, therefore the parameters adopted are the following:  $a = 200$  and  $b = 125$ . This approximation has appeared sufficiently accurate concerning the fact that currently available data on groundwater aquifer depth and hydrogeological parameters are rather approximated, uncertain and with low resolution (Kobierska et al., 2015; Zomlot et al., 2015; Hayashi, 2020; Huscroft et al., 2018).

$$\frac{dh_{groundwater}(t)}{dt} \cong \frac{\Delta h_{groundwater}(t)}{\Delta t} \pm \frac{F_{GW}(t)}{\Delta x * \Delta y} = L_{per}(t) - Ex_{GW}(t) \quad (45)$$

The groundwater table is generated by the percolated water  $L_{per}(t)$  coming from the upper layer Eq. (5). The groundwater lateral flow  $F_{GW}(t)$ , expressed in  $[m^3 s^{-1}]$ , is then calculated using the Dupuit approximation according to which the filtration rate is given by the product of hydraulic permeability for the tangent of the slope of the impermeable substrate, supposed parallel to the slope (Klaus and Jackson, 2018; Anderson, 2005; Bresciani et al., 2014).  $Ex_{GW}(t)$  e.g., groundwater exfiltration, is the term that describes the leakage of water after the complete saturation of the groundwater storage, simulating the water springs.

$$\frac{dh_{runoff}(t)}{dt} \cong \frac{\Delta h_{runoff}(t)}{\Delta t} \pm \frac{F_{kin-dyn}(t)}{\Delta x * \Delta y} = R(t) + Ex(t) + Ex_{GW}(t) \quad (6)$$

$$\frac{dh_{runoff}(t)}{dt} \cong \frac{\Delta h_{runoff}(t)}{\Delta t} = R(t) + Ex(t) + Ex_{GW}(t) \pm F_{kin-dyn}(t) \quad (5)$$

At the groundwater reservoir, the sub-surface flow is generated thanks to the percolated water from the upper layer Eq. (4). The flow is calculated using the Dupuit approximation according to which the filtration rate is given by the product of hydraulic permeability for the tangent of the slope of the impermeable substrate, supposed parallel to the slope (Klaus and Jackson, 2018; Anderson, 2005; Breseciani et al., 2014). The sub-surface flow has been modelled considering a special distribution of the groundwater depth (Fan et al., 2007; de Graaf et al., 2015; Pelletier et al., 2016). This approximation has appeared sufficiently precise concerning the fact that up to now available data on groundwater aquifer depth and hydrogeology parameters are rather approximated and uncertain with respect to the affordability of the superficial layers data (Kobierska et al., 2015; Zomlot et al., 2015; Hayashi, 2020; Huseroft et al., 2018).

uperficial runoff is defined as the sum of  $R(t)$ ,  $Ex(t)$  and  $Ex_{GW}(t)$  and it is stored in  $h_{runoff}(t)$  in Eq. (6).  $h_{runoff}(t)$  The sum of the surface and the emerged sub-surface runoffs are propagated across the overland surface along the lines of maximum slope and inside the river network using two possible methods available in PCRaster libraries (kinematic and dynamic) that are deputed for the flow routing process (Chow et al., 1988; Lee and Pin Chun, 2012; Collischonn et al., 2017; Bancheri et al., 2020).  $F_{kin-dyn}(t)$  flux, expressed in  $[m^3 s^{-1}]$ , is Both derived from the simplification of De Saint Venant's one-dimensional equations of motion, expressed in -. The first kinematic algorithm is generally used applied in sections where the slopes are accentuated so it is possible to approximate the hydraulic gradient with the slope of the channel (Chow et al., 1988). The second dynamic algorithm instead introduces further terms that allow a better simulation of the outflow in correspondence to the flat areas where when the other terms of the De Saint Venant equation are no longer negligible (Chow et al., 1988), but requires precise information about the geometry of rivers sections to carry out the flood wave propagation (Karssenberget al., 2010).

### 395 2.2.3 Geo-hydrological module and equations

In order to study geo-hydrological instability it is of paramount importance to analyse the triggering causes of landslides and the dynamic of erosion and sediment transport processes (Guzzetti et al., 2005; Remondo et al., 2005; Montrasio and Valentino, 2016; Bovololo and Bathurst, 2012). For this purpose, an ad-hoc In the following paragraphs, the new “landslide module” features (Figure 3, n° 7) has been included developed in CRHyME are described (Fig. 3, n° 7).

400

#### 2.2.3.1 Stability models for shallow landslides and debris flows

Shallow landslides triggering is strongly correlated with meteorological and climatic forcing (Abbate et al., 2021a). The abrupt modifications of the local hydrology with the alternation of dry and wet conditions of soil induced by precipitation are responsible for undermining the stability of the slopes (Iverson, 2000; Chen and Young, 2006). Here are described briefly the four stability models included in CRHyME: 1) the Iverson model (Iverson, 2000), Eq. (7), 2) the Harp model (Harp et al., 2006), Eq. (8), 3) the Milledge model (Milledge et al., 2014) and, Eq. (9), 4) the SLIP model (Montrasio, 2008; Montrasio and Valentino, 2016), Eq. (10). In slope stability analysis, the limit equilibrium method based on Mohr-Coulomb criterion is usually adopted to calculate slope stability. The one-dimensional theory considers the hypothesis of an infinitely extended slope characterized by soil thickness  $Z$  [m], plane inclination  $\alpha$  [°], saturated soil  $\gamma_s$  and water  $\gamma_w$  specific weight [ $\text{kN m}^{-3}$ ]. The slope the stability is evaluated by the Factor of Safety ( $FS$ ), defined as the ratio between the resistant forces due to the friction and to the mobilizing forces due to the weight component parallel to the slope. In CRHyME, the one-dimensional model was implemented by imagining each cell as a slope element for which the value of the safety factor  $FS$  is calculated. Typical values of the friction angle and cohesion for superficial terrains have been obtained from literature references, while the water content is the result of the hydrological balance carried out by hydrological modules. According to the principle of effective stress, as the soil moisture increases, normal efforts are reduced by an aliquot equal to the pressure generated by the water itself (Iverson, 2000).

415

$FS = \frac{\tan(\varphi)}{\tan(\alpha)} - \frac{\psi\gamma_w \tan(\varphi)}{\gamma_s Z \sin(\alpha) \cos(\alpha)} + \frac{c}{\gamma_s Z \sin(\alpha) \cos(\alpha)}$	(7)
$FS = \frac{\tan(\varphi)}{\tan(\alpha)} + \frac{m\gamma_w \tan(\varphi)}{\gamma_s \tan(\alpha)} + \frac{c}{\gamma_s Z \sin(\alpha)}$	(8)
$FS = \frac{2F_{rl} + F_{rb} + F_{rd} - F_{du}}{F_{dc}}$	(9)
$FS = \frac{N' \tan \varphi + C'}{W' \sin \alpha + F'}$	(10)

The key parameters of the Iverson (Iverson, 2000) Eq. (7) and Harp (Harp et al., 2006) models Eq. (8) are essentially 3: the friction angle  $\varphi$  [°] and the cohesion of the soil  $c$  [kPa] which are a function of the terrain granulometry, and the superficial soil moisture  $S_m(t)$  [m]. Inside the Iverson's model, the soil moisture influence is described by through the groundwater pressure head of the local aquifer  $\psi = f(S_m(t))$ , expressed in [kPa], while inside the Harp model is described by the dimensionless variable  $m = \frac{h_{soilwater}(t)}{Z \cdot n}$ , comprised between 0 (completely dry) and 1 (completely wet). The Milledge model (Milledge et al., 2014) in Eq. (9) considers not only the friction effects along the sliding surface  $F_{rb}$  expressed in [N], but also the shear resistance along the two parallel and vertical side walls  $F_{rl}$  in [N], the passive force of the upstream terrain  $F_{du}$ , in [N], the active force of the valley terrain  $F_{rd}$  in [N], and the mobilizing force due to the terrain weight  $F_{dc}$ , in [N]. In the SLIP model (Montrasio, 2008; Montrasio and Valentino, 2016) shown in Eq. (10) the terms are expressed in [N]:  $N'$  is the normal component of the weight as a function of porosity  $n$  and soil moisture  $S_m(t)$ ;  $C'$  is the cohesion term;  $W'$  is the slope

425

parallel component of the weight as a function of porosity  $n$  and soil moisture  $S_m(t)$ ;  $F'$  is the term that expresses the seepage forces that are related to the presence of the temporary water table. Since ~~at catchment scale~~ slopes are vegetated, two other factors should be included: the additional cohesion of the root system of trees and the additional weight of plant biomass (Cislighi et al., 2017; Yu et al., 2018; Rahardjo et al., 2014). ~~In fact~~ ~~As a matter of fact~~ ~~In fact~~, in the absence of root cohesion, several slope ~~portions~~ ~~areas~~ ~~were~~ would be perpetually in conditions of instability with  $FS < 1$ . The addition of root cohesion, varying between 1 – 10 kPa depending on the tree species and the type of land use was included in the ~~estimates of the stability model~~ ~~stability evaluation~~ (further details in Abbate and Mancusi, 2021a).

A debris flow represents movements of mass that are often triggered on steep slopes and travel long distances reaching the fan close to the watershed outlet (Takahashi, 2009). Debris flows are classified as landslides, although they are among the more fluid types of landslides (Iverson et al., 1997). Therefore, solid concentration within the saturated deposit and the presence of superficial water flowing above are the key parameters for assessing the triggering condition. As can be appreciated by ~~the~~ Eq. (11) and (12), two criteria are at least to be included. The first one is derived from the theory of infinite slope stability where the solid concentration parameter  $C_*$  is included as the principal triggering factor. The solid concentration  $C_*$  is the grain concentration by volume in the static debris bed and can be expressed by the ratio between the soil amount [ $m^3$ ] to the sum of the soil amount [ $m^3$ ] and soil water volume [ $m^3$ ]. Increasing the local water volume, the solid concentration starts to progressively reduce. The first criterium in Eq. (11) requires the indication of soil density  $\sigma$  [ $kg\ m^{-3}$ ], water density  $\rho$  [ $kg\ m^{-3}$ ], the surface runoff height  $h_{runoff}$  [ $m$ ] and the parameter  $a_{df}$  that can be assumed equal to the representative diameter of the soil deposit, such as  $D_{50}$ , expressed in [ $m$ ]. The second criterium in Eq. (12) considers that specific superficial runoff discharge  $q_l = \frac{F_{kin-dyn}(t)}{\Delta x}$ , in [ $m^2\ s^{-1}$ ], flowing above the debris deposit, satisfies the threshold condition  $\geq 2$  for the non-dimensional water discharge  $q^*$  [-], where  $g$  is gravity acceleration [ $m\ s^{-2}$ ]. If these criteria are satisfied under a predetermined rainfall condition that basin could be ~~affected by~~ ~~subjected to~~ debris flow triggering.

$FS_{debris} = \frac{C_*(\sigma - \rho)}{C_*(\sigma - \rho) + \rho \left(1 + \frac{h_{runoff}(t)}{a_{df}(D_{50})}\right)} \tan \varphi$	(11)
$q_* = q_l / \sqrt{D_{50}^3 * g} \geq 2$	(12)

## 2.2.3.2 Erosion production and bed-load solid transport ~~evaluation~~ routing

Gavrilovic's method (summarized in Eq. 13-14-15) is a semi-quantitative method capable of giving an estimation of erosion and sediment production in a basin (Longoni et al., 2016; Milanese et al., 2015; Globevnik et al., 2003; Brambilla et al., 2020). ~~Initially, it~~ was ~~initially~~ developed in southern ex-Yugoslavia and then successfully applied in Switzerland and Italy. The mean annual volume of eroded material  $G$ , expressed in [ $m^3\ yr^{-1}$ ], is a product of  $W_s$  and  $R_{EPM}$ , which are respectively the mean annual production of sediment due to surface erosion, expressed in [ $m^3\ yr^{-1}$ ] Eq. (13), and the retention coefficient, ~~non~~dimensional [-] in Eq. (15) considers the possible re-sedimentation of the eroded material across the watershed.

$G = W_s R_{EPM}$	(13)
$W_s = \pi \bar{P} \bar{H} \tau_G(\bar{T}) \bar{Z}_{EPM}^{\frac{3}{2}} A_{Basin} \rightarrow W_{s\ downscaled} = \pi P(t) \bar{H} \tau_G(T(t)) \bar{Z}_{EPM}^{\frac{3}{2}}(x, y) \Delta x \Delta y$	(14)
$R_{EPM} = \frac{\sqrt{OD}(l + l_{lat})}{(l + 10)A_{basin}}$	(15)

The terms that appear in the equations are:  $\tau_G$  —temperature coefficient [ $^{\circ}C$ ] in ~~the~~ function of watershed mean annual temperature  $\bar{T}$  in [ $^{\circ}C$ ],  $\bar{P}$  mean annual precipitation value [ $mm\ yr^{-1}$ ],  $\bar{Z}_{EPM}$  mean erosion coefficient [-],  $A_{basin}$  basin area [ $km^2$ ],  $O$  perimeter of the basin [ $km$ ],  $D$  mean elevation of the basin [ $km$ ],  $l$  length of the main watercourse [ $km$ ],  $l_{lat}$  the

total length of the lateral tributaries [km]. The Gavrilovic method was developed to work with annual data of mean precipitation and temperature. Since with CRHyME, we are interested in a continuous simulation, the method has been temporally and spatially downscaled (Eq. 14) by substituting  $\bar{P}$  and  $\bar{T}$  with the time-series of precipitation  $P(t)$  [mm timestep<sup>-1</sup>] and  $T(t)$  temperature [C°] and calculated for each domain cell ( $A_{Basin} \rightarrow \Delta x * \Delta y$ ). The values of  $Z_{EPM}$  are correlated to the land use characteristics and geological maps (Milanesi et al., 2015; Abbate and Mancusi, 2021a) therefore the coefficient was spatially distributed through these parameters using the conversion table relation proposed by (Globevnik et al., (2003).

The Gavrilovic method defines  $W_s$  as the source of available sediment ~~that can be~~ routed through the watershed until the outlet. In CRHyME the sediment routing has been modelled considering its strong relation with the liquid discharge. First of all, ~~The latter is corrected by recalling the theory of incipient motion of Shields that states the starting motion of sediments in the function of  $D_{50}$  quantity,~~ the median diameter of the soil granulometric curve (Chow et al., 1988; Merritt et al., 2003; Vetsch et al., 2018), is evaluated implemented (Figure 4). ~~In particular, the~~ solid discharge is evaluated in two manners ways. A first calculation considers a pure Transport Limited stream-power formula for bed load transport (Morgan and Nearing, 2011; Shobe et al., 2017; Campforts et al., 2020). Here, the solid discharge  $Q_s$ , expressed in [m<sup>3</sup> s<sup>-1</sup>], is in function of the reach hydraulic and geometrical characteristics (Figure 4) and it doesn't consider the local availability of the eroded material in the channel that may decrease/increase the amount of sediment delivered. This first implementation of solid transport routing ~~and balance is founded on the hypothesis of~~ is also defined as Transport Limited (TL) since only the reach transport capacity is determined as a prevalent condition. ~~The latter is corrected by recalling the theory of incipient motion of Shields that states the starting motion of sediments in the function of  $D_{50}$  quantity (Chow et al., 1988; Merritt et al., 2003; Vetsch et al., 2018).~~  
 A second calculation represent consists of an adaptation of the kinematic model for clear water to the sediment transport, under the hypothesis that the velocity of sediment transport is assumed ~~like~~ similar to the water flow. The application of the kinematic method requires the estimation of stage-discharge relations for the sediment in analogy with the clear water stage-discharge functions. Several authors (Govers, 1989; Govers et al., 1990; Rickenmann, 1999) have considered this hypothesis reasonable when no further additional information about solid transport is available. For this second case, ~~In both cases,~~ the sediment balance is required and it has been assessed in each cell domain through Eq. (16) considering: the erosion rate  $E_s$  equal to the source term  $W_s$  computed by EPM and the deposition rate  $D_s$ , following (Shobe et al., (2017), expressed in [m<sup>3</sup> yr<sup>-1</sup>]; and the transport term  $T_s$  considering the kinematic model adapted for sediment routing, expressed in [m<sup>3</sup> s<sup>-1</sup>]; the sediment amount  $h_{solid}(t)$  in [m], converted in volume [m<sup>3</sup>] if multiplied by cell area extension [m<sup>2</sup>], with Eq. (15). This second implementation is representative of the Erosion Limited (EL) condition where the ~~material available~~ sediment availability in the river or ~~across~~ the slopes tends to limit is limited by their effective availability-effective water erosion, as it frequently happens (Shobe et al., 2017; Campforts et al., 2020; Chow et al., 1988; Davy and Lague, 2009).

$\frac{dh_{solid}(t)}{dt} \cong \frac{\Delta h_{solid}(t)}{\Delta t} \pm \frac{T_s(t)}{\Delta x * \Delta y} = D_s(t) - E_s(t)$	(16)
--	------

In CRHyME both TL and EL methods are evaluated for assessing quantitatively sediment transport yield within a physically reasonable range. According to Papini et al. (2017); Ivanov et al. (2020a); Dade and Friend (1998a); Lamb and Venditti (2016); Peirce et al. (2019); Pearson et al. (2017) and; Ancy, (2020), the sediment transport dynamic is an active research frontier. In this sense, the spatial distribution of  $D_{50}$  is a critical point because is difficult to be reconstructed at the catchment scale (Abeshu et al., 2021). Moreover,  $D_{50}$  distribution influences incipient motion threshold that sensibly modifies the local sediment routing leading to wrong estimations of the watershed sediment yield (Fig. 4). Since a close formulation doesn't exist for indirectly estimating the granulometry in the absence of an on-field survey dataset, empirical approaches have been proposed by (Nino (2002); Sambrook Smith and Ferguson (1995); Lamb and Venditti (2016) and; Berg (1995).

According to these authors, morphological, climatic, hydrological, and geological factors can influence river granulometry in a particular section. Slope-like factors have shown a quite significant correlation with  $D_{50}$  and in some cases  $slope \rightarrow D_{50}$  relations (power-laws in the form like  $D_{50} = a_x S slope^{b_x}$ ) were retrieved (Nino, 2002). Namely,  $D_{50}$  tends to increase with slope steepness. These relations mimic the formula proposed by Berg (1995) where the  $D_{50}$  is indirectly determined using a power-law function describing the river morphology evolution. Even though  $slope \rightarrow D_{50}$  represent a crude approximation it has a physical meaning since in the upper catchment (where slopes are steepness) coarse granulometries are generally prevalent while at the outlet (where slopes are lower) the sediment fine fraction becomes more significant (Tangi et al., 2019). In CRHyME, the  $D_{50}$  is a necessary granulometric data, therefore an ensemble of empirical  $slope \rightarrow D_{50}$  curves have been proposed to assess automatically  $D_{50}$  distribution across the catchment using the slope data. Curve's parameters were calibrated ad hoc in the examined areas comparing simulated sediment yields to the available measurements and with on-site granulometry surveys.

(Abeshu et al., 2021) In CRHyME both TL and EL methods are considered and evaluated for solid transport assessment. According to (Papini et al., 2017; Ivanov et al., 2020a; Dade and Friend, 1998; Lamb and Venditti, 2016; Peirce et al., 2019; Pearson et al., 2017; Ancy, 2020), the sediment transport dynamic is an active research frontier. In this sense, the spatial distribution of  $D_{50}$  is a critical issue because is difficult to be reconstructed at catchment scale. Moreover,  $D_{50}$  distribution influences incipient motion threshold that sharply modify sensibly the local sediment routing leading to wrong estimations of the watershed sediment yield.

empirical According to these authors, several morphological, climatic, hydrological, and geological factors can influence the river granulometry. Among them, slope-like factors have shown a quite significant correlation with  $D_{50}$  and in some cases sfound (Nino, 2002). formula  $D_{50}$  function Even though s represent a crude approximation it has a physical meaning since in the upper catchment (where slopes are steepness) coarse granulometries are prevalent while at the outlet (where slopes are lower) the sediment fine fraction becomes important. In CRHyME's model  $D_{50}$  is a necessary data, therefore a bunch of empirical  $slope \rightarrow D_{50}$  curves have been implemented. Curve's parameters were calibrated ad hoc with respect to the available sediment yield measurements and on-site granulometry surveys conducted in the examined areas.

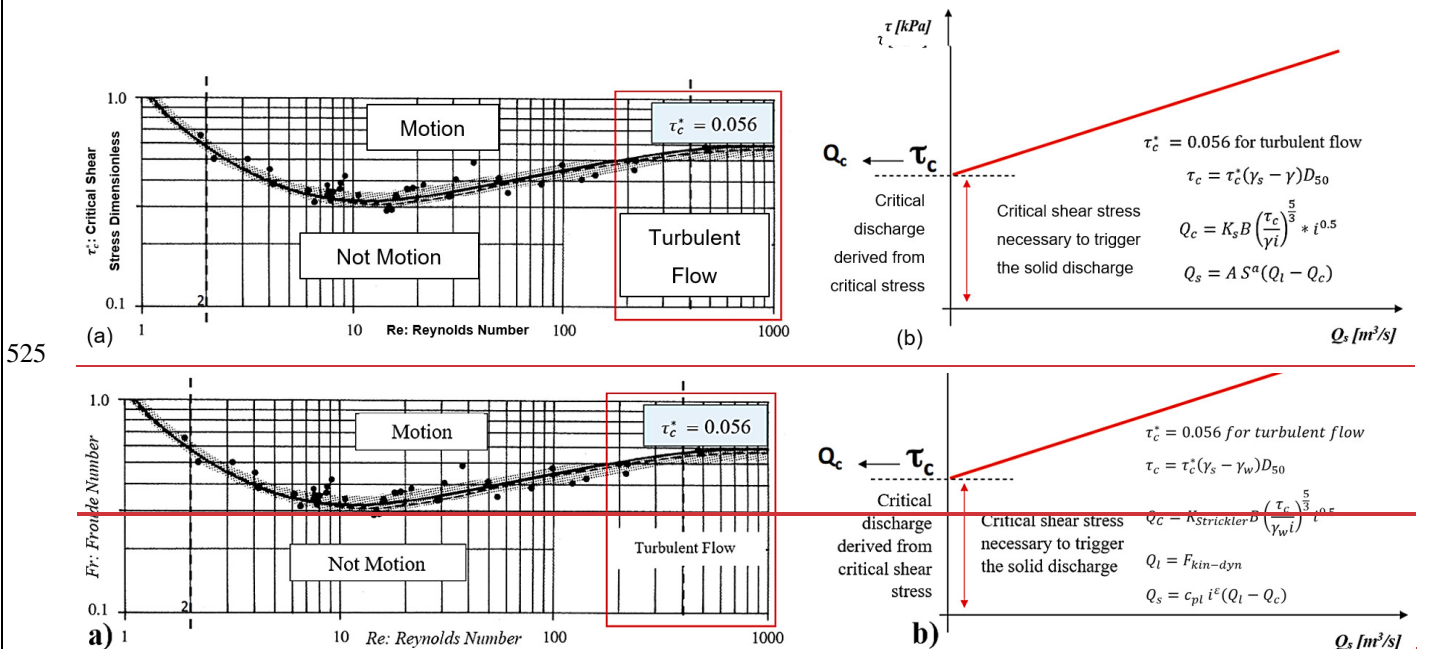


Figure 4: (a) Shield abacus (Chow et al., 1988) for solid transport incipient motion under different conditions of turbulence ( $Re$  Reynolds number) and flow regime ( $Fr$  number). In the red box is defined the typical range of turbulent flow in rivers with a critical dimensionless shear stress  $\tau_c^*$  of 0.056; (b) evaluation of the incipient motion condition for solid transport discharge  $Q_s$  using power-law relation where: the critical shear stress  $\tau_c$  [kPa] and the critical liquid discharge  $Q_c$  [ $m^3 s^{-1}$ ] are a function of saturated grain  $\gamma_s$  and  $\gamma_w$  and water specific weights [ $kN m^{-3}$ ], the local granulometry through the parameter  $D_{50}$  [mm], the roughness  $K_{Strickler}$  [-], the channel width  $B$  [m], the reach slope  $i$  [%] and the two coefficients  $\epsilon$  [-] (comprised between 1 and 2) and  $c_{pl}$  [-] (comprised 0.94 and 5.8) (Vetsch et al., 2018).



535 In the recent literature, some simplified models of sediment erosion and transport have been proposed to fulfil the need to quantify  
these processes (Tangi et al., 2019; Bizzi et al., 2021; Czuba, 2018; Gilbert and Wilcox, 2020; Beveridge et al., 2020). The models  
described represent a strong idealization of what can happen at the catchment scale. Some authors have proposed a framework  
where the river network is discretized in “segments” where the mass balance of water and solid are assessed starting from the top  
of the basin up to the outlet. These “topological” frameworks are fast and rather simple to interpret and have the peculiarity to  
540 include all the infrastructures, such as dams, that can perturb the sediment balance at reached levels (Tangi et al., 2019; Bizzi et al.,  
2021; Schmitt et al., 2018). One of their main worth points is the possibility to include statistical analysis on inputs and making  
Montecarlo iterations to reach the best accordance with monitoring field data. Montecarlo statistical technique is applied especially  
for assessing the granulometry of each reach of the catchment where the sediment source strongly depends on the characteristic  
diameters (Tangi et al., 2019). In several cases, an automatic procedure has been implemented and rather large catchments have  
545 been studied (Bizzi et al., 2021; Schmitt et al., 2018). However, these models suffer from the same problems as the distributed ones:  
the scarcity of reference data that are necessary to select the more realistic Montecarlo simulation and the not complete  
understanding of the erosion-transport processes. According to (Beveridge et al., 2020; Sklar et al., 2017), the erosion processes on  
the hillslopes are rather complex and are difficult to conceptualize in a unique framework since several factors work together at  
different scales and at different times to manipulate the soil granulometry. In particular, sediment delivery to river reaches depends  
550 on landslides that occurred in the past that are a barely random process without a characteristic of periodicity (Gilbert and Wilcox,  
2020; Sklar et al., 2017). Moreover, several assumptions on transport dynamics are assumed in these models such as the hypothesis  
of equilibrium of the sediment supply across the rivers (Bizzi et al., 2021; Gilbert and Wilcox, 2020) that, in some cases, maybe not  
be representative of the real condition that is again barely unknown. Due to their simplicity, these models are generally not integrated  
with a hydrological routine because are intended to focus only on sediment transport mechanisms (Bizzi et al., 2021; Gilbert and  
555 Wilcox, 2020; Beveridge et al., 2020). So, liquid discharge data series are required to be initialized and some hypothesis about  
uniform flow motion using Gauckler-Manning-Strickler formula are needed to associate a proper discharge value at eac

### Connections within among simulated geo-hydrological processes

The processes here described may occur simultaneously inside a catchment, especially during heavy rains or after periods of  
prolonged precipitation (Abbate et al., 2021a). In CRHyME, the erosion and sediment transport are well integrated within the  
560 hydrological routines following the state-of-the-art in the literature (Vetsch et al., 2018). Here, both the triggering function  
(sediment detachment and incipient motion) and the magnitude (amount of sediment eroded and transported) are quantified.  
On the other side, for shallow landslide and debris flow, only the triggering condition of failure has been analysed while the  
mass wasting propagation across the catchment has not been included in the code yet. This choice is motivated by the fact that  
mass wasting failures, especially for debris flows, are characterized by large uncertainties in their volume quantification related  
565 mainly to the entrainment processes and their runout strongly depends on DEM accuracy and spatial resolution (i.e. they are  
spatial scale dependent) (Jakob and Hungr, 2005; Scheidl and Rickenmann, 2011). The entrainment effect is difficult to be  
modelled in a closed form and it may perturb the volume estimation by orders of magnitude (D’Agostino and Marchi, 2001).  
Mass wasting processes may have a strong incidence on sediment transport dynamic and compared to widespread erosion,  
which is a “low intensity” process, landslides may change abruptly the geo-morphological characteristics of the catchment  
570 (Iida, 1999; D’Odorico and Fagherazzi, 2003). These issues are under study, but preliminary results are not investigated in  
this present work but are under study.

### **2.3 Model performance**

The PCRaster libraries implemented in CRHyME have the advantage of being fully parallelized to work with multicore  
processors (Karszenberg et al., 2010). This is an important aspect of our code that permits us to decrease sharply the time-  
575 consuming of each simulation. The intrinsic parallelization of the PCRaster libraries simplifies and facilitates code  
maintenance and updating, without any further optimizations. In Table 1 the operating time calculation ranked for the model  
CRHyME is reported for different numbers of core processors (worker thread).

<u>CPU cores</u>	<u>PCRaster N° Worker Thread</u>	<u>Single Operation on LANDSURFACE Module with a large file (10'000 cells)</u>	<u>Single Cycle (1° to 7° Module) of Model Iteration with a large file (10'000 cells)</u>
<u>2 cores</u>	<u>2</u>	<u>4.07 s</u>	<u>Around 20 – 25 s</u>
<u>4 cores</u>	<u>4</u>	<u>1.48 s</u>	<u>Around 8 – 10 s</u>
<u>8 cores</u>	<u>8</u>	<u>1.05 s</u>	<u>Around 5 – 6 s</u>

**Table 1: Performances of the CRHyME model working on different CPU core sets. By increasing the number of cores available, the computation time for a particular operation can drop significantly.**

### 2.3.1 Hydrological ~~error metrics~~ ~~Indexes~~ and sediment ~~transport assessment~~ ~~and assessment~~

Assessing hydrological performance at basin outlets is evaluated through error indexes that compare water discharges recorded by the local hydrometer and the water discharge simulated by the model (Chow et al., 1988; Bancheri et al., 2020). The most common ~~error metrics used in hydrology~~ ~~indexes~~ are the Nash–Sutcliffe Efficiency (NSE), and the Root-Mean-Square Error (RMSE). The Nash–Sutcliffe Efficiency (NSE) in Eq. (17) is a normalized model efficiency coefficient where  $S_i$  and  $M_i$  are respectively the predicted (or simulated) and measured (or observed) values at a given time step  $i$ . The NSE varies from  $-\infty$  to 1, where 1 corresponds to the maximum agreement between predicted and observed values. The Root-Mean-Square Error (RMSE) in Eq. (18) is given by where  $S_i$  and  $M_i$  are respectively the predicted (or simulated) and measured (or observed) time series, and  $N$  is the number of components in the series.

$NSE = 1 - \frac{\sum_{i=1}^n (S_i - M_i)^2}{\sum_{i=1}^n (M_i - \bar{M}_i)^2}$	(17)
$RMSE = \sqrt{\frac{1}{N} \sum_{i=1}^n (M_i - S_i)^2}$	(18)

For the sediment transport assessment, the periodical bathymetry campaigns carried out inside hydropower reservoirs can be considered as a reference ~~for the sediment yield measurement~~ (Pacina et al., 2020; Langland, 2009; Marnezy, 2008) ~~of the sediment yield measurement~~. Compared to hydrometric data which can be easily gathered from local environmental agencies (Rete Monitoraggio ARPA Lombardia; Rete Monitoraggio ARPA Emilia), bathymetries are generally not accessible to the public (ITCOLD, 2009, 2016). Therefore, the calibration and validation of erosion and sediment transport models have considered the seasonal volume estimation in hydropower reservoirs and the event-based volume estimation only where available. For the case studies analysed, these data were retrieved also from specific reports (Milanesi et al., 2015; Ballio et al., 2010; Brambilla et al., 2020).

### 2.3.2 ROC curves for local landslide prediction

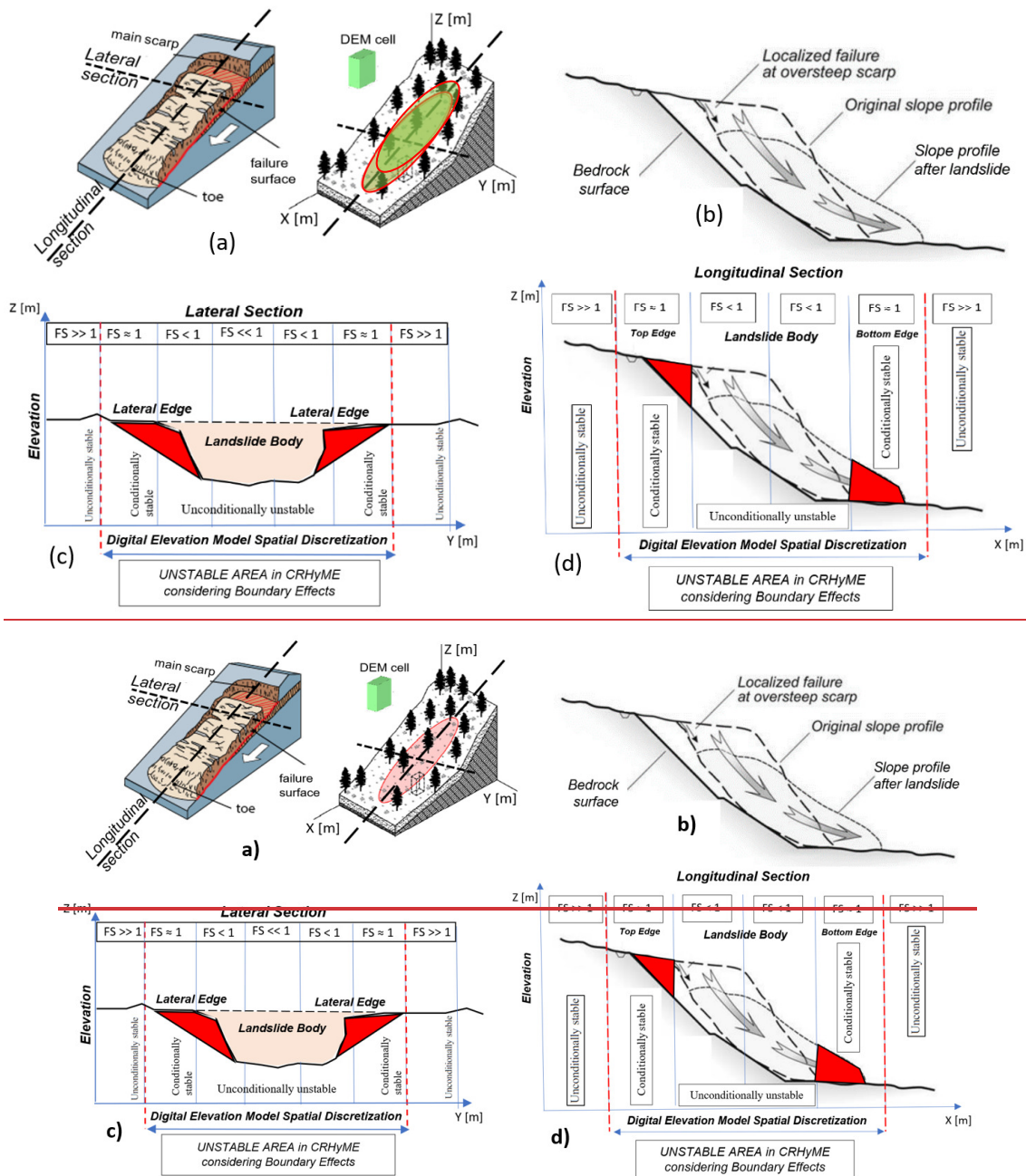
According to ~~several authors~~ (Formetta et al., (-2016), Pereira et al., (-2016), Vakhshoori and Zare, (-2018), Gudiyangada Nachappa et al., (-2019), Kadavi et al., (-2018) and Fawcett, (-2006), a useful technique to assess the ~~good~~ prediction performances of a slope stability models is the Receiver Operating Characteristic (ROC) methodology. ~~The ROC curve is a graphical plot that~~ illustrates the diagnostic ability of a binary classifier system as its discrimination threshold is varied. In landslide stability assessment, the binary classificatory is the condition of  $FS \gg 1$  (stable) or  $FS < 1$  (unstable) characterizing each pixel of the model domain (Formetta et al., 2016; Vakhshoori and Zare, 2018). ~~In CRHyME, model doesn't build a susceptibility map but it simply counts~~ the number of the landslide activations ~~is counted~~. ~~On each timestep, a 0-1 map is produced if the where the instability condition destabilized pixels (of  $FS < 1$ ) are signed as 1 is verified while stable pixels ( $FS \geq 1$ ) are signed with 0~~. This landslide-triggering algorithm is rather simple to be implemented inside a code and other authors have also followed this approach (Harp et al., 2006; Milledge et al., 2014; Formetta et al., 2016). However, ~~The spatial scale~~

610 where the activations are represented is the pixel dimension of the HydroSHED DEM. This resolution may be sufficient to spot a single shallow landslide activation but there are uncertainties on its real extension that could be in principle lower or greater than single pixel size.

~~in our opinion, the~~ inclusion of a “*pixel-~~buffer~~range*” in the surrender area of a detected unstable pixel (prone to shallow landslide failure) is necessary to describe ~~more more physically~~ the instability ~~of shallow landslide~~ activation. Generally speaking, landslide instability areas are not confined to the landslide body but could extend to surrounding boundaries; in the upper part, the landslide crown could experiment with further collapse since other cracks may generate and propagate retrogressively (Ivanov et al., 2020b); in the bottom part, the landslide may evolve into soil slip or earth flow and travel along the slope following the maximum gradient (Jakob and Hungr, 2005); the lateral boundaries could be also affected by landslide instability due to shear stress perturbation and reduced lateral roots cohesion (Rahardjo et al., 2014) that develops during landslide collapsing. Bearing in mind that a single-pixel slope failure evaluation may be ~~too reductive~~ not conservative from a hazard perspective, in CRHyME the unstable area related to the predicted unstable pixel has been extended considering also the surrounded ~~eight~~ adjacent cells, as reported in Figure 6.a.

~~A ousbecause italso DTM resolutionTo assure the reasonability of this choice, awithinFFI landslide inventory rainfall induced shave mean and median equal to 20'000 and 10'000 m<sup>2</sup> respectively, which correspond an indicative pixel size comprised between 150 100 m. DTM (sampled at the equator) becomes 70 m at the latitude of the tested case study due to geographical transformation (Lehner et al., 2008).Therefore, a approximation could bring equal to 7 40'000, slightly larger compared to inventory but within the same order of magnitude calculated from the IFFI inventory. However, the exact landslide geometry is not definable “a priori” since it has large variability in terms of extension and shape (areas span mostly 10<sup>3</sup> to 10<sup>6</sup> m<sup>2</sup> according to Tanyaş et al., 2019) which could be larger or narrower compared to DTM resolution (Figures 5.a and 5.c). Moreover, Oguz et al., 2022, Zheng et al., 2020, Legorreta Paulin et al., 2010, Michel et al., 2014 have shown how DTM resolution and its accuracy may significantly perturb the local stability at the top and bottom edges, extending or reducing the effective unstable slopes (Figures 5.b and 5.d). According to Legorreta Paulin et al., 2010 a higher DTM resolution could improve the unstable area description reducing size over/underestimation but it would increase sensibly the computational cost of the hydrological model (Zhang et al., 2016). These issues will be further discussed in section 4.4.~~

625  
630



635

640

Figure 5: Scale dependence in the infinite slope stability assessment. (a) geometrical sections (longitudinal and lateral) of shallow landslides, (b) landslide kinematics along the longitudinal section, (c) exemplification of the stable and unstable areas in the lateral section, (d) exemplification of the stable and unstable areas in the longitudinal section with respect to DEM resolution. In red are highlighted the lateral, top and bottom edges of the landslide affected by instabilities are highlighted.

645

A 9-pixel counting may overestimate in some cases the extension of the hazardous area because it is also dependent on the DEM resolution. To assure the reasonability of this choice, a survey conducted within the IFFI (Inventario Fenomeni Franosi Italiano) landslide inventory (ISPRA, 2018; Guadagno et al., 2003; Guzzetti and Tonelli, 2004) has shown that typical rainfall-induced shallow landslides have mean and median spatial extension equal to  $\sim 20'000 \text{ m}^2$  and  $\sim 10'000 \text{ m}^2$  respectively, which correspond an indicative pixel size comprised between 150 – 100 m. In our case, the 90 m DEM resolution (sampled at the equator) becomes  $\sim 70 \text{ m}$  at the latitude of the tested case study due to geographical transformation (Lehner et al., 2008). Therefore, a 9-pixel approximation could bring the overall landslide extension equal to  $(70 \cdot 3)^2 \sim 40'000 \text{ m}^2$ , slightly larger compared to the IFFI inventory range but within the same order of magnitude. However, the exact landslide geometry is not definable “a priori” since it has large variability in terms of extension and shape (areas span mostly  $10^3$  to  $10^6 \text{ m}^2$  according to Tanyaş et al (2019)) which could be larger or narrower compared to DEM resolution (Fig. 5.a and 5.c). Moreover, Oguz et al.

650

(2022), Zheng et al. (2020), Legorreta Paulin et al. (2010) and Michel et al. (2014) have shown how DEM resolution and its

accuracy may significantly perturb the local stability at the top and bottom edges, extending or reducing the effective unstable slopes (Fig. 5.b and 5.d). According to Legorreta Paulin et al. (2010) a higher DEM resolution could improve the unstable area description by reducing size over/underestimation but it would increase sensibly the computational cost of the hydrological model (Zhang et al., 2016). These topics will be further discussed in section 4.4.

Since the reference data on historical landslides in the IFFI inventory comes from several sources, the localization of the shallow instability could not be georeferenced-geo-localized with high precision, especially for historical events where sometimes only triggering point locations (not the landslide polygon) are reported (ISPRA, 2018). To carry out the ROC methodology and avoid reference data issues, a buffer zone with different radii around each landslide point was created: 250 m, 500 m, 1000 m and 2000 m (Fig. 6). This radius represents an attempt to cope with the uncertainties about the real position and extension of the triggered landslide.

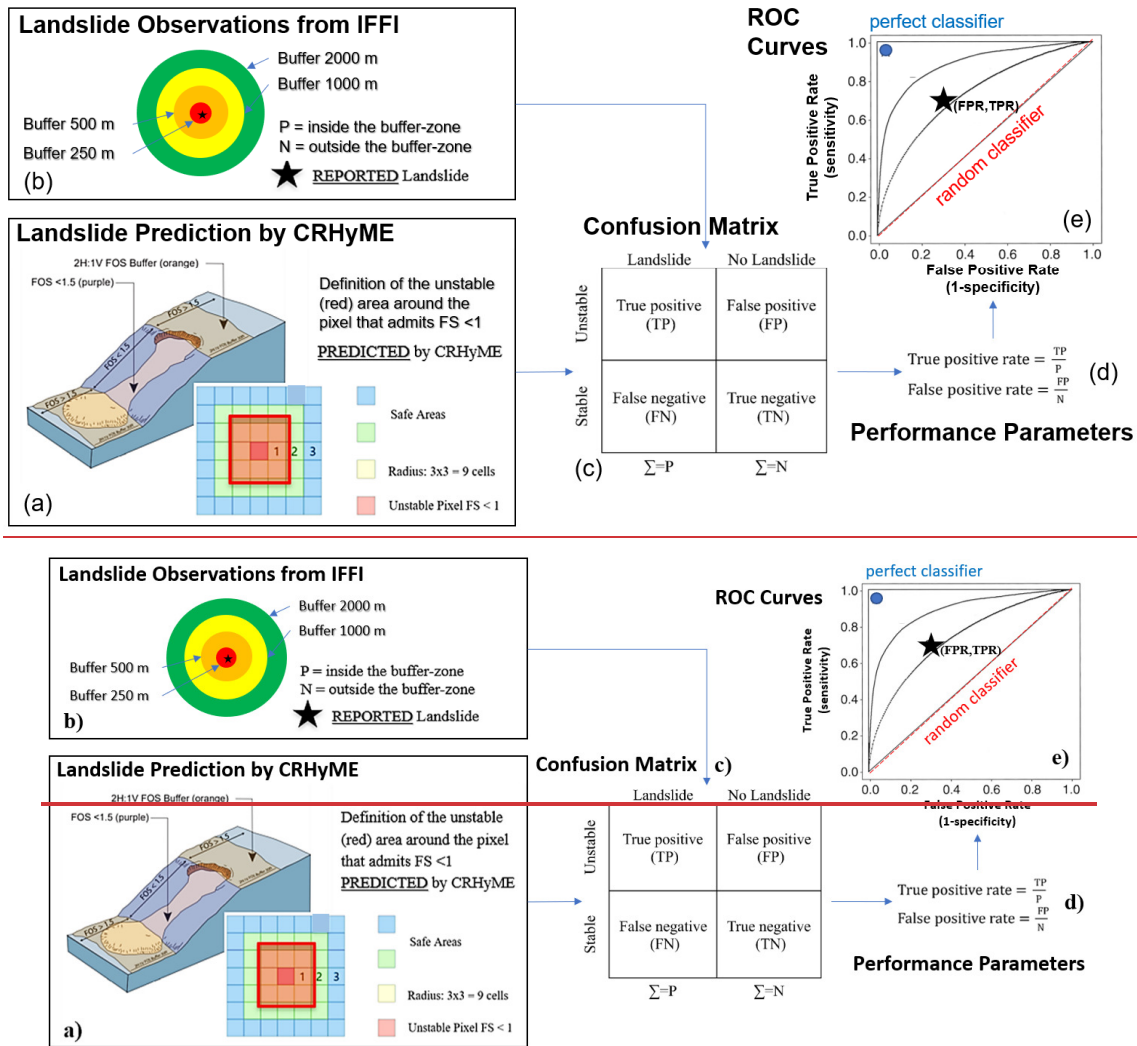


Figure 6: ROC methodology scheme to assess the CRHyME model performances in detecting landslide failures that occurred after a rainfall event. (a) unstable areas predicted by CRHyME considering the surrounded 8 cells, (b) unstable area reported in IFFI considering buffer-zones due to geo-localization uncertainties, (c) confusion matrix and parameters TP, FN, TN and FP calculation, (d) evaluation of performance parameters TPR and FPR for the graphical representation of the ROC curves (ed).

Knowing the observed and the predicted instabilities (retrieved by IFFI) and simulated by CRHyME referring to a specific geo-hydrological event, the ROC assessment was conducted. The ROC curves were built following the scheme presented in Fig. 6. Through a confusion matrix (Fig. 6.c), the False Positive Rate (1-specificity, FPR) Eq. (19) and the True Positive Rate (sensitivity, TPR) Eq. (20) are calculated (Fig. 6.d), and the point (FPR, TPR) is reported in the ROC graph (Fig. 6.e). The upper left corner of the graph (TPR = 1 and FPR = 0) represents the perfect performance (or perfect classifier), and

the diagonal line, represents the random classification or “no skill”. As the point (FPR, TPR), the prediction skill) plotted on the ROC graph is closer to the upper left, the prediction capacity of the CRHyME model is better.

$FPR = \frac{FP}{N} = \frac{FP}{FP + TN}$	(19)
$TPR = \frac{TP}{P} = \frac{TP}{TP + FN}$	(20)

## 2.4 2.4 Cases sStudied

The case ~~studies of study considered simulated for with~~ CRHyME ~~simulations are located in~~ are located in Northern Italy ~~and are here presented and presented in~~ (Figure 7.).

680

The Caldone basin (Figure Fig. 7.a) represents the on-field laboratory of the University of Politecnico di Milano (Brambilla et al., 2020). The basin is about 27 km<sup>2</sup> situated near the city of Lecco (Lombardy region) across the Pre-Alps and is characterized by intense sediment transport. The catchment is well monitored by 5 rain gauge stations, a hydrometer at the outlet and two sediment check-dams where the sediment yield is constantly monitored with periodic bathymetric surveys. The lithology of the area is constituted by consolidated calcareous rocks with good strength properties but rather susceptible to rainfall erosivity. Karst is present in the surrounding region but is not relevant in the Caldone catchment (Papini et al., 2017). From a climatic viewpoint, the area has a mean precipitation of 2000 mm yr<sup>-1</sup> (Rete Monitoraggio ARPA Lombardia).

685

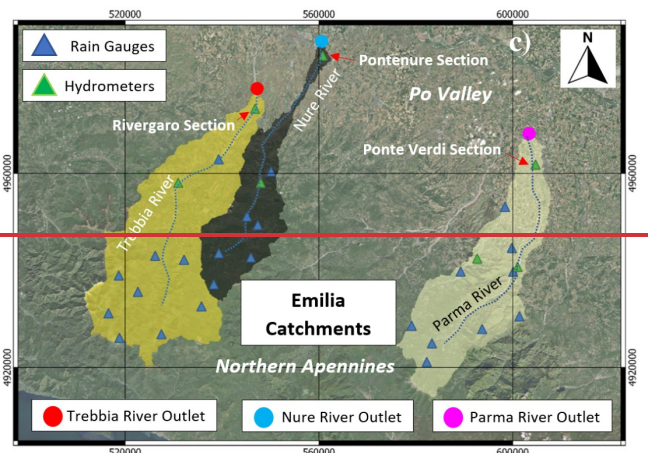
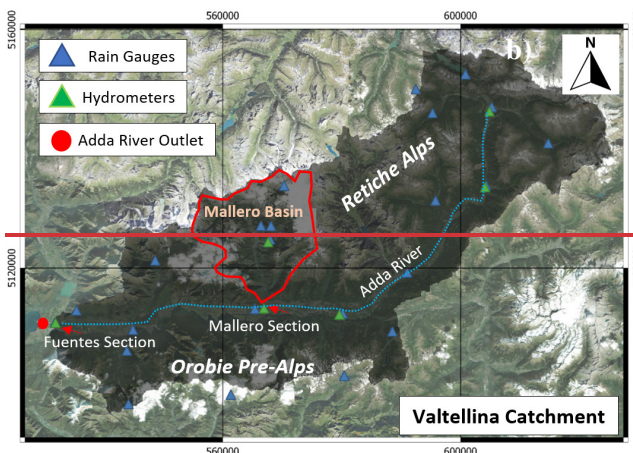
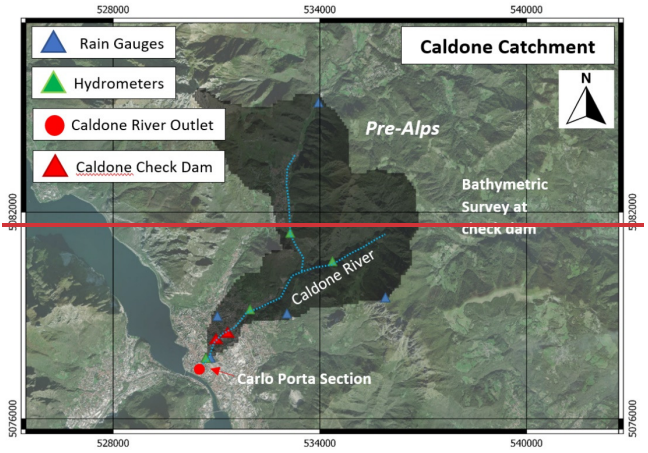
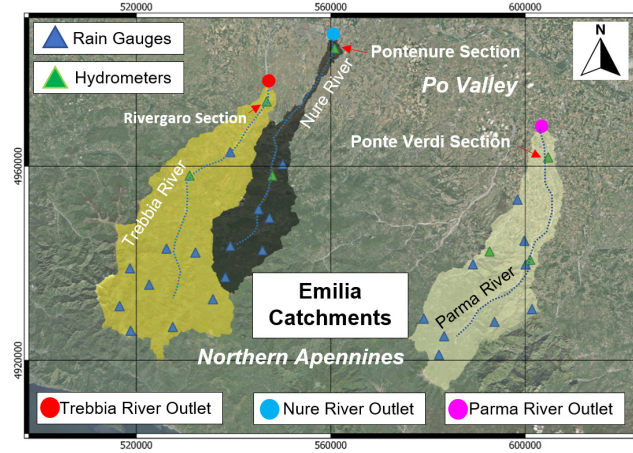
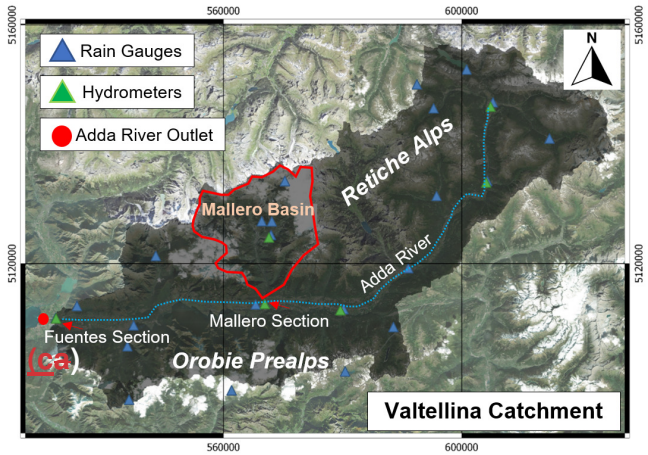
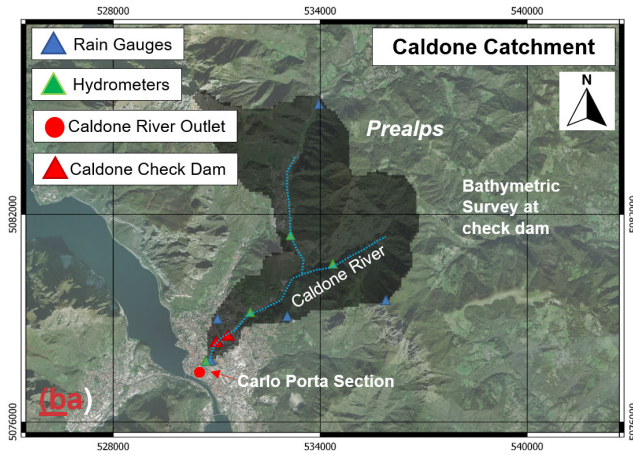
690

The Valtellina valley catchment (Figure Fig. 7.b) is settled in the northern part of the Lombardy region across the Central Alps and in 1987 experienced a dramatic geo-hydrological episode triggered by rather intense intense and prolonged rainfalls (Abbate et al., 2021a). The effects on the territory were severe: shallow landslides, debris flows, and flash floods were recorded causing human injuries and fatalities and extensive damage to infrastructure and buildings (Luino, 2005). The secondary branch of Mallerio River also experienced intense sediment transport during the 1987 flood, which affected Sondrio town. Similar events iteratively hit the area in November 2000 and 2002. The Valtellina valley has E-W topographical development, and its geomorphology is characterized by a strong difference between the opposite slopes. In the southern flank of the valley, the Orobic Pre-Alps are constituted by consolidated metamorphic rocks (Gneiss) while across the Retiche Alps (northern flank), magmatic and sedimentary rocks alternate with metamorphic. The most prevalent type of soil texture is formed by sandy loam and silty loam (Crosta and Frattini, 2003; Longoni et al., 2016). The valley catchment is characterized by a strong precipitation variability in the range of a minimum of 600 mm yr<sup>-1</sup> in the north-eastern part of the Retiche Alps and a maximum of 3500 mm yr<sup>-1</sup> in the south-western sector of the Orobic Pre-Alps (Rete Monitoraggio ARPA Lombardia). According to this, two different meteorological datasets were examined here to test the ability of CRHyME to deal with different rainfall datasets. The first one has considered the meteorological data provided by the Regional Agencies for Environmental Protection (ARPA Lombardia) (Rete Monitoraggio ARPA Lombardia) ground-based weather stations. The second one is MERIDA, the MEteorological Reanalysis Italian Dataset (Bonanno et al., 2019). MERIDA consists of a dynamical downscaling of the new European Centre for Medium-range Weather Forecasts (ECMWF) global reanalysis ERA5 using the Weather Research and Forecasting (WRF) model, which is configured to describe the typical weather conditions of Italy.

695

700

705



710

715 **Figure 7: The Caldone (a), the Valtellina (b) and the Emilia (c) catchments studied. Rain gauges, hydrometer stations and river outlets are indicated in (a), b), c). Hydrometric stations considered for assessing the CRHyME performances are located at Carlo Porta section (for the Caldone River), Fuentes and Mallero sections (for the Adda and the Mallero Rivers) in the Valtellina catchment, and Rivergaro (for Trebbia River), Pontenure (for Nure River) and Ponte Verdi (for Parma River) sections across the Emilia area. Base layer from © Google Maps 2023.**

720 The Emilia area is situated in the Northern Apennines (Figure Fig. 7.c) and experienced intense geo-hydrological episodes in October 2014 and September 2015 (Ciccarese et al., 2020). Three watersheds were particularly affected: the Trebbia, Nure and Parma catchments. The event of October 2014 mainly hit the Parma catchment while the event of September 2015 hit the Trebbia and Nure catchments. From a geomorphological viewpoint, the Northern Apennines represent a “fold-and-thrust” mountain chain where several landslide instabilities are present due to the post-failure weathering of claystone, sandstone, and limestone rock fragments. These deposits are in residual strength conditions and can be quite easily mobilised and trigger debris flows during heavy rain episodes (Parenti et al., 2023). The Emilia region is characterized by a rainfall distribution with a south-north gradient where a maximum amount of 2000 mm yr<sup>-1</sup> is recorded in the highest relief of the Apennines (south) while the 700 mm yr<sup>-1</sup> characterizes the floodplain areas of the Po Valley in the northern part (Rete Monitoraggio ARPA Emilia).

730 ~~During the CRHyME calibration and validation of the CRHyME model procedure, some~~ monitoring points for checking the water discharge and volume were chosen in correspondence with the reference hydrometers located at the catchment outlets (green triangles in Figures Fig. 7.a,b,c). ~~Check dams and h~~Hydropower reservoirs were considered for estimating reference sediment yield: a check dam close to the outlet for the Caldone catchment (red triangles in Figure Fig. 7.a), three hydropower reservoirs of Campo Tartano, Valgrosina and Cancano for the Valtellina case study (red triangles in Figure Fig. 10.a) and AdBPo reference data (Autorità di Bacino Distrettuale del Fiume Po, 2022) for the Emilia case study. Regarding ~~the~~ shallow landslides and debris flows ~~triggered during the investigated geo-hydrological events~~, a literature survey has been conducted within the IFFI inventory ~~and scientific literature~~ to find an available inventory of the ~~occurred~~ failures (Figures Fig. 11.a and 13.a) ~~that occurred during the past geo-hydrological events simulated.~~

### 3 Results

740 In the next paragraphs, the results obtained for the three case studies are presented in this way: description of the simulation settings, reporting of hydrological and sediment transport performances, and showing landslide and debris flow ROC assessment.

#### 3.1 Caldone case study

745 The Caldone catchment was investigated to verify the numerical conservativity of hydrological and sediment balances ~~conservativity of hydrological and sediment balance~~ calculated by CRHyME, to explore the sensitivity to the variation of spatial resolution of the input data (e.g. ~~DTMDEM~~) and to calibrate and validate the  $slope \rightarrow D_{50}$  empirical relations. According to Rocha et al. (2020) ~~and~~ Tavares da Costa et al. (2019), a spatially distributed hydrological model is sensitive to input data spatial resolution. The reconstruction of the catchment parameters, such as the flow accumulation and the flow direction, depends on the characteristics of the ~~DTMDEM~~. As a result, routing methods, which also depend on the flow direction accuracy, may experience differences in results under different cell resolutions. Moreover, increasing the ~~DTMDEM~~ resolution is ~~generally time-consuming~~ time-consuming due to the ~~large number~~ considerable number of cells within the computational domain. ~~To test these aspects in CRHyME, for the Caldone catchment were executed four runs~~ were executed in a short period of 6 months, considering four different ~~DTMDEM~~ resolutions: 90 m, 50 m, 20 m and 5 m. In Table 2 the simulation settings are resumed.



<u>Simulation Settings and Error Analysis</u>	<u>Simulation 1</u>	<u>Simulation 2</u>	<u>Simulation 3</u>	<u>Simulation 4</u>
<u>Spatial Resolution</u>	<u>90 m</u>	<u>50 m</u>	<u>20 m</u>	<u>5 m</u>
<u>Starting Date</u>	<u>01/06/2020</u>	<u>01/06/2020</u>	<u>01/06/2020</u>	<u>01/06/2020</u>
<u>Ending Date</u>	<u>10/10/2020</u>	<u>10/10/2020</u>	<u>10/10/2020</u>	<u>10/10/2020</u>
<u>Initial Soil Moisture</u>	<u>90%</u>	<u>90%</u>	<u>90%</u>	<u>90%</u>
<u>NSE (Volume) [-]</u>	<u>0.765</u>	<u>0.777</u>	<u>0.777</u>	<u>0.656</u>
<u>NSE (Discharge) [-]</u>	<u>0.341</u>	<u>0.650</u>	<u>-1.333</u>	<u>-2.610</u>
<u>RMSE (Discharge) [m<sup>3</sup> s<sup>-1</sup>]</u>	<u>1.605</u>	<u>0.699</u>	<u>1.804</u>	<u>2.244</u>

**Table 2: Settings adopted for the Caldone River simulations, and hydrological volume and discharge error metrics calculated at Carlo Porta hydrometric station, testing different DEM spatial resolutions.**

To initialize CRHyME, the meteorological data series were gathered from ARPA Lombardia agency (Rete Monitoraggio ARPA Lombardia) (Figure 6.a). The hydrometers data and the local stage discharge relation were retrieved from the Lecco municipality station located at Via Carlo Porta (Figure 7.a). The rain gauges was spatially interpolated using the IDW technique (Chow et al., 1988) with a temporal resolution of 1 day. As can be appreciated from Table 2, the model's ability into the reproduction of a realistic water discharge tends to degrade progressively using a higher resolution. Looking at NSE scores for the discharge, the best accordance with the reference is reached in correspondence of a 50 m resolution. RMSE for the discharge is lower for 50 m simulation. The model is conservative since the NSE for the volume is close to 0.8, verifying that almost all the precipitation volume has arrived at the outlet within the simulated period. The NSE for the volume is a parameter that is rather invariant with respect to the resolution while the NSE for the discharge is spatial scale dependent.

As can be appreciated from Table 2, the model's ability into the reproduction of a realistic water discharge tends to degrade progressively using a higher resolution. Looking at NSE scores for the discharge, the best accordance with the reference is reached with a 50 m resolution. RMSE for the discharge is lower for a 50 m simulation. The model is conservative since the NSE for the volume is close to 0.8, verifying that almost all the precipitation volume has arrived at the outlet within the simulated period. The NSE for the volume is a parameter that is rather invariant with respect to the resolution while the NSE for the discharge is spatial scale dependent. The meteorological data series necessary to run the model were gathered from the ARPA Lombardia agency (Rete Monitoraggio ARPA Lombardia) (Fig. 6.a). The hydrometers data and the local stage-discharge relation were retrieved from the Lecco municipality station located at Via Carlo Porta (Fig. 7.a). The rain gauges were spatially interpolated using the IDW technique (Chow et al., 1988) with a temporal resolution of 1 day.

The influence of the  $slope \rightarrow D_{50}$  curves parameterization was the second aspect investigated in the Caldone catchment. A long-term simulation has been carried out from 1 January 2019 up to 30 November 2021 (Figure 8.a), with the a DTMDDEM resolution of 50 m and after a "spin-up" period of 2 years for raising the model to realistic initial conditions. Considering the limited extension of the watershed, this period has revealed sufficient for assessing the performance of solid discharge. The sediment discharge was computed considering both TL (Transport Limited) and EL (Erosion Limited) options.

In Table 3 Figure 8.b can appreciate can be noticed that NSE for water discharge and volume exhibit a rather high score, about 0.462 and 0.719 respectively. The former states that the reproduction of the hydrological part has been assessed almost correctly by CRHyME. Four  $slope \rightarrow D_{50}$  functions have been tested in the form like  $D_{50} = a_x S slope^{b_x}$  (Table 43): set 1, set 2, set 3 and set 4. Results have shown that the choice of  $slope \rightarrow D_{50}$  can sensibly modify the outlet's sediment yield: the cumulated sediment amount increases with a decrease of in the mean diameter. These data were compared with the onsite bathymetric surveys that were carried out four times across during the investigated period (Table 5)4. From the bathymetry measurements, a sediment yield of about 1000 m<sup>3</sup> yr<sup>-1</sup> was considered representative of Caldone River. In our sensitivity analysis, this value has matched the reference using set 2: 2993 m<sup>3</sup> for 1055 days  $\approx$  3 yrs correspond to  $\approx$  1000 m<sup>3</sup> yr<sup>-1</sup>. Set

n° 2 is rather slightly higher than the functions considered for Valtellina and Emilia simulations ~~that are better represented by set n° 3.~~

Simulation Settings and Error Analysis	Simulation 1	Simulation 2	Simulation 3	Simulation 4
Spatial Resolution	90 m	50 m	20 m	5 m
Starting Date	01/05/2020	01/06/2020	01/06/2020	01/06/2020
Ending Date	10/10/2020	10/10/2020	10/10/2020	10/10/2020
Initial Soil Moisture	90%	90%	90%	90%
NSE (Volume)	0.765	0.777	0.777	0.656
NSE (Discharge)	0.341	0.650	-1.333	-2.610
RMSE (Discharge) [m <sup>3</sup> ·s <sup>-1</sup> ]	1.605	0.699	1.804	2.244

**Table 21: Setting properties adopted for the Caldone River simulations and hydrological indexes ranking of volume and discharge testing different spatial resolutions of the DTM.**

795

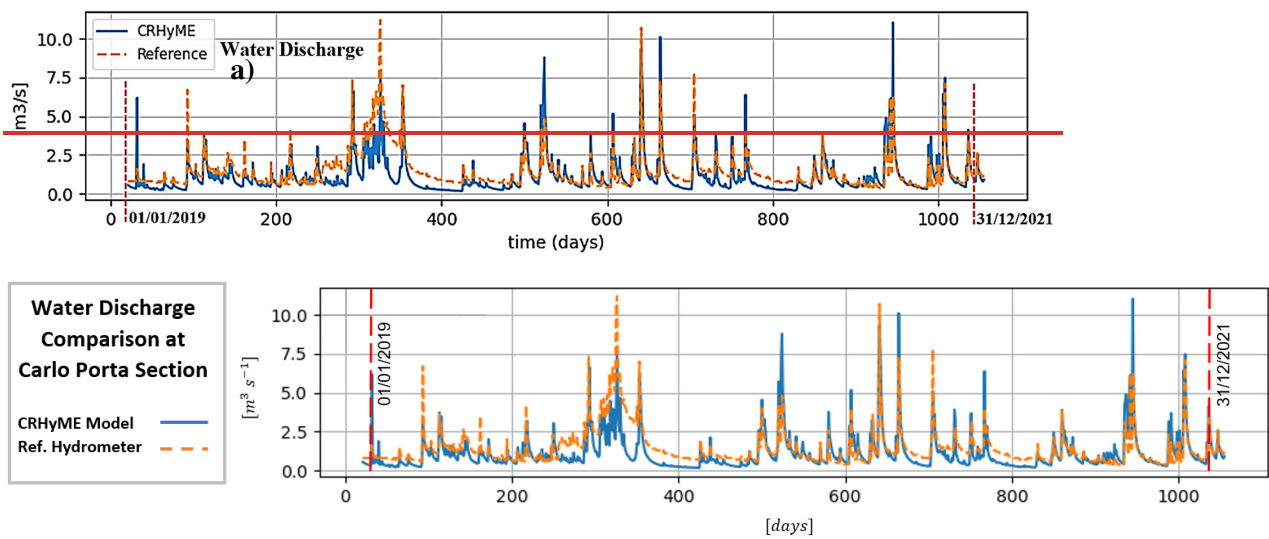
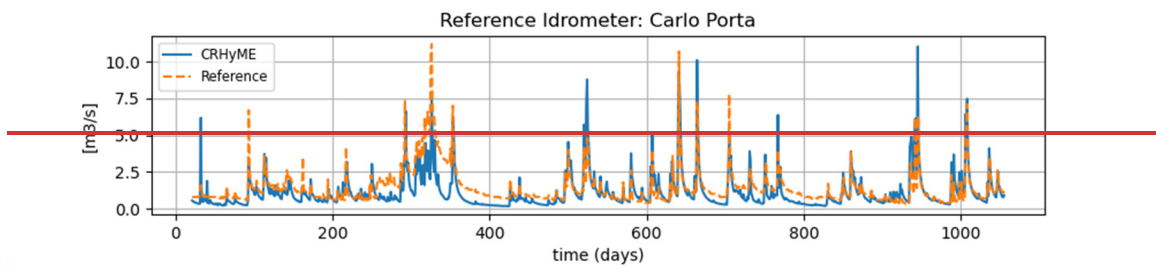


**Figure 8: Hydrological simulation carried out for sediment transport assessment in the Caldone catchment with 50 m DTMDEM resolution from 01/01/2019 up to 31/12/2021: a) simulated water discharge (blue line) vs. reference hydrometer at the Carlo Porta section (orange line), and b) hydrological indexes ranking of volume and discharge.**

800



b)	NSE (Discharge)	NSE (Volume)	RMSE (Discharge) [m <sup>3</sup> s <sup>-1</sup> ]
Error Analysis	0.462	0.719	0.900

805

**Figure 8: Hydrological simulation carried out for sediment transport assessment in the Caldone catchment with 50 m DTM resolution from 01/01/2019 up to 31/12/2021: a) simulated water discharge (blue line) vs. reference hydrometer at the Carlo Porta section (orange line) and b) hydrological indexes ranking of volume and discharge.**

**Table 3: NSE and RMSE error metrics of the previous hydrological simulation for the volume and discharge quantities.**

Curve Set	$a_x$ parameter	$b_x$ parameter	Slope $\rightarrow D_{50}$ Equations	Total Sediment Volume [m <sup>3</sup> ]
Set 1	5604.8	2.38	$D_{50} = 5604.8 \cdot slope^{2.38}$	2608
Set 2	1786.9	1.79	$D_{50} = 1786.9 \cdot slope^{1.79}$	2993
Set 3	1453.1	1.61	$D_{50} = 1453.1 \cdot slope^{1.61}$	5947
Set 4	285.3	0.8	$D_{50} = 285.3 \cdot slope^{0.80}$	16446

810 **Table 342:** Slope  $\rightarrow D_{50}$  functions tested in the Caldane catchment, and the volume of the total sediment simulated by CRHyME at the basin outlet.

815

Bathymetry survey	Total Sediment Volume [m <sup>3</sup> ]
20 July 2019 - 20 July 2020	$\approx 294 \pm 100$
20 July 2020 - 13 October 2020	$\approx 438 \pm 100$
13 October 2020 - 15 November 2021	$\approx 800 \pm 100$
<u>Estimated Sediment Yield [m<sup>3</sup> yr<sup>-1</sup>]</u>	<u><math>1532 / 2.32 = 660</math></u>

**Table 453:** Bathymetric survey and total volume stored at the check dam close to the Caldane catchment outlet. An average sediment yield was calculated around 660 m<sup>3</sup> yr<sup>-1</sup>. Due to possible measurement uncertainties and relatively short time series, a representative sediment yield value of 1000 m<sup>3</sup> yr<sup>-1</sup> was considered in the simulations.

### 820 3.4.2 Valtellina Case Study

The analysis conducted for the Valtellina area has followed the setting steps reported in Table 265. The CRHyME calibration was carried out for three years between 1 September 2015 and 31 August 2018 after a “spin-up” period of 2 years for acquiring realistic initial conditions. Then, a subsequent validation period started on 1 September 2018 up to 31 December 2019. In Fig. 9 the water discharges and the total volumes computed by CRHyME in the two reference sections of Fuentes (basin area = 2600 km<sup>2</sup>) and Mallero (basin area = 320 km<sup>2</sup>) are reported.

825

Simulation settings of Valtellina case study. The first calibration and validation of the model have considered more than 4 years of data on daily basis gathered from ARPA (Environmental Agency) (Rete Monitoraggio ARPA Lombardia) weather stations and the MERIDA reanalysis database (Bonanno et al., 2019). These event based simulations were carried out for significant geo-hydrological events of July 1987, November 2000 and November 2002.

830

Settings for <u>Valtellina catchment</u>	Geo-Hydrological Event Simulated	Starting Date	Ending Date	Rainfall Dataset used
Calibration	-	01/09/2015	31/08/2018	ARPA Lombardia and MERIDA
Validation	October 2018	01/09/2018	31/12/2019	ARPA Lombardia and MERIDA
Validation	July 1987	01/09/1984	31/07/1987	ARPA Lombardia
Validation	November 2000	01/09/1997	30/11/2000	ARPA Lombardia
Validation	November 2002	01/12/2000	31/12/2002	ARPA Lombardia

**Table 56:** Simulation settings of the Valtellina case study. The calibration and validation of the model have considered more than 4 years of data on a daily basis gathered from ARPA Lombardia (Environmental Agency) weather stations and the MERIDA reanalysis database (Bonanno et al., 2019). These event-based simulations were carried out for significant geo-hydrological events of July 1987, November 2000, November 2002 and October 2018. ~~Table 2: Simulation settings of Valtellina case study. The first calibration and validation of the model have considered more than 4 years of data on daily basis gathered from ARPA (Environmental Agency) (Rete Monitoraggio ARPA Lombardia) weather stations and the MERIDA reanalysis database (Bonanno et al., 2019). These event based simulations were carried out for significant geo-hydrological events of July 1987, November 2000 and November 2002.~~

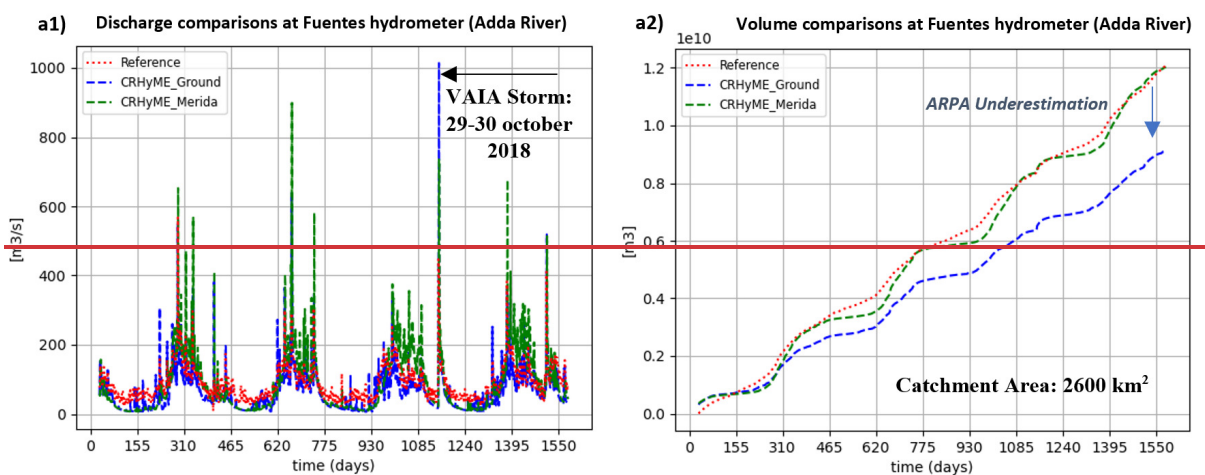
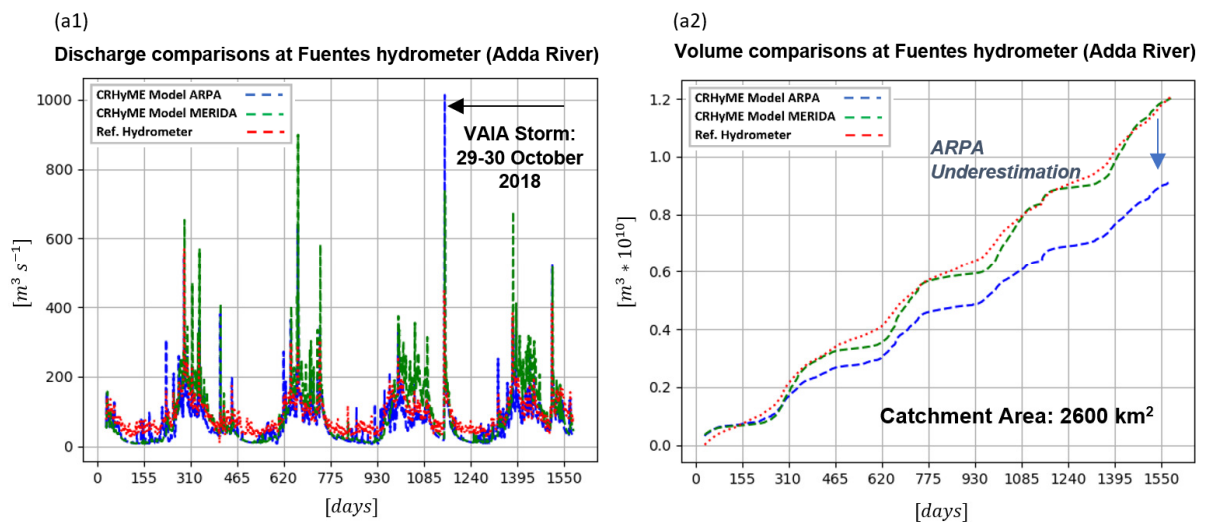
835

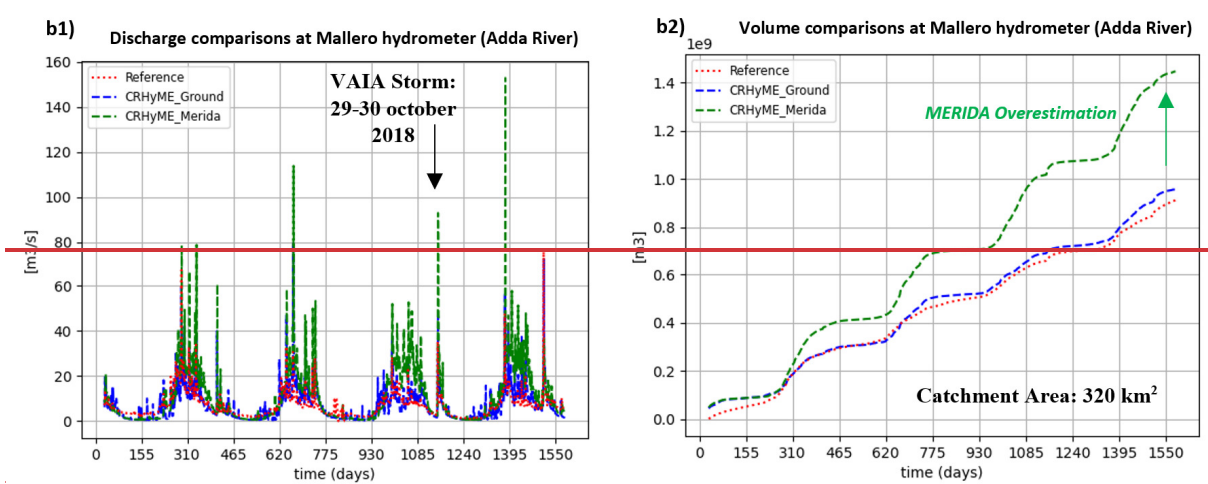
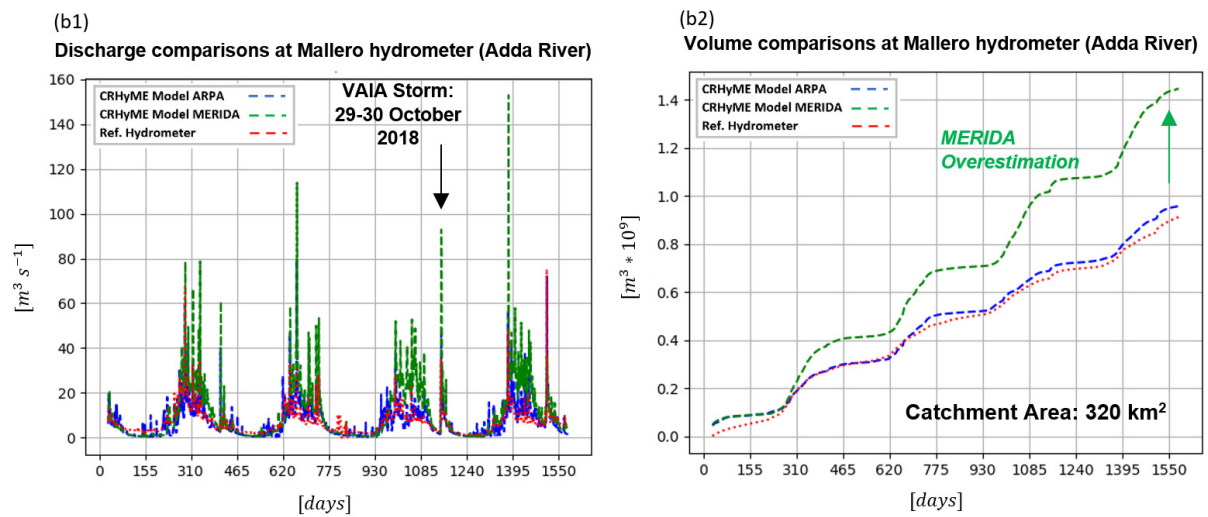
840 Looking at the simulation driven by the ARPA dataset, the total volume transited at the Fuentes section (blue line, Fig. 9.a) is underestimated if compared to the local hydrometric reference (line red), while at the Mallero section (blue line, Fig. 9.b) simulated and recorded volumes are in agreement. NSE scores for volumes also highlight this fact since Mallero's NSE is  $\sim 1$  while Fuentes's NSE is about 0.783 (Table 7). Transited volume is the integral of water discharge that has been better reproduced for the Mallero section (agreement among the blue and red line in Fig. 9.b and NSE = 0.325 in Table 7) rather than Fuentes's section (disagreement among the blue and red line with underestimation of the mean flow during winter periods in Fig. 9.b and NSE = 0.199 in Table 7) by the model.

845 Opposite results were obtained considering MERIDA's dataset. There, the Fuentes section has performed well both in discharge and volume computation rather than the Mallero section. The volume NSE at Fuentes is now closer to the perfect agreement while at Mallero station the transited volume is sensibly overestimated. In both cases, NSE scores for discharges are badly represented with values below the '0' threshold. This fact is also well depicted in Fig. 9.a and 9.b where discharge spikes simulated from the ARPA dataset (blue line) are lower compared to the green ones simulated from the MERIDA dataset. The CRHyME model performed numerically conservatively in both cases without code instabilities so that these outcomes are supposed to be perturbed by the different reconstructions of rainfall fields. From these results can be noticed how the influence of rainfall data is determinant in the hydrological assessment. Looking at RMSE scores in Table 7, the simulation with the

850 are badly represented with values below the '0' threshold. This fact is also well depicted in Fig. 9.a and 9.b where discharge spikes simulated from the ARPA dataset (blue line) are lower compared to the green ones simulated from the MERIDA dataset. The CRHyME model performed numerically conservatively in both cases without code instabilities so that these outcomes are supposed to be perturbed by the different reconstructions of rainfall fields. From these results can be noticed how the influence of rainfall data is determinant in the hydrological assessment. Looking at RMSE scores in Table 7, the simulation with the

855 ARPA dataset was better performed giving lower values of the index, around  $4.7 \text{ m}^3 \text{ s}^{-1}$  and  $45.4 \text{ m}^3 \text{ s}^{-1}$  for the Mallero and Fuentes sections respectively. This means that discharge uncertainties propagate proportionally increasing the catchment extension and CRHyME's performances are sensibly higher for small catchments.





Error Analysis of Hydrological Variables	NSE [-]	RMSE [mm]	NSE_MERIDA [-]	RMSE_MERIDA [mm]
Discharge Fuentes (Adda River)	0.199	45.370	-0.603	64.172
Volume Fuentes (Adda River)	0.783	$1.587 \cdot 10^9$	0.993	$2.931 \cdot 10^8$
Discharge Mallero (Adda River)	0.325	4.695	-2.369	10.494
Volume Mallero (Adda River)	0.988	$2.852 \cdot 10^7$	-0.145	$2.736 \cdot 10^8$

865 **Figure 9:** CRHyME model simulation results of water discharges (a1 and b1) and volume (a2 and b2) at the Fuentes (a), and the Mallero (b) hydrometers for the period 2015-2019 and using ARPA weather stations and MERIDA dataset. **As can be appreciated, the Volume performances are better than Discharge performances: the Valtellina basin is strongly regulated by hydropower plants and dams that operate a consistent lamination of the peak discharge during major rainfall events; the kinematic routing may be not sufficiently accurate for flood propagation across the valley floodplain since dynamic lamination may occur. As a result, green and blue spikes overestimate the peak discharge compared to the reference.** The geo-hydrological event that occurred in late October 2018 (The Vaia Storm (Davolio et al., 2020)) has been recognized by CRHyME as one of the most intense, especially at the Fuentes section.

Error Analysis of Hydrological Variables	NSE [-]	RMSE [ $m^3 s^{-1}$ ]	NSE_MERIDA [-]	RMSE_MERIDA [ $m^3 s^{-1}$ ]
Discharge Fuentes (Adda River)	0.199	45.370	-0.603	64.172
Volume Fuentes (Adda River)	0.783	=	0.993	=
Discharge Mallero (Adda River)	0.325	4.695	-2.369	10.494
Volume Mallero (Adda River)	0.988	=	-0.145	=

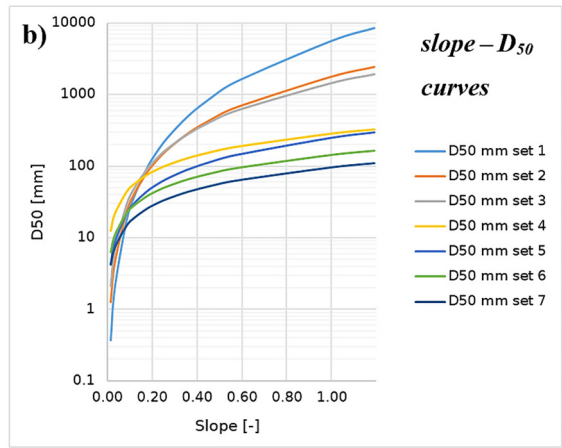
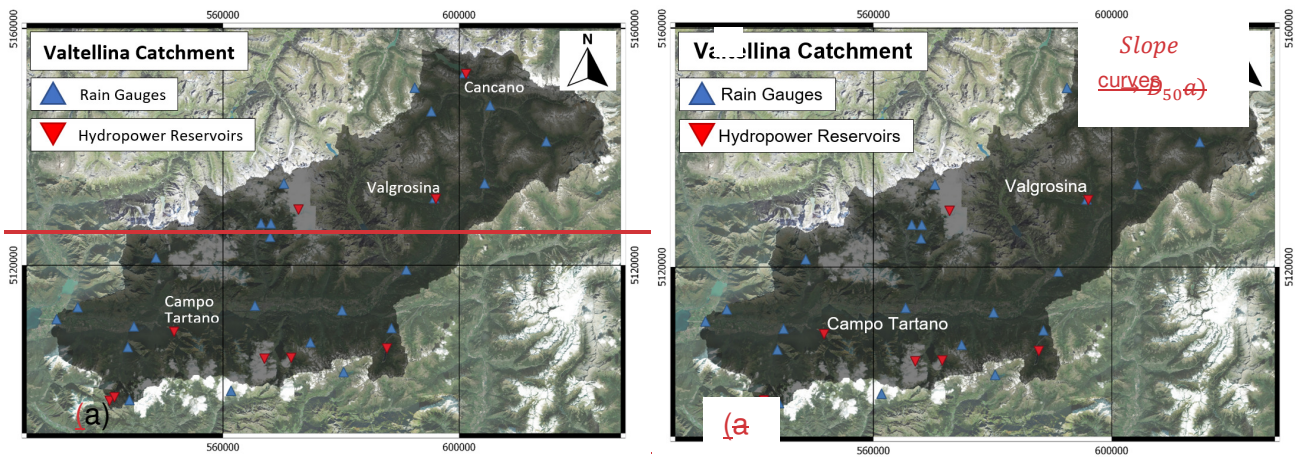
875

**Table 7: NSE and RMSE error metrics of the previous hydrological simulation for the volume and discharge quantities. As can be appreciated, the volume performances are better than the discharge: the Valtellina basin is strongly regulated by hydropower plants and dams that operate a consistent lamination of the peak discharge during major rainfall events; the kinematic routing may be not sufficiently accurate for flood propagation across the valley floodplain since dynamic lamination may occur. As a result, green and blue spikes overestimate the peak discharge compared to the reference.**

880

Sediment transport results were checked in correspondence with three hydropower reservoirs of Campo Tartano, Valgrosina and Cancano (Fig. 10.a) considering ARPA dataset simulations. For each reservoir, a literature survey has been conducted to estimate the yearly mean sediment accumulation rate (Ballio et al., 2010; Milanesi et al., 2015; ITCOLD, 2016). The sensitivity parameter for sediment yield is represented by the  $slope \rightarrow D_{50}$  curve that was adjusted during the calibration period (Fig. 10.b and 10.c). Among others, the set n°6 was retained sufficiently representative of the Valtellina area. In Table 9 the results obtained from CRHyME simulations show that the sediment yields evaluated yearly have matched the reference data for the three reservoirs investigated. For the Campo Tartano dam, the difference between the simulated and the reference is around -11.7%, for the Valgrosina dam is about +2.15% while for the Cancano reservoir is around -11.9%.

885



(c)

<u>Curve Set</u>	<u><math>a_x</math> parameter</u>	<u><math>b_x</math> parameter</u>	<u>Slope <math>\rightarrow D_{50}</math> Equations</u> $D_{50} = a_x \text{ slope}^{b_x}$	<u>Literature Reference and Curve Calibration</u>
<u>Set 1</u>	<u>5604.8</u>	<u>2.38</u>	$D_{50} = 5604.8 \text{ slope}^{2.38}$	<u>From Berg (1995), <math>b_x = 2.38</math></u>
<u>Set 2 (Caldone)</u>	<u>1786.9</u>	<u>1.79</u>	$D_{50} = 1786.9 \text{ slope}^{1.79}$	<u>Decreasing <math>a_x</math> and <math>b_x</math></u>
<u>Set 3</u>	<u>1453.1</u>	<u>1.61</u>	$D_{50} = 1453.1 \text{ slope}^{1.61}$	<u>Decreasing <math>a_x</math> and <math>b_x</math></u>
<u>Set 4</u>	<u>285.3</u>	<u>0.8</u>	$D_{50} = 285.3 \text{ slope}^{0.80}$	<u>Decreasing <math>a_x</math></u>
<u>Set 5</u>	<u>246.7</u>	<u>0.8</u>	$D_{50} = 246.7 \text{ slope}^{0.80}$	<u>Decreasing <math>a_x</math></u>
<u>Set 6 (Valtellina-Emilia)</u>	<u>142.6</u>	<u>0.8</u>	$D_{50} = 142.6 \text{ slope}^{0.80}$	<u>From Nino (2002), <math>b_x = 0.8</math></u>

	<u>Set 7</u>	<u>95.1</u>	<u>0.8</u>	$D_{50} = 95.1 \text{ Slope}^{0.80}$	<u>Decreasing <math>a_x</math></u>
(c)	<u>Curve Set</u>	<u><math>a_x</math> parameter</u>	<u><math>b_x</math> parameter</u>	<u>Slope <math>\rightarrow D_{50}</math> Equations</u>	<u>Literature Reference and Curve-Calibration</u>
	<u>Set 1</u>	<u>5604.8</u>	<u>2.38</u>	$D_{50} = 5604.8 \text{ Slope}^{2.38}$	<u>From (Berg, 1995), <math>b_x = 2.38</math></u>
	<u>Set 2</u>	<u>1786.9</u>	<u>1.79</u>	$D_{50} = 1786.9 \text{ Slope}^{1.79}$	<u>Decreasing <math>a_x</math> and <math>b_x</math></u>
	<u>Set 3</u>	<u>1453.1</u>	<u>1.61</u>	$D_{50} = 1453.1 \text{ Slope}^{1.61}$	<u>Decreasing <math>a_x</math> and <math>b_x</math></u>
	<u>Set 4</u>	<u>285.3</u>	<u>0.8</u>	$D_{50} = 285.3 \text{ Slope}^{0.80}$	<u>Decreasing <math>a_x</math></u>
	<u>Set 5</u>	<u>246.7</u>	<u>0.8</u>	$D_{50} = 246.7 \text{ Slope}^{0.80}$	<u>Decreasing <math>a_x</math></u>
	<u>Set 6</u>	<u>142.6</u>	<u>0.8</u>	$D_{50} = 142.6 \text{ Slope}^{0.80}$	<u>From (Nino, 2002), <math>b_x = 0.8</math></u>
	<u>Set 7</u>	<u>95.1</u>	<u>0.8</u>	$D_{50} = 95.1 \text{ Slope}^{0.80}$	<u>Decreasing <math>a_x</math></u>

d)	<u>Sediment Yield Error Analysis</u>	<u>Campo Tartano Dam</u>	<u>Valgrosina Dam</u>	<u>Cancano Dam</u>
	<u>Literature Reference</u>	<u>38'037 m<sup>3</sup>/yr</u>	<u>33'600 m<sup>3</sup>/yr</u>	<u>21'450 m<sup>3</sup>/yr</u>
	<u>Simulated 2015-2019</u>	<u>33'604 m<sup>3</sup>/yr</u>	<u>34'324 m<sup>3</sup>/yr</u>	<u>18'893 m<sup>3</sup>/yr</u>
	<u>% difference</u>	<u>-11.7 %</u>	<u>+2.15 %</u>	<u>-11.9 %</u>

890 **Figure 10:** (a) Valtellina case study area where hydropower reservoirs of Campo Tartano, Valgrosina and Cancano are indicated; (b) and (c)  $Slope \rightarrow D_{50}$  relations tested and implemented in CRHyME based on the theory of (Berg, (1995) and; Nino, (2002) and considering on-site surveys; (d) Sediment yield estimations for the three dams of Campo Tartano, Valgrosina and Cancano where can be noticed the correct estimation with respect to the ITCOLD reference (ITCOLD, 2009, 2016). Base layer from © Google Maps 2023.

895

<u>Sediment Yield Error Analysis</u>	<u>Campo Tartano Dam</u>	<u>Valgrosina Dam</u>	<u>Cancano Dam</u>
<u>Literature Reference</u>	<u>38'037 m<sup>3</sup> yr<sup>-1</sup></u>	<u>33'600 m<sup>3</sup> yr<sup>-1</sup></u>	<u>21'450 m<sup>3</sup> yr<sup>-1</sup></u>
<u>Simulated 2015-2019</u>	<u>33'604 m<sup>3</sup> yr<sup>-1</sup></u>	<u>34'324 m<sup>3</sup> yr<sup>-1</sup></u>	<u>18'893 m<sup>3</sup> yr<sup>-1</sup></u>
<u>% difference</u>	<u>-11.7 %</u>	<u>+2.15 %</u>	<u>-11.9 %</u>

**Table 9:** (d) Sediment yield estimations for the three dams of Campo Tartano, Valgrosina and Cancano where can be noticed the correct estimation with respect compared to the ITCOLD reference (ITCOLD, 2009, 2016).

900 Looking at the simulation driven by the ARPA dataset, the total volume transited at the Fuentes section (blue line, Figure 9.a) is underestimated if compared to the local hydrometer reference (line red), while at the Mallero section (blue line, Figure 9.b) simulated and recorded volumes are in agreement. Also, NSE scores for volumes highlight this fact since Mallero's NSE is -1 while Fuentes's NSE is about 0.783. Transited volume is the integral of water discharge that CRHyME has better reproduced for the Mallero section (agreement among blu and red line in Figure 9.b and NSE = 0.325) rather than Fuentes's section (disagreement among blu and red line with underestimation of the mean flow during minter periods in Figure 9.b and NSE = 0.199). Opposite results were obtained considering MERIDA's dataset. There, the Fuentes section has performed well both in discharge and volume computation rather than the Mallero section. The volume NSE at Fuentes is now closer to the perfect agreement while at Mallero station the transited volume is strongly overestimated. In both cases, NSE scores for discharges are badly represented with values below the '0' threshold. This fact is also well depicted in Figures 9.a and 9.b where discharge spikes simulated from the ARPA dataset (blue line) are lower compared to the green ones simulated from the MERIDA dataset. The CRHyME model performed numerically conservatively in both cases without code instabilities so that these outcomes are supposed to be perturbed by the different reconstructions of rainfall fields. From these results can be noticed how the influence of rainfall data is determinant in the hydrological assessment. Looking at RMSE scores, the simulation with the ARPA dataset was better performed giving lower values of the index, around 4.7 mm and 45.4 mm for the Mallero and Fuentes sections respectively. This means that discharge uncertainties propagate proportionally increasing the extension of the catchment and CRHyME's performances are sensibly higher for small catchments.

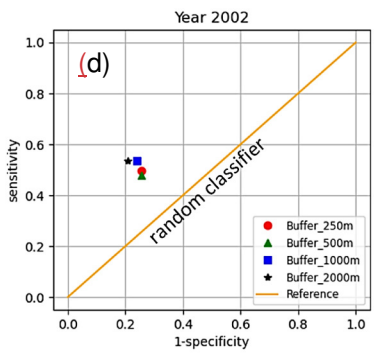
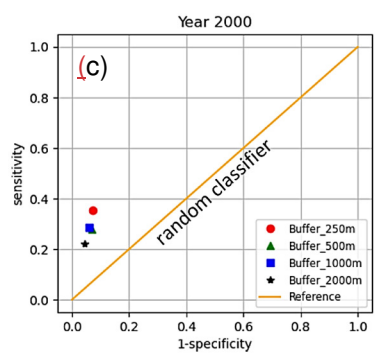
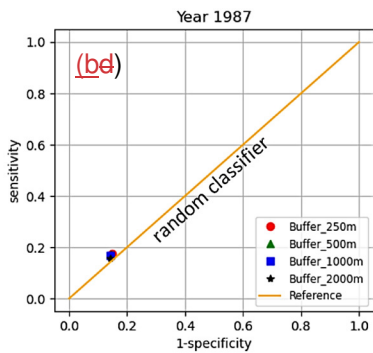
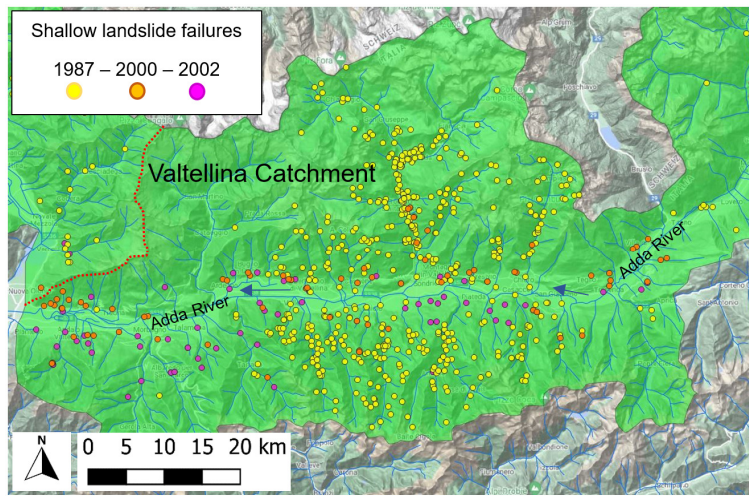
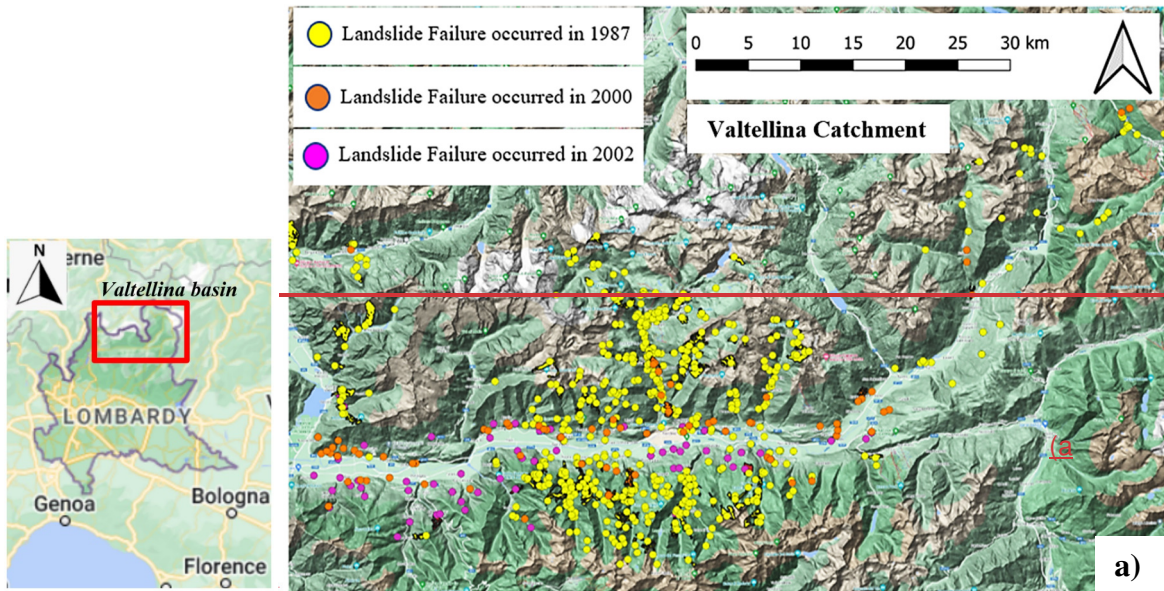
915

Results were checked in correspondence with three hydropower reservoirs of Campo Tartano, Valgrosina and Caneano (Figure 10.a) considering ARPA dataset simulations. For each reservoir, a literature survey has been conducted to estimate the yearly mean sediment accumulation (Ballio et al., 2010; Milanesi et al., 2015; ITCOLD, 2016).

920 The sensitivity parameter for sediment yield is represented by the  $slope \rightarrow D_{50}$  curve that was adjusted during the calibration period (Figure 10.b and 10.c). Since it doesn't exist a close formulation for indirectly estimating the granulometry in absence of a field survey dataset different functions have been proposed taking into account literature surveys and approaches proposed by (Nino, 2002; Sambrook Smith and Ferguson, 1995; Lamb and Venditti, 2016; Berg, 1995). Several Slope  $\rightarrow D_{50}$  relations were retrieved from the studies and obtained varying the parameters of the curves. These relations mimic the functions  
925 proposed by (Berg, 1995) where the  $D_{50}$  is determined as a function of the river morphology evolution, varying the two power-law coefficients. Among others, the set n°6 was retained sufficiently representative for the Valtellina area. In Figure 10.d the results obtained from CRHyME simulations are reassumed where the sediment yields evaluated yearly have matched the reference data for the three reservoirs investigated. For the Campo Tartano dam, the difference between the simulated and the reference is around -11.7%, for the Valgrosina dam is about +2.15% while for the Caneano reservoir is around -11.9%.

930 The capacity of CRHyME to predict the localization of shallow landslides triggered during the events of 1987, 2000 and 2002 events was investigated through the ROC scores. Figures 11.b, 11.c and 11.d describe the ROC assessment for the shallow landslides that occurred across the Valtellina valley during the July 1987, November 2000 and November 2002 events. To compare the four shallow landslide instability models included in CRHyME (Iverson, Harp, Milledge, and SLIP) has been carried out were compared, ranking the Harp model as the most accurate one (Fig. 11e, 11.f and 11.g) and with stable  
935 performances. A realistic combination of friction angle values has been considered among the broader ranges available in the literature (Abbate and Mancusi, 2021a) for the area:  $40^\circ$  for gravels,  $35^\circ$  for sand,  $33^\circ$  for silt and  $30^\circ$  for clay similar to those proposed by (Crosta and Frattini, 2003). In analogy with root cohesion, to obtain a spatial distribution of the friction angle was spatially distributed, this combination has been weighted by considering the fraction of soil composition (%coarse, %sand, %silt, %clay); within the superficial layers retrieved directly (Hengl et al., 2017) from available soil data. Using the  
940 Harp model and considering different buffer extensions of 250 m, 500 m, 1000 m and 2000 m. Among others, the Harp model has performed best with respect to the others, followed in the order by Milledge, Iverson and SLIP models. In Figure 11 are reported the results obtained by Harp model varying the buffer extension around the census landslide point. For the three events ease, the ROC curves have assessed a model CRHyME's performance above the "random classifier" threshold line. The sensitivity (True Positive Rate) of the model is comprised between 0.2 and 0.6 while the 1-specificity (False Positive Rate) is around 0.2. The distorted distribution of the shallow landslide inventory related to 1987 may have influenced the performance predictions, lowering the ROC assessment compared to the events that happened in 2000 and 2002 events. The buffer's choice of the buffer extension can influence the redistribution among TP and FP: and generally, the performance may tend to be slightly lower when large buffers are considered, especially for 1000 m and 2000 m radii, while tends to increase with. On the other hand, the radius of 250 m and 500 m are closest to the actual extension of shallow landslide  
950 movements recorded.

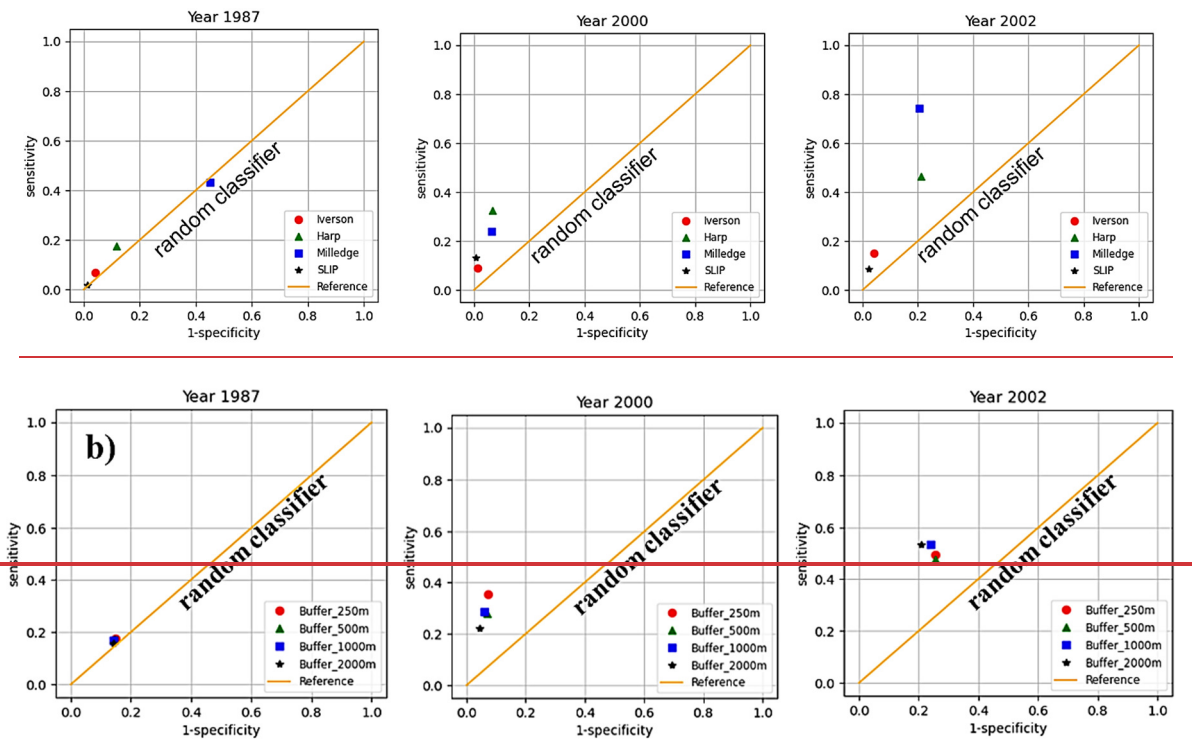




(ee)

(fe)

(ge)



955

Figure 11: (a) Triggered shallow landslides during the events of July 1987 (yellow points), November 2000 (orange points) and November 2002 (fuchsia points) across the Valtellina area reported by the IFFI inventory across the Valtellina area; (b, c, d) Representation of the ROC curves for 1987, 2000 and 2002 events considering the model-Harp model with different landslide position's buffers of 250 m, 500 m, 1000 m and 2000 m; (d, e, f) Representation of the ROC curves for 1987, 2000 and 2002 events considering a buffer of 250 m and comparing the four stability models. The Milledge model behaved best for the 2002 event but was the worst for 1987, while the Harps model showed the most stable performances. -Base layer from © Google Maps 2023. For the examined case studies, the model has shown a good ability to correctly individuate the location of the triggered landslide.

960

In every case, the ROC curves have assessed a model performance above the “random classifier” threshold line. The sensitivity (True Positive Rate) of the model is generally comprised of between 0.2 and 0.6 while the 1-specificity (False Positive Rate) is around 0.2. The distorted distribution of the shallow landslide census related to 1987 may have influenced the performance predictions, lowering the ROC assessment with respect to 2000 and 2002 events. The choice of the buffer extension can influence the redistribution among TP and FP and generally, the performance may tend to lower when large buffers are considered, especially for 1000 m and 2000 m radii. On the other hand, the radius of 250 m and 500 m are closest to the actual extension of shallow landslide movements. For the examined case studies, the model has shown a good ability to correctly individuate the location of the triggered landslide.

965

970

### 3.1.3 Emilia Case Study

For the Emilia case study, CRHyME was tested following a similar schedule for Valtellina area. Simulations were carried out considering a period of 5 years from 01/09/2011 up to 31/01/2016 where the investigated geo-hydrological events of 13/10/2014 and 14/09/2015 have been recorded in the area (Table 3.106). To raise the model to a realistic initial condition, a spin-up period of 900 days comprised between 01/09/2011 and 28/02/2014 have has been considered carried out. ARPA Emilia meteorological dataset (Rete Monitoraggio ARPA Emilia) was considered for rainfall and temperature variables.

975

Settings for Emilia's catchments	Geo-Hydrological Event Simulated	Starting/Ending Date for the Spin-Up Period		Starting/Ending Date for Validation Period	Rainfall and Temperature Dataset
River Trebbia	September 2015	01/09/2011	28/02/2014	31/01/2015-2016	ARPA Emilia

<u>River</u> Nure	September 2015	01/09/2011	28/02/2014	<u>01/09/2016</u> <del>31/12/2015</del>	ARPA Emilia
<u>River</u> Parma	October 2014	01/09/2011	28/02/2014	<u>01/09/2015</u> <del>31/12/2015</del>	ARPA Emilia

**Table 610: Simulation settings of the Emilia case study considering the ARPA Emilia (Environmental Agency) rainfall and temperature data.** **Table 5: Simulation settings of Emilia case study considering the ARPA Emilia (Rete Monitoraggio ARPA Emilia)**

up to the similar in Figure 12.a rivers F, NSE scores River 2.a

The hydrology of Trebbia, Nure and Parma rivers has shown scores similar to the Valtellina area (Fig. 12). Looking at NSE in Table 11.a, we can appreciate that higher scores are assessed for the water volume of Nure (0.978), Parma (0.820) and Trebbia (0.773) rivers. For water discharges, NSE scores are better for Trebbia (0.272) and Parma rivers (0.452) while for Nure River are lower (0.102), also confirmed by the RMSE index (Table 11.a).

Looking at the solid transport quantification in Table 11.b, the AdBPo (Autorità di Bacino del fiume Po) reports have been taken into consideration as reference data for the comparisons (Autorità di Bacino Distrettuale del Fiume Po, 2022). Keeping the same calibration of the  $slope \rightarrow D_{50}$  curve (set n°6) that was adopted for the Valtellina (no granulometry data were found in the examined catchments), the results obtained after the simulations have shown fairly good accordance with the reference. In the three cases, the order of magnitude of the sediment yield delivered each year at the outlet is similar to AdBPo data especially for Trebbia (+12.6%) and Parma (-24.7%) basins while for Nure we have a slightly larger difference (-35.7%). Perhaps, finer granulometry should have been taken into account for simulating the Parma and Nure rivers, decreasing the  $D_{50}$ . This suggests how the sediment transport dynamics are sensitive to the  $slope \rightarrow D_{50}$  parameterization that strongly depends on the geological and lithological characteristics of the catchment.

After running CRHyME for the entire simulation period, keeping the calibration parameters assessed for the Valtellina case study, the model scores have been examined. The hydrology of Trebbia, Nure and Parma rivers has shown better scores in water discharge reproduction for the tested period. Looking at NSE, we can appreciate that higher scores are assessed for the water volume especially for Nure (0.978) and Trebbia (0.773) rivers while for Parma large errors were shown (0.482). However, with respect to Valtellina area, the scores for water discharges are sensibly better for Trebbia (0.272) and Parma rivers (0.452) while for Nure the scores are lower, also confirmed by the RMSE index (Figure 10).

Looking at the solid transport quantification, the AdBPo (Autorità di Bacino del fiume Po) (Autorità di Bacino Distrettuale del Fiume Po, 2022) estimations obtained for the three basins have been taken into consideration for the comparisons. The AdBPo data were calculated by applying the EPM. Keeping the calibration of the  $D_{50}$  slope curve that was adopted for Valtellina, the results obtained after the simulations has shown good accordance with respect to the reference. In the three cases, the order of magnitude of the sediment yield delivered each year at the outlet is similar to AdBPo data especially for Trebbia (+12.6%) and Parma (-24.7%) basins while for Nure we have a slightly larger difference (-35.7%).

(a)	Error Analysis of Hydrological Variables	NSE [-]	RMSE [ $m^3 s^{-1}$ ]
	Discharge Rivergaro (Trebbia River)	0.272	27.915
	Volume Rivergaro (Trebbia River)	0.773	$5.450 \cdot 10^8$
	Discharge Pontenure (Nure River)	0.102	33.468
	Volume Pontenure (Nure River)	0.978	$3.765 \cdot 10^7$

Discharge Ponte Verdi (Parma River)	0.452	14.898
Discharge Ponte Verdi (Parma River)	0.4820	<del>3.704 10<sup>8</sup></del>

(b)

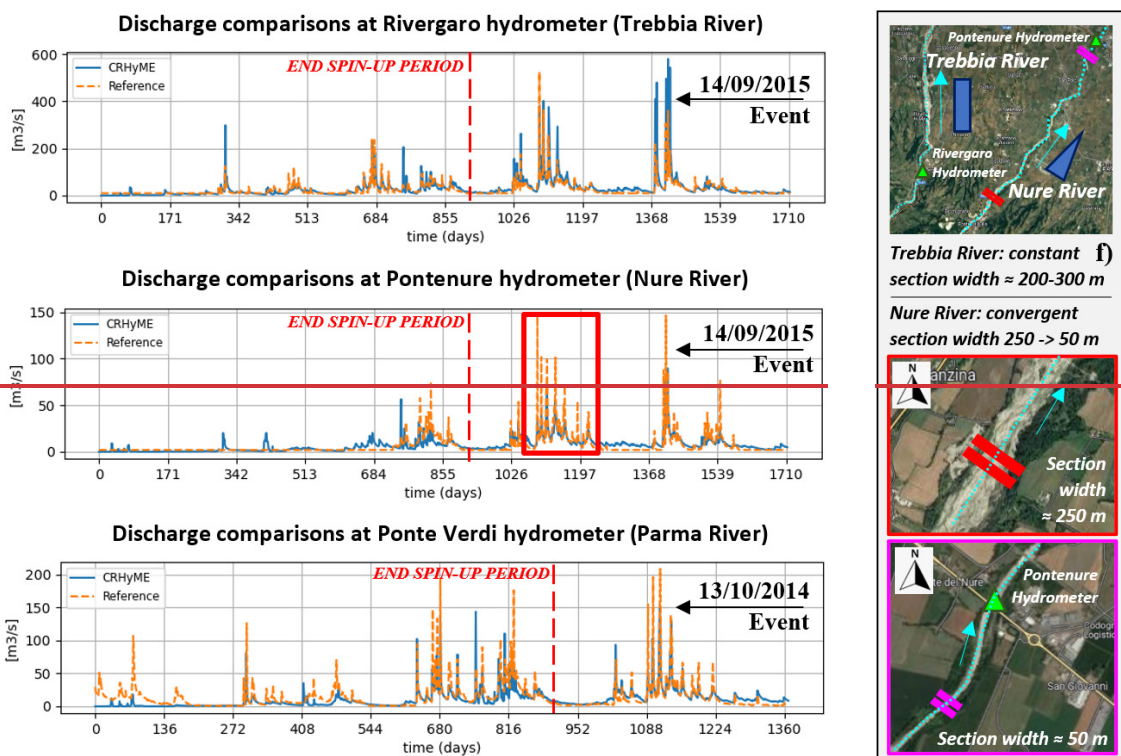
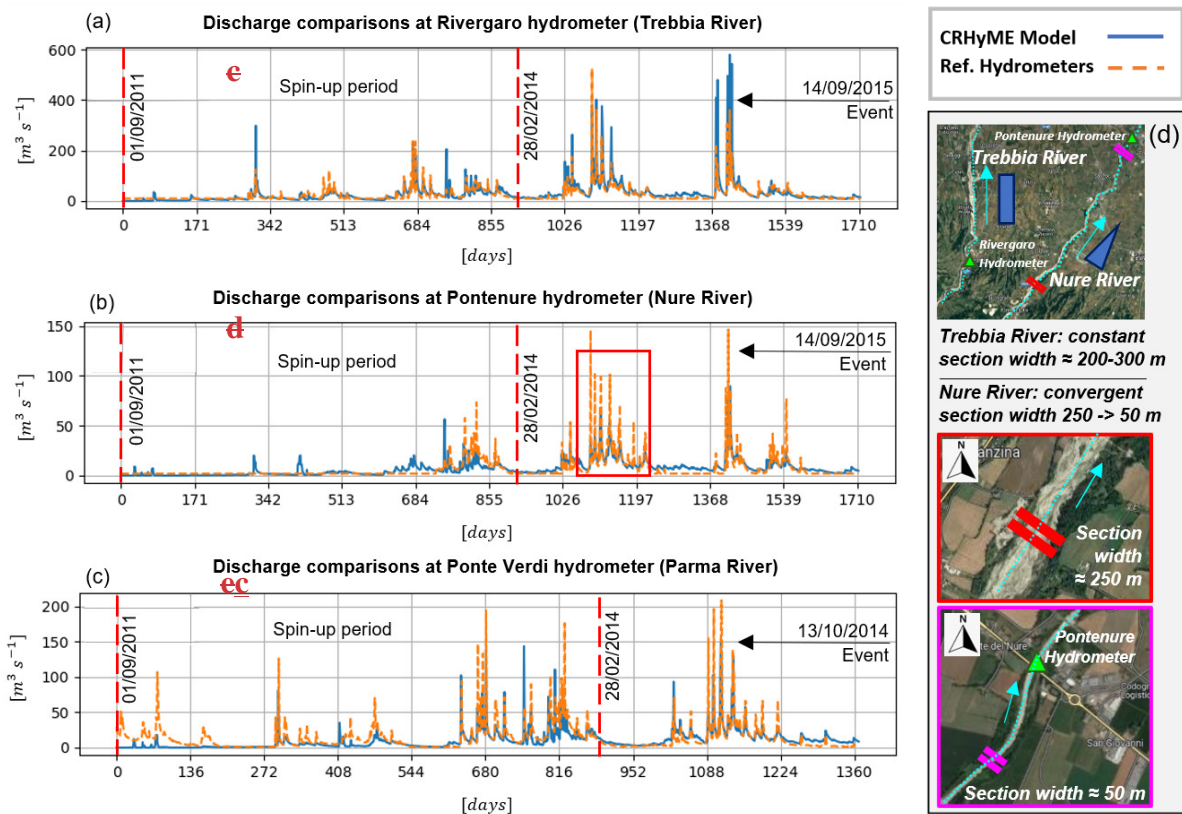
Sediment Yield Error Analysis	Trebbia River	Nure River	Parma River
AdbPo Reference	247.2 10 <sup>3</sup> m <sup>3</sup> yr <sup>-1</sup>	69.4 10 <sup>3</sup> m <sup>3</sup> <del>yr</del> <sup>1/yr</sup>	101.1 10 <sup>3</sup> m <sup>3</sup> yr <sup>-1</sup>
Simulated 2011-2015	278.3 10 <sup>3</sup> m <sup>3</sup> yr <sup>-1</sup>	44.6 10 <sup>3</sup> m <sup>3</sup> <del>yr</del> <sup>1/yr</sup>	76.1 10 <sup>3</sup> m <sup>3</sup> yr <sup>-1</sup>
% difference	+12.6 %	-35.7 %	-24.7 %

**Table 11: CRHyME model error analysis for hydrological discharge and volume (a), sediment yield (b) for the Emilia's catchments at Rivergaro (Trebbia River), Pontenure (Nure River), Ponte Verdi (Parma River) hydrometers.**

1015 The performance of CRHyME in detecting the triggered debris flow during the events of October 2014 and September 2015 (Fig. 13) was assessed again through ROC. A new calibration on the friction angle was carried out since the value provided for the Valtellina was too conservative for stability. This fact could be explained by the Apennines's lithologies which are characterized by higher percentages of clay compared to the Central Alps, reducing the soil friction resistance (Raj, 1981; Hengl et al., 2017). The highest ROC scores were obtained by slightly decreasing (-20%) the slope friction angles and reducing

1020 the soil cohesion to the minimum, supposed to be representative of incoherent deposits. In most cases the model has outperformed the random classifier, showing a sensitivity (TPR) comprised between 0.1- 0.4 and a higher value of specificity (1-FPR) depending on the chosen buffer extension around the triggering point. In our simulations, debris flow failure has been effectively detected across a small valley impluvium, confirming the onsite observations carried out by Ciccarese et al. (2020, 2021): the highest scores were obtained for the Nure catchment, intermediate rank for Parma basin and poor description of

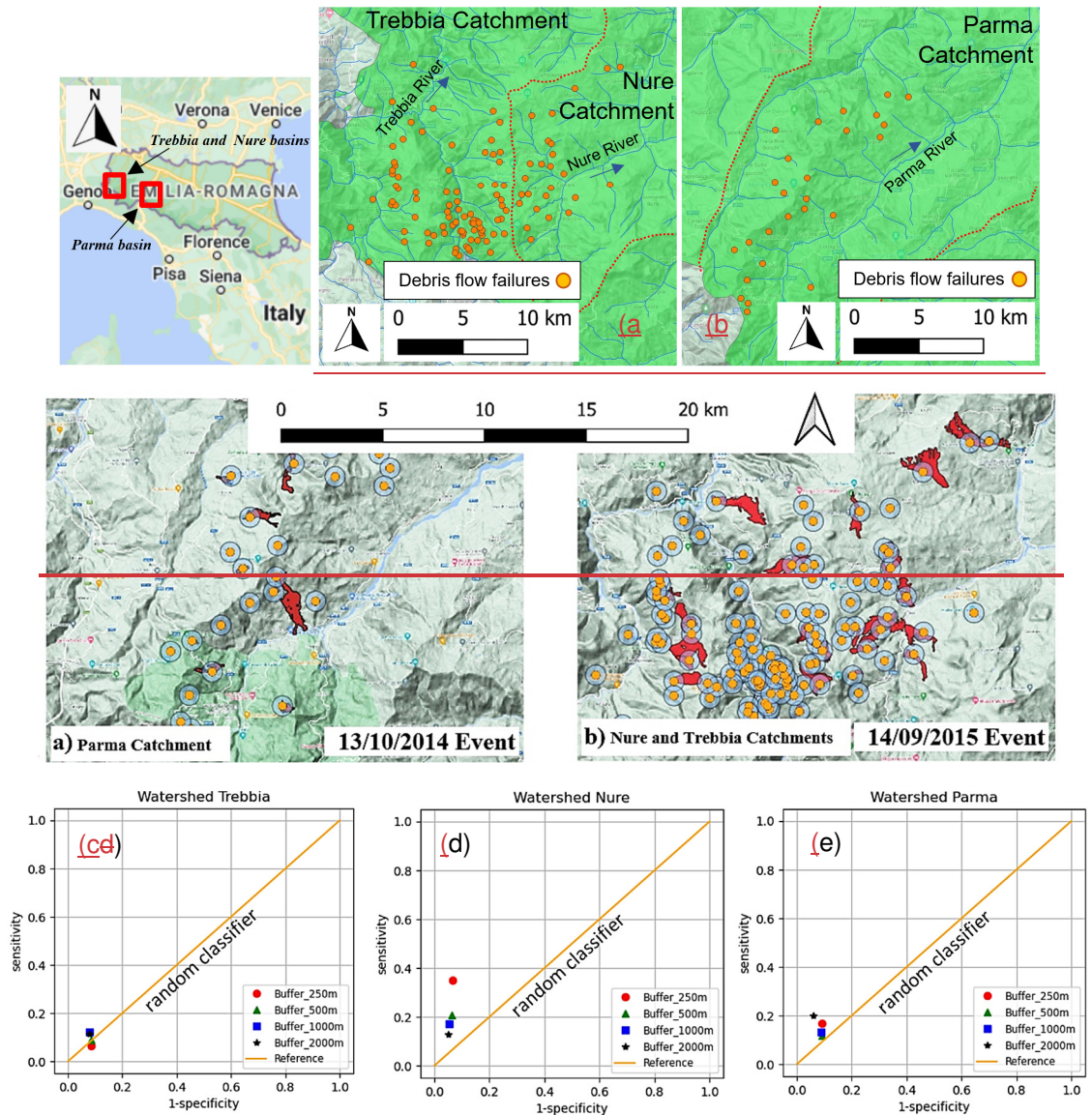
1025 instabilities for Trebbia watershed.



**Figure 12: CRHyME water discharges comparisons for the Emilia's catchments at (a) Rivergaro (Trebbeia River), (b) Pontenure (Nure River), (c) Ponte Verdi (Parma River) hydrometers for the period 2011-2016. The first 900 days of each simulation are considered for model "spin-up" to a realistic initial condition. In the red box (b) is highlighted the peak discharge underestimation for the Nure River due to section variation along floodplain (d). Base layer from © Google Maps 2023.**

**Figure 12: CRHyME model error analysis for hydrological discharge and volume a), sediment yield b) for the Emilia's catchments at e) Rivergaro (Trebbeia River), d) Pontenure (Nure River), e) Ponte Verdi (Parma River) hydrometers for the period 2011-2015. The first 900 days of each simulation are considered for model "spin-up" to a realistic initial condition. In the red box d) are highlighted the peak discharge underestimation for the Nure River due to section variation along floodplain f). Base layer from © Google Maps 2023.**

The performance of CRHyME in detecting the triggered debris flow during the events of October 2014 and September 2015 (Figure 113) was assessed again through ROC methodology. A new calibration on the value of the friction angle was carried out since the value provided for the Valtellina was too conservative with respect to stability. This fact could be explained by the Apennines's lithologies which are characterized by higher percentages of clay with respect to the Central Alps that slightly reduce the soil friction resistance (Raj, 1981; Hengl et al., 2017). The highest ROC scores were obtained by slightly decreasing (20%) the slope friction angle and reducing the soil cohesion to the minimum, supposed to be representative of incoherent deposits. In most cases the model has outperformed the random classifier, showing a sensitivity (TPR) comprised between 0.1–0.4 and a higher value of specificity (1-FPR) depending on the chosen buffer extension around the triggering point. In our simulations, debris flow failure has been effectively detected across a small valley impluvium confirming the onsite observations carried out by (Ciccarese et al., 2020, 2021).



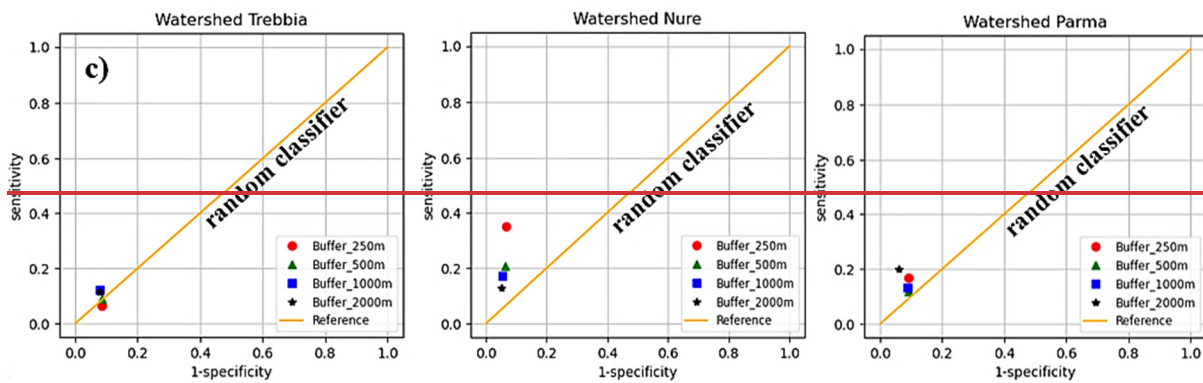


Figure 1313: a) Trebbia–Nure landslide triggered during the event of September 2015 (left) (a, b) Debris flows triggered in Trebbia and Nure the Parma–basins during the event of September 2015–October 2014 and (b) debris flows triggered in Trebbia and NureParma basins during the event of October 2014. Orange points are the mass wasting starting points reported by (Ciccarese et al., 2020, 2021) after the event, blue circles represent a buffer of 500 m around those points and red polygons are historical landslide inventory mapped in the area before the 2014 and 2015 events by the IFFI inventory. Representation of ROC curves for Trebbia (c), Nure (d) and Parma (e) watersheds for the events of October 2014 and September 2015 and October 2014. Base layer from © Google Maps 2023.

## 4 Discussion

### 4.1 CRHyME sensitivity analysis: spatial resolution and sediment diameters

The CRHyME model sensitivity in reproducing hydrological cycle has been tested considering four different spatial resolutions within the Caldane catchment (27 km<sup>2</sup>): 90 m, 50 m, 20 m and 5 m. CRHyME results were obtained with sufficient accuracy and faster computation for cell resolution > 10 m. The computational time was observed to be proportional to the number of domain cells: the 90 m, 50 m and 20 m simulations were concluded in one to two minutes while for the 5 m simulation, the time was raised to 5 min. However, increasing spatial resolution doesn't mean always increasing the accuracy (Rocha et al., 2020; Zhang et al., 2016) and with CRHyME the best performance was acquired for DEM resolutions of 50 m and 20 m and not for 5 m. The variation of the DEM resolution can change sensibly the flow direction of the rivers (“*ldd.map*”) and the basin drainage density, affecting discharge computation. According to the literature (López Vicente et al., 2014; Erskine et al., 2006), the routed runoff could be perturbed by “numerical diffusion”, a known problem of the spatially distributed models that is predominant with fine spatial resolution, which depends on the algorithm applied for flow direction computation (Barnes, 2017, 2016). To preserve CRHyME's solution accuracy and to maintain affordable computational times, we suggest applying the HydroSHEDS DEM model at 90 m resolution for quite large basins > 500 km<sup>2</sup> while higher resolutions are advisable for smaller basins.

Within the Caldane catchment, the dependence of the sediment transport processes on the soil granulometry was tested. The distribution of  $D_{50}$  that increase as a function of the slope is a reasonable representation of the geomorphological processes encountered in mountain catchments (Brambilla et al., 2020; Ivanov et al., 2020a; Ballio et al., 2010). According to Nino (2002), among slope and  $D_{50}$  exist a slight correlation, but non-linearities are caused by sediment processes occurring within river granulometry (sorting and armoring). Recently, data-driven approaches were explored in the USA to define a map of the  $D_{50}$  along the river stream (Abeshu et al., 2021). To evaluate the map, these authors have chosen a series of geomorphological predictors of  $D_{50}$  (elevation, slope, curvature etc.), verifying results with the available databases at country-based they have retrieved the USA  $D_{50}$  map. Not surprisingly, one of the most important predictors is the basin slope which has the highest correlation coefficient with a  $D_{50}$  but stated other geomorphological factors (river path length and elevation) have a similar correlation with  $D_{50}$ . It seems clear that a unique formulation of the  $D_{50}$  as a function of morphological and hydrodynamical parameters cannot be assessed straightforwardly. Since  $D_{50}$  is required for incipient motion of bed-load sediment transport (Chow et al., 1988), and bearing in mind its complexity in spatial evaluation, slope  $\rightarrow D_{50}$  curves

implemented in CRHyME represent a crude but efficacious simplification. Moreover,  $slope \rightarrow D_{50}$  have the advantage of being easily calibrated ~~data~~ if on-site data are available.

#### 4.2 CRHyME's hydrological performances

1090 For the Valtellina case study, CRHyME hydrological performances ~~for regarding~~ the water discharge (NSE ~ 0.2-0.3) were not  
comparable to the ones obtained for ~~the~~ Caldone River (NSE ~ 0.46). A possible explanation resides within the characteristics  
of the Valtellina catchment, which is bigger (2600 km<sup>2</sup>) than the Caldone basin (27 km<sup>2</sup>). Bigger computation domains mean  
increased landscape heterogeneity which implies higher uncertainties in the reproduction of infiltration-runoff-groundwater  
processes (Morbidelli et al., 2018; Mishra et al., 2003; Chow et al., 1988). Comparing volume and discharge scores for the  
1095 Valtellina area driven by the ARPA dataset, a general tendency to overestimate the peak discharge during rainfall seasons  
(spring, summer, and autumn) can be noticed while an underestimation of the discharges during winter is detected (Fig. 9.a).  
This effect is more significant at the Fuentes hydrometer but is less evident at the Mallerio station. After analysing these results,  
three main error components were disentangled into 1) infiltration, 2) losses, and 3) routing parameterizations. They represent  
key processes that should be paid attention to during the calibration phase (Morbidelli et al., 2018) since if they are wrong-  
1100 conditioned may also cause numerical instabilities, losing the water-balance ~~balance~~-conservativity of the code. As reported  
by (Abbate and Mancusi (2021a), infiltration models strongly regulate runoff generation. Their parameterization depends on  
land surface coverage and terrain composition which are sometimes affected by high uncertainties: onsite measurements are  
generally not available and coverage layers have low resolution. For CRHyME, this fact may imply cascade effects on landslide  
processes causing underestimation of the landslides triggered due to the reduced subsurface pore pressure caused by wrong  
1105 soil moisture balance predictions. Water recirculation inside the groundwater reservoir affects water balance in the long term.  
In this regard, Alps and Apennines have complex hydrogeology (ISPRA, 2018) which affects the groundwater dynamics that  
a simple Dupuit model may oversimplify. Unfortunately, the unavailability of local piezometric reference data for calibration  
has not permitted us to assess model performance for this part. To cope with these uncertainties, several sensitivity and  
calibration tests (not reported here) were conducted during model construction, varying groundwater parameterization to  
1110 achieve the best performances. Another source of error is embedded in the runoff-routing algorithm. The kinematic algorithm  
adopted in CRHyME is sufficiently representative of the small lateral catchment rainfall-runoff processes (as for Caldone or  
Mallerio rivers) but maybe not be suitable for interpreting floodplain flood evolution where dynamic processes are prevalent  
(Chow et al., 1988). Moreover, across the Valtellina catchment, river discharges are regulated by several hydropower plants  
(ITCOLD, 2009, 2016). Dams can smooth and shift floods peaks and perturb seasonal water discharges recorded at the outlet's  
1115 hydrometer lowering the CRHyME performances: in the current version of the model lakes and dams are not considered  
explicitly. Among others, this fact could explain the best water discharge score (NSE = 0.325) of the Mallerio sub-catchment  
(less regulated, only 2 dams) with respect to the Fuentes outlet (NSE = 0.199) for the whole Valtellina catchment (Fig. 7).  
The hydrological performances of Emilia catchments have scores similar to the Mallerio River. The water discharge assessment  
for the tested period shows the best agreement for Trebbia (NSE ~ 0.27) and Parma (NSE ~ 0.45). These basins are less  
1120 regulated by hydropower reservoirs compared to the Valtellina, and, since they are smaller (about 1/3 of the extension), the  
kinematic approach for runoff routing is more representative. Nevertheless, the lower scores for the Nure River were caused  
by an underestimation of the peak discharges (Fig. 12). Several simulations conducted in the Nure basin have shown a  
systematic bias within the reference data. The latter could be explained by the location of the reference hydrometer, which is  
settled far away across the flood plain where the river is constricted to flow within a narrow section (~10 m) compared to the  
1125 upper catchment (~ 250 m) (Fig. ~~ure~~ 12.d). Looking at Fig. 7, the Pontenure (Nure River) hydrometer is located across the  
flood plain ~20 km downstream of the catchment for the Rivergaro (Trebbia River, ~1 km) and the Ponte Verdi (Parma River,  
~10 km) stations. Similarly to the Valtellina case, where a flood lamination is likely to occur, to describe river  
behaviour across a floodplain, the dynamic approach should be preferred instead of kinematic routing. In fact, including section



130 geometry as input could increase the simulation accuracy, improving the model's performances in hydrographs and discharge  
reconstruction (Lee and Pin Chun, 2012; Chow et al., 1988).

### 4.3 CRHyME's geo-hydrological performances

135 Geo-hydrological processes have been consistently reproduced by CRHyME. The sediment yields in the Valtellina  
catchment have matched the available reference data of Campo Tartano, Valgrosina and Cancano dams after a calibration of  
the slope  $\rightarrow D_{50}$  to distribute grain size parameters across the catchment. The good reproduction of the annual sediment yield  
(~ 10% underestimation for Valtellina) has been confirmed also for the Emilia case study where the order of magnitude was  
comparable compared to the AdBPo reference (~  $\pm$  20% depending on the basin).

140 Since the  $D_{50}$  perturbs the threshold that activates the sediment transport (Vetsch et al., 2018), it has revealed the critical  
parameter to be assessed in the CRHyME model. For the Valtellina and Emilia areas, the optimal slope  $\rightarrow D_{50}$  curve (set n°  
6, Fig. 10) was different compared to the one adopted for the Caldane catchment (set n° 2, Fig. 10). From a geological  
viewpoint, the Caldane catchment is located in the Prealps where calcareous rocks are prevalent while metamorphic bedrock  
is more diffused across the Valtellina catchment (ISPRA, 2018). Depending on the state of fracture, metamorphic could be  
less strength than calcareous and more prone to be fragmented into small diameters (D'Agostino and Marchi, 2001). Moreover,  
the maturity of the watershed influences the granulometry distribution across the landscape (Pérez-Peña et al., 2009; Strahler,  
1952). Large basins such as the Valtellina and Emilia catchments are more "mature" than the small Caldane catchment,  
145 therefore, a finer granulometry at the outlet is expected. This fact seems to justify why a lower slope  $\rightarrow D_{50}$  curve was optimal  
for these catchments while a higher one was more suitable for the Caldane basin.

150 The CRHyME model has identified the localization and the timing of landslide failures during the extreme events that have  
affected the studied catchment. Looking at ROC scores for the Valtellina area, 1987, 2000 and 2002 events were reproduced  
consistently. The best scores were acquired for 2000 and 2002 events where a good quality inventory was available for the  
investigated area. For 1987-4-b, the incompleteness of the available inventory (yellow points in Fig. 11.b) affected the model's  
final score. However, independently from the specific case, the ROC methodology has highlighted how much the choice of  
the stability parameters (friction angle and cohesion) has a critical influence on the final results. This fact has been confirmed  
also by the sensitivity analysis carried out for debris flow episodes in the Emilia case study during the events of 2014 and  
2015. Here, to reach the best ROC scores against the random classifier, the friction angles calibrated for Valtellina have been  
155 slightly reduced by about 20% confirming the dependence of this parameter on soil texture and lithology and texture.

### 4.4 Model limitations

160 The sensibility of the CRHyME model to precipitation mapping, initial hydrological conditions settings, DEM scale-  
dependency and geo-hydrological cycle parametrization have affected the result accuracy and performances. Since they  
represent possible the current limitations on the widespread applicability of the code a brief discussion is here developed  
suggesting possible solutions.

165 Correctly assessing the precipitation distribution is mandatory to define a realistic representation of the external forcing that  
triggers geo-hydrological failures (Abbate et al., 2021b). Especially across mountain regions, the higher local variability of  
meteorology and the absence of a dense rain gauge network can complicate the reconstruction of a representative rainfall field.  
This aspect was investigated for the Valtellina case study, where simulations derived by MERIDA (Bonanno et al., 2019) and  
ARPA (Rete Monitoraggio ARPA Lombardia) datasets were compared. Using MERIDA, we would expect a better  
performance from CRHyME but this didn't happen in all situations. Looking at water volumes transited across the Fuentes  
hydrometer during the period 2015-2019, the MERIDA dataset has performed better than ARPA stations. On the other hand,  
looking at the Mallero hydrometer, the MERIDA dataset has scored worse than ARPA stations. What is the possible  
explanation for this contradictory fact? MERIDA gives a rainfall map that has a spatial resolution of ~ 4 km while the ARPA

170 station data are interpolated geometrically using the Inverse Distance Weight (IDW) techniques (Daly et al., 1997; Chow et  
al., 1988). A trade-off exists between the ARPA's rain gauge network density and the spatial resolution of MERIDA. In large  
catchments, MERIDA is more representative since it can cover ungauged areas while in small catchments, lower spatial  
resolution may be insufficient for describing local rainfall variability. This is why MERIDA has performed worse than IDW  
in the Mallerio catchment where several ground-based weather stations are uniformly distributed across a limited area of 320  
175 km<sup>2</sup> (Figure 7). Moreover, reanalysis datasets could sometimes smooth the rainfall peaks leading to a wrong interpretation of  
the net rainfall that occurred over a limited area (Abbate et al., 2021b; Bonanno et al., 2019; Ly et al., 2013). This is another  
key issue that generally influences the ability/performance of the slope stability model implemented in CRHyME to detect  
landslides triggered by rainfalls. In this regard, a better integration within rainfall sources coming from the ground-based  
station, reanalysis models, radar maps and satellite data is advisable to reduce possible rainfall uncertainties (Abbate et al.,  
180 2021b).

The choice of a realistic initial catchment's moisturizing is another common issue in every deterministic spatially-distributed  
hydrological model (Uber et al., 2018; Trambly et al., 2010; Chow et al., 1988). Historical measures about the superficial soil  
moisture, groundwater piezometry and superficial runoff are difficult to gather, especially across small mountain basins where  
monitoring systems are not provided (Schoener and Stone, 2020; Chiarelli et al., 2023). Moreover, soil moisture is a quantity  
185 that can vary abruptly across different terrain types, so it is not common to implement a network that permits the acquisition  
of distributed information across a catchment (Lazzari et al., 2018). In CRHyME, to overcome these difficulties, a "spin-up  
period" was introduced within each simulation. This period represents the minimum time required by the model for reaching  
an automatic adjustment of the initial condition that depending on the extension of the basin, can be comprised within a few  
months up to some years. The spin-up simulation permits a re-distribution of the water across the cells of the domain  
190 (horizontally) and among each layer of the model (vertically), reducing the "time lag" between rapid (runoff) and slow  
(groundwater) catchment dynamics. This "time lag" effect was rather evident for the Emilia case study, where a realistic regime  
condition was reached only after three years, rather slower than for the Adda basin (two years). This fact could be explained  
by the different soil compositions and lithology that influence hydrogeological parameters. In the Apennines, the presence of  
clay decreases the speed of soil recharge (lower permeability) slowing down the groundwater recharge (Ronchetti et al., 2009;  
195 Ciccarese et al., 2020; Parenti et al., 2023) compared to the Alps, where coarser terrain granulometry increases soil  
permeabilities. From a practical viewpoint, running the model up to realistic hydrological conditions is time-consuming. In  
CRHyME, PCRaster libraries are already parallelized and can reduce sensibly the computational cost of this operation.  
Moreover, CRHyME can set a "restart" condition, saving the hydrological storage outputs  
 $h_{snow}(t)$ ,  $h_{soilwater}(t)$ ,  $h_{groundwater}(t)$  and  $h_{runoff}(t)$  computed during the spin-up period which could be reused for  
200 subsequent running.

For evaluating shallow landslide and debris flow triggering the simple theory of the infinite slope stability model has been  
implemented. According to the literature (Harp et al., (2006); Iverson, (2000); Takahashi, (2009); Oguz et al., (2022) and;  
Milledge et al., (2014), this methodology is rather affordable for cell-based landslide susceptibility models and mapping thanks  
to its fast coding. However, its strong dependence on DEM resolution represents the main drawback since varying it different  
205 results in slope stability assessment are expected to vary depending on DEM resolution. This fact was not directly experienced  
with CRHyME since in the Caldane catchment, where spatial scale dependence was tested for the hydrological part, the IFFI  
inventory was not available for landslides investigation. Legorreta Paulin et al. (2010) and Zheng et al. (2020) have pointed  
out how the simple infinite slope theory needs to be applied carefully. First of all the inaccuracy of the infinite slope method  
is related to the fact that each pixel is considered independent from the other settled at the boundary (Iverson, 2000). For very  
210 large DEM pixel size, namely > 100 m this may be an acceptable hypothesis since 100\*100 m<sup>2</sup> represents the typical  
order of magnitude of a rainfall-induced shallow landslide or a debris spatial extension (~ 10'000 m<sup>2</sup>). For pixels ≤ 100 m this  
is not properly correct since the cell size is lower than the typical dimension: surrounding areas may participate in the landslide

collapse due to boundary effects, especially at the top and bottom edges (Fig. 5), caused by strength redistribution (Zheng et al., 2020; Milledge et al., 2014). In CRHyME, having a spatial resolution of about ~70 m, we have preferred to include the surrounding 8 pixels close to the unstable areas, following a rather conservative choice justified by the physical interpretation of landslide kinematics. On the other hand, varying ~~DTMDEM~~'s resolution causes a modification of the local slope gradients which are the main drivers of failures: lower resolutions can operate an unphysical smoothing of the surface reducing cliff and scarp that may trigger small landslides. As a result~~In principle~~, the best ~~DTMDEM~~ resolution available may lead to the most accurate results but this choice is generally adopted for static landslide susceptibility mapping while may not be suitable for dynamic routines (Legorreta Paulin et al., 2010; Zhang et al., 2016). In CRHyME hydrological balance is computed at each time step and then the slope stability calculation is evaluated recursively: increasing the spatial resolution the computational times rise fast so that a trade-off between model performance and result accuracy should be acquired. Bearing in mind this, ~~is~~ a critical issue, improvements on landslide hazards are planned in the future version of the code, making the slope stability hazard assessment routine less scale-dependent and less conservative.

According to (Gariano and Guzzetti, 2016), reconstructing the whole geo-hydrological cycle that drives the erosion and mass wasting processes through numerical models is a challenge. In this regard, CRHyME is not an exception: the EPM is considered for erosion; empirical power-law relationships are implemented for sediment routing; only landslide and debris flow triggering conditions are evaluated by stability models, not including runout evolutions. This subdivision was adopted firstly to simplify the phenomena interactions and secondly to guarantee the fast functioning and stability of the CRHyME code. Following this sequential scheme, geo-hydrological processes are computed after the hydrological assessment, but possible feedbacks are not explicitly taken into account. On a long-term timescale, geo-hydrological processes contribute to a landscape modification, e.g. ~~DTMDEM~~'s height changes. The former is not included by CRHyME since the code has been built with a different purpose with respect to landscape-evolutions models (Campforts et al., 2020; Bovy et al., 2020; Salles, 2019). However, all geo-hydrological hazards also play an important role in the short-term period, modifying temporarily or permanently the local soil depth (Sklar et al., 2017): landslide and debris flow runout can redistribute the local terrain changing the soil depth (asportation at the crown and accumulation at the toe) and modifying the ~~DTMDEM~~ height. Therefore, finding a "closure" for the superficial geo-hydrological balance is a non-trivial task from a theoretical and numerical viewpoint (D'Odorico and Fagherazzi, 2003). The CRHyME experience has shown how landslides and debris flow stability assessment cannot be treated deterministically since their triggering strongly depends on the choice of the model type (FS equations) and on stability parameters (the friction angle and the cohesion) which are parameters generally measured on the field or in a laboratory. In CRHyME, (Abbate and Maneusi, 2021a) following some literature studies (Hengl et al., 2017; Yu et al., 2018; Chow et al., 1988; Dade and Friend, 1998), the cohesion was spatially distributed in the function of vegetation coverage bearing in mind the roots contribute to stability while the friction angle was correlated with the soil composition. On the other side, friction angle is in function of the soil texture, granulometry and consolidation, depending also on complex sediment dynamics and geological processes (de Vente and Poesen, 2005; Merritt et al., 2003; Shobe et al., 2017; Ballio et al., 2010; Kondolf, 1997). As a result, the calibration procedure within a sensitivity analysis was necessary case-by-case since these parameters correlate with several geo-morphological predictors.

The assessment of the superficial geo-hydrological cycle cannot be evaluated precisely since its monitoring is currently still insufficient on a catchment scale (ISPRA, 2018; Gariano and Guzzetti, 2016). Even though surface mapping and inventory are supposed to increase their accuracy and completeness in the future thanks to remote sensing data (Ciampalini et al., 2016), some doubts remain about the possible improvements for other fundamental data required for slope stability and sediment transport spatially distributed models routines. However, the databases adopted in CRHyME (Hengl et al., 2017; Huscroft et al., 2018; Ross et al., 2018) represent the very first attempt to overcome these issues having already made an important homogenization of the essential data required for geo-hydrological modelling.

1255 ~~4 (Barnes, 2017, 2016)(Albano et al., 2017; Brunner et al., 2015; Hunter et al., 2008)(Barnes, 2016)(ISPR, 2018)(Dade and Friend, 1998b)(Abeshu et al., 2021)~~

#### ~~4.1 The hydrological performance of Valtellina and Emilia case studies~~

1260 As shown in the previous paragraph, CRHyME hydrological performances are not particularly satisfactory regarding the water discharge reproduction (NSE = 0.2-0.3), especially for the case study of Valtellina considering both ARPA and MERIDA datasets. The characteristics of Valtellina catchments, where river discharges are regulated by the presence of a consistent group of hydropower plants (ITCOLD, 2009, 2016) can decrease the CRHyME performances in reconstructing the water discharges peaks recorded at the outlet. In fact, in the current version of the model lakes and dams are not considered since still data about how they operate and flood regulations are not available to the public. On the other hand, the kinematic routing of runoff, which is sufficiently representative of the small lateral catchment rainfall-runoff processes (Chow et al., 1988), maybe not be suitable for interpreting floodplain flood evolution where dynamic routing should be considered. In fact, due to its morphology, Valtellina valley has a rather long floodplain (70-80 km) where larger river sections are present together with 4 in-line reservoirs that can operate important flood lamination during intense rainfall events. This explains the best score of the Mallero sub-catchment (NSE = 0.325) with respect to the Fuentes section (NSE = 0.199) related to whole Adda catchment.

1270 As a counter-example, the hydrology of Emilia rivers has similar scores of Mallero in water discharge reproduction for the tested period with the best agreement for Trebbia (NSE = 0.27) and Parma (NSE = 0.45). These basins are less regulated by hydropower reservoirs with respect to the whole Valtellina, and, since they are smaller (about 1/3), also the kinematic approach for runoff routing is much more representative of the catchment behaviour. Nevertheless, for the Nure river, the lower scores are caused by the appreciable differences between CRHyME discharge peaks that overestimate during rainfall periods the ones recorded by the hydrometer, even though the catchment behaviour seems to be represented correctly thanks to the volume conservation (NSE = 0.978). Looking at Figure 5, Pontenure hydrometer is located across the flood plain 20 km downstream of the catchment with respect to the Rivergaro (-1 km) and Ponte Verdi (-10 km) stations. Similar to Valtellina, a flood lamination is likely to occur before reaching the stations so a dynamic approach should be tested instead of kinematic routing in order to increase the discharge agreements.

1280 The higher performances in the volume quantification obtained by CRHyME in almost all tested cases (NSE = 0.8-0.9) assure that the routine is numerically and hydrologically conservative. Numerical stability has been guaranteed by built-in PCRaster libraries adopted for computations where some stability criteria have been matched especially for kinematic and dynamic routing functions. Since hydrological balance and water redistribution across the catchment domain are rather articulated, CRHyME calculates the ratio among the water Inflows and Outflows at each time step: if the model works numerically conservatively it is kept equal to 1. The high value of the NSE index has shown that the behaviour of the catchment dynamic over a long period of simulation is correctly interpreted. This is true especially for the Valtellina case study, using the ARPA dataset, and for Trebbia and Nure basins while only for Parma the score was sensible lower. A possible explanation may reside in some errors that affected the early simulation period where the CRHyME model has not already reached the regime condition giving a non-optimal reconstruction of the water discharge.

1290 ~~Comparing volume and discharge scores a general tendency to overestimation of the peak discharge during rainfall seasons can be noticed while an underestimation of the discharges during winter is detected. The main reason should be imputed also in part to the water recirculation inside the groundwater reservoir that, as already anticipated in section 2, has been included bearing in mind several assumptions due to the data scarcity and hydrogeological uncertainties. In this regard, Alps and Apennines have a different geological history that may affect the groundwater dynamics and this aspect may have not been glimpsed totally by the Dupuit model implemented in CRHyME. Unfortunately, the unavailability of reference piezometric data has not permitted us to assess model performance for this part (Morbidelli et al., 2018)(Mishra et al., 2003)(ISPR, 2018)~~  
Comparing volume and discharge scores a general tendency to overestimation of the peak discharge during rainfall

seasons can be noticed while an underestimation of the discharges during winter is detected. The main reason should be imputed also in part to the water recirculation inside the groundwater reservoir that, as already anticipated in section 2, has been included bearing in mind several assumptions due to the data scarcity and hydrogeological uncertainties. In this regard, Alps and Apennines have a different geological history that may affect the groundwater dynamics and this aspect may have not been glimpsed totally by the Dupuit model implemented in CRHyME. Unfortunately, the unavailability of reference piezometric data has not permitted us to assess model performance for this part.

#### 4.1.1 Precipitation uncertainties: datasets across the Alps

Correctly assessing the precipitation distribution is mandatory to define a realistic representation of the external forcing that influences mainly the dynamic of the geo-hydrological cycle (Abbate et al., 2021b). Unfortunately, especially across mountain regions, the higher local variability of meteorology and the absence of a distributed network of stations can complicate the reconstruction of a continuous field, especially for rainfall. Differences were appreciated using two different datasets for the Valtellina case study, revealing that ARPA stations are settled ground-based and represent the most accurate indication of the effective rainfall drop into the soil surface. The former is the data required by CRHyME and in this sense, reanalysis data such as ones from MERIDA (Bonanno et al., 2019) are preferable because they already produce precipitation as a spatially distributed map, covering also area without rain gauges. Using MERIDA, we would expect a better performance from CRHyME runs but this hypothesis has not been confirmed in all situations. Looking at water volumes transited across the Fuentes hydrometer during the period 2015-2019, the MERIDA dataset has performed better than ARPA stations with respect to the reference. On the other hand, looking at the Mallerio hydrometer, the MERIDA dataset has scored worse rather than using directly ARPA stations. What is the possible explanation for this contradictory fact?

The main difference resides in the different reconstructions of the rainfall field from the two datasets since the model has driven the simulations by keeping the same calibration parameters. MERIDA gives an already corrected rainfall map that has a spatial resolution of 4 km while the ARPA stations data are interpolated geometrically using the Inverse Distance Weight (IDW) techniques. The former is a good interpolator when the network density is rather high and uniformly distributed across the landscape and this is a good and fast solution for flat areas while across complex terrain, the orography can increase the errors in IDW (Abbate et al., 2021b). In the Valtellina case study, since it is a valley without a uniform rain gauge network, the IDW method has performed worse than MERIDA. Nevertheless, the power of MERIDA is valid if the watershed is rather large, while the performance may decrease for a smaller basin. In the Valtellina case study, this situation has emerged for the Mallerio catchment (Figure 5) that represents a branch of the main reach Adda. Analysing the water discharge volume, across the Mallerio basin, MERIDA has performed worse rather than IDW. In this case, the coarse resolution of MERIDA has represented a critical point while the rainfall field has been reconstructed in a better way by local ARPA stations. It is important to mention that the Mallerio catchment is a well-monitored basin where around ~10 weather stations are distributed across an area of 320 km<sup>2</sup> so that IDW can interpolate better the precipitation field. This evidence is following some literature studies (Abbate et al., 2021b; Bonanno et al., 2019; Ly et al., 2013) where the problems related to the smoothing of the rainfall peak operating by meteorological models are highlighted.

#### 4.1.2 Initial hydrological condition uncertainties

The choice of a realistic initial condition for the catchment's soil moisture and its dependence on rainfall field reconstruction represents a common problem for a deterministic model (Uber et al., 2018; Trambalay et al., 2010; Chow et al., 1988). In some cases, it is very difficult to have sufficient measures about the superficial water content of the soil, groundwater piezometric and superficial discharges. Regarding water flows, precise quantification of the discharge is generally produced by hydrometers that are normally located at the outlets of the basins. These data series are barely distributed and sometimes may fail to give useful data, especially during extreme events where they may be discontinued due to a lack of electric power. Finally, soil moisture is a quantity that can vary abruptly across different terrain types, so it is not common to implement a network that permits the acquisition of distributed information across a catchment (Lazzari et al., 2018).

In CRHyME, these problems have been in part skipped considering that the model reached an automatic adjustment after some time steps that, depending on the extension of the basin, can be comprised of a few months up to some years. The former is a sort of automatic auto-calibration of the model. In fact, the long-run simulation permits a distribution of the water across the cells of the domain (horizontally) and across each layer of the model (vertically). This effect was rather evident for the Emilia case study, where a realistic regime condition was reached only after a couple of years, and it was rather slower than for the Adda basin. The regime conditions have been acquired less rapidly since to the different soil compositions and morphology between the two areas. In the Apennines, the presence of clay can generally decrease the speed of soil saturation slowing down the groundwater recharge (Ronchetti et al., 2009; Ciccarese et al.,

2020). As a result, the regime condition can take several times with respect to the Alps, where coarser terrain granulometry can reduce it due to higher soil permeabilities. Two-three years are generally sufficient to reach a regime condition since the fact that liquid discharge recorder at the outlets starts to match the hydrometric series.

## 4.2 The geo-hydrological performance of Valtellina and Emilia case studies

### 4.2.1 Solid Transport

Regarding the geo-hydrological hazard quantification, bearing in mind the limited availability of historical and reference data and their embedded uncertainties, landslide and solid transport processes have been reproduced with good affordability. The sediment yields calculated on a yearly based have been matched with respect to the available data of Tartano, Valgrosina and Caneano dams after a calibration procedure that has involved the application of the function for redistributing  $D_{50}$  grain size parameter across the catchment. The good reproduction of the annual sediment yield ( $\sim 10\%$  underestimation for Valtellina) has been confirmed also for the Emilia case study where the order of magnitude was correctly reproduced with respect to AdBPo reference ( $\pm 20\%$  depending on the basin).

Since the  $D_{50}$  is embedded into the threshold that activates the sediment transport (Vetsch et al., 2018), it has revealed the critical parameter to be assessed in the CRHyME model. (ISPRA, 2018)(Inventario Fenomeni Franosi)(D'Agostino and Marchi, 2001)(Pérez Peña et al., 2009; Strahler, 1952)In the literature, there is plenty of studies that have investigated the dynamic of solid transport, but they lack giving a comprehensive theory that could be applied in those case where field data are not available. The empirical formulation proposed for CRHyME is an attempt in this direction, but since it is a currently open problem further research is planned for future versions of the model.

### 4.2.2 Shallow landslide and debris flow

The CRHyME model has identified correctly the localization and the timing of landslide failure during the extreme events that have affected the studied catchment. For the Valtellina area, 1987, 2000 and 2002 events were reproduced consistently by looking at ROC scores. The best scores were acquired for 2000 and 2002 events also a good quality census was available for the investigated area. For 1987, as can be appreciated in Figure 9, the incompleteness of the available census (yellow points) has affected the model's final score. However, independently from the specific case, the ROC methodology has permitted us to highlight how the choice of stability parameters (friction angle and cohesion) has a critical influence on the final results. This fact has been confirmed also by the sensitivity analysis carried out for debris flow episodes in the Emilia case study during the event of 2014 and 2015. Here, in order to reach the best ROC scores with respect to the random classifier, the friction angles calibrated for Valtellina have been slightly reduced by about 20%.

CRHyME experience has shown how landslides and debris flow stability assessment cannot be treated deterministically even with an infinite slope model equation if some key data are not available or tuned indirectly from the others. In particular, the friction angle of the natural slope, and the cohesion of the superficial soil represent the most uncertain parameters that unfortunately cannot be estimated even if a terrain sample is analysed in the laboratory. The former cannot be properly done if the aim of the study is to investigate the slope stability at the catchment scale. Up to now, there are still few examples of the spatial distribution prediction of these two quantities that are essential for simulating geo-hydrological hazards, especially for landslide susceptibility mapping. In this regard, stochastic techniques are sometimes implemented to fulfil these needs (Vardon et al., 2016). In the simulations of Valtellina and Emilia case studies, a brief sensitivity analysis was carried out considering ranges given by the literature survey but without implementing a Montecarlo simulation of stability coefficients. The tuning procedure is difficult since (Hengl et al., 2017; Yu et al., 2018; Dade and Friend, 1998b; Chow et al., 1988) depends also on the large uncertainties that can be found inside the reference database that is used for validating the carried-out simulation. Moreover, friction angle depends on soil consolidation which is barely unknown while soil granulometry is the final result of the complex sediment dynamics and geological processes that have not been clarified at all (de Vente and Poesen, 2005; Merritt

1395 et al., 2003; Shobe et al., 2017; Ballio et al., 2010; Kondolf, 1997). Similarly, to the  $D_{50}$  parameter, these problems represent a research frontier that will be further strengthened in the future version of the model.

### 4.3 Geo-hydrological uncertainties: superficial geo-hydrological cycle

1400 CRHyME is intended to simulate superficial geo-hydrological processes occurring at the catchment scale. Through a multi-hazard approach is possible to quantify these phenomena giving insight into their potential effects on the territory, useful for engineering and Civil Protection purpose. In this regard, CRHyME is one of the first examples of an integrated model.

1405 The existing methodologies used in the engineering field have the main drawbacks of threatening separately geo-hydrological processes, not giving a comprehensive framework of the geo-hydrological cycle (ISPRA, 2018; Vetsch et al., 2018; Ali et al., 2019; Gariano and Guzzetti, 2016). In literature, models that assess jointly the erosion processes with shallow landslide instabilities at the catchment scale are rare (Baartman et al., 2012; Roo et al., 1996; Van Der Knijff et al., 2010) since the approaches adopted, the data required for simulations and their availability have historically limited the applicability inside a spatially distributed model (Sutanudjaja et al., 2018; Strauch et al., 2018). Moreover, these processes have been studied in the past not always taking into account the high dynamicity of hydrological assessment, making strong assumptions on its stationarity, i.e. complete saturation of the slopes (Montgomery and Dietrich, 1994; Mandal and Maiti, 2015; Zhu and Xiao, 2020). In CRHyME, the hydrological aspect represents the main engine that, coherently with the observed reality, can trigger 1410 geo-hydrological instability at different locations and times.

Thanks to the PCRaster functions, CRHyME is a tool that overcomes the limitation related to lumped parameter erosion model, stream power solid transport methodologies and to static susceptibility mapping for shallow landslide and debris flow. PCRaster permits to work with spatially distributed data and combine them to better describe the characteristic of a territory especially related to the local morphology, soil composition and coverages. Embedded routing functions are able to route the material (water or solid) through the whole catchment, extending the investigation of geo-hydrological in a spatial and time perspective. Processes are not evaluated at a specific river section or single slope under the hypothesis of stationarity, but they are simulating through the entire domain and considering their transient. Moreover, CRHyME could produce dynamic susceptibility maps, highlighting for shallow landslide phenomena the area that could destabilise at a particular time step of simulation, extending the concept of static susceptibility mapping where time components driven by meteorological triggering factors (rainfalls) are not always taken into account (Meisina et al., 2013; Ali et al., 2019; Atkinson and Massari, 1998; Benni Thiebes et al., 2017).

1415 According to (Gariano and Guzzetti, 2016), reconstructing the whole geological cycle that drives the superficial erosion process and landslide formation is a challenge. CRHyME model is not an exception: EPM semi-quantitative model is considered for simulating the erosion process while landslide and debris flow triggering do not involve their runout. The runout processes can redistribute the local terrain changing the soil depth (asportation at the crown and accumulation at the toe) and modifying the DEM height. This dynamic is rather difficult to simulate consistently on a 2D domain even though a specific problem is addressed (Scheidl and Rickenmann, 2011). It represents one of the main assumptions for guaranteeing a fast functioning of the implemented routines in CRHyME: geo-hydrological assessment is computed after the hydrological assessment (one-directional sequence) and possible feedbacks, such as DEM modifications, are not taken into account up to 1420 now.

1425 Uncertainties about hydrological simulations are present in CRHyME but can be “controlled” through the hydrometer stations if available locally. On the other hand, the assessment of the “superficial geological cycle” cannot be evaluated precisely since the monitoring of these geo-hydrological phenomena is still insufficient on a catchment scale (Inventario Fenomeni Franosi; ISPRA, 2018). Even though surface mapping and census are supposed to increase their accuracy and completeness in the future, some doubts remain about possible improvements in other fundamental data. To correctly assess the landslide triggering, a uniform soil layer cannot be sufficient sometimes but further information about local geology in terms of 1435

lithological material, strata inclination and immersion and the eventual presence of faults should be included to have a complete picture of dynamics and triggering of the local geo-hydrological processes (Montgomery and Dietrich, 1994; Bovolò and Bathurst, 2012; Cevaseo et al., 2014; D'Amato Avanzi et al., 2004). Up to now, these data are still represented in the geological sections that depict an accurate profile of the possible configuration of the layers. Unfortunately, geological sections are not available digitally and cannot be included directly inside the models even though a complex 3D mesh is available and required by the program. The former is beyond the scope of CRHyME that can be in principle classified as a 2.5D model. Nevertheless, the possibility to include those data could help in interpreting superficial and groundwater fluxes to reduce uncertainties, especially for larger catchments. In this sense, the databases already adopted in CRHyME (Hengl et al., 2017; Huseroft et al., 2018; Ross et al., 2018) have made an important homogenization of superficial soils properties that permit to implement in CRHyME stability models.

In conclusion, the deterministic reproduction of the “superficial geological cycle” poses some open problems still unresolved. Geo-hydrological processes cannot be perfectly coupled with the hydrological cycle since feedbacks are difficult to be taken into account and empirical formulations are necessary to try to simplify these complex interactions. CRHyME is one of the first attempts that aim to describe geo-hydrological processes coupled with hydrological dynamics deterministically and in an efficient way using the potentiality of PCRaster functions.

(Daly et al., 1997; Chow et al., 1988)(Abbate et al., 2021b)(Campforts et al., 2020; Bovy et al., 2020; Salles, 2019)(Sklar et al., 2017)

## 5 Conclusion

Geo-hydrogeological processes have been conventionally studied separately in many engineering fields (hydrology, geology etc.). Hypothesis and simplifications adopted to make them more tractable have sometimes partially neglected their mutual interactions, possible chain effects and their embedded interdisciplinarity. Therefore, hydrological models that assess jointly the erosion, and sediment transport processes and evaluate shallow landslide instabilities are quite rare. In this sense, the CRHyME model was designed as a tool able to show a complete picture of the most significant geo-hydrological hazards processes that may occur at the catchment scale.

In this work, the new model CRHyME and its applications are reported. CRHyME model was built ex-novo using with Python programming language, have the same framework and implementing faster PCRaster libraries that can simulate hydrological processes in a very efficient way. CRHyME includes some of the common features of the classical spatially distributed hydrological model but with an additional focus on quantitative reconstruction of geo-hydrological hazards.

CRHyME is characterized by six modules that reproduce water-hydrological balance over terrain and by a brand-new module deputed to simulate all the processes related to the geo-hydrological hazards (e.g. erosion, solid transport, shallow landslide and debris flow triggering at the catchment scale). In the field of geo-hydrological risk assessment, CRHyME includes some of the common features of the classical hydrological model but with an additional focus on geo-hydrological hazards. Particular attention has been devoted to the study and to the implementation of the erosion and solid transport processes that can typically occur in a river catchment. Moreover, shallow landslide and debris flow stability models have been included. The integration of all those processes in a spatially distributed hydrological model represents a novelty in the field of geo-hydrological risk assessment. Of course, some hypotheses were assumed since it is quite impossible to implement accurately all the existent geo-hydrological mechanisms: some dynamics are still unknown or are too complex to be reduced to a 2D interpretation.

Since the aim of our study was to build and facilitate the usage of the model indistinctly in any area of the globe, a deep investigation of the open-source repositories available for initial data has been carried out. The user-defined calibration parameters have been reduced to the minimum. Among them, erosion coefficients, average sediment diameters, cohesion and



friction angle have been tuned following the strategies presented above. A sensitivity analysis has been carried out to simplify and accelerate the reconstruction of realistic hydrological initial conditions, adding the possibility to activate the restart option after a spin-up period. Moreover, the DEM's resolution scale dependency was investigated and detected by the results. CRHyME was intensively tested to make it as general as possible and reproducible in whatever catchments. A model is affordable if correctly calibrated and validated. Calibration procedures are a critical part of the most common hydrological model since they measure how the results may be affected by the chosen parameters. Since the aim of our study was to build and use a model indistinctly in any area of the globe, the user defined calibration parameters have been reduced to the minimum. In this way, we have reduced the possibility of parameter overfitting to a particular case study, making the CRHyME model rather general and usable in all catchments. Our case studies, the ~~of~~ Caldane basin, the Valtellina Valley catchment, and the Emilia area, were chosen with respect to looking at the availability of historical data that which are of paramount importance for model validation. The results have shown a fairly good reproduction of the past observations: the model is numerically stable (thanks to PCRaster libraries), conservative (no water or solid leakages outside the domain) and hydrologically conservative consistent (compared to the reference hydrometers, ~~the routed water volume of water recirculating across the basin is~~ shows  $NSE \approx 0.8-0.9$  while discharges have lower performance,  $NSE \approx 0.2-0.4$ , especially for larger catchments regulated by hydropower plants conserved), and numerically stable (thanks to PCRaster libraries); the solid discharge reproduced with downscaled EPM Gavrilovic's method is consistent with the observations (errors around  $\pm 20\%$ ), even though there are some uncertainties on  $D_{50}$  parameter; the triggering of shallow landslides and debris flows is comparable in number and spatial localization with respect to the reference inventory (confirmed by ROC assessment). However, CRHyME's performances are rather sensitive to the quality of rainfall field data that should be accurate in spatial and temporal resolution to allow the code to correctly detect landslide triggering.

The efforts conducted in this study with the creation of CRHyME go are in the direction of a better investigation and reproduction of geo-hydrological hazards. CRHyME is a multi-hazard model able to address and quantify at catchment scale several geo-hydrological processes that may occur simultaneously, are physically coupled and coupled and cannot be interpreted separately. With CRHyME is possible to overcome the software fragmentation that is currently present in the geo-hydrological field, answering the recent needs required for multi-hazard quantification and multi risk quantification evaluation required not only for in back analysis studies but also for a multi-risk now-casting evaluation at the Civil Protection level.

## Appendix A

In this section Here, an example of the CRHyME ".INT" file that was written for the computations is reported. Each module has contains its options where the parameters, variables and other settings required for the model ~~run for the computations~~ are specified. The ".INT" file essentially reports reports the simulation time settings (e.g., starting date and ending date), the spatially distributed input data and the meteorological and climatological data series, the settings options of each computational module and the name of the output files. The ".INT" file is read by the "deterministic\_runner.py" file that starts the CRHyME model and its internal routines (Fig. ~~are~~ 2): in "pre-processing.py", "reporting.py" and "plot.py" modules, variables are respectively defined, saved, and plotted following the formats and standards of the PCRaster libraries (Sutanudjaja et al., 2018; Karssenberget al., 2010). CRHyME's results are reported in two formats, as a ".csv" datasheet or a ".netcdf" map (Jacob et al., 2014; Sutanudjaja et al., 2018). The first type is generally used used to pick up information of a particular quantity at one location such as in the correspondence of a rain gauge or hydrometric station. The datasheet is organized with a first column containing the time step value while the subsequent columns contain picked information of one or more monitoring points. The ".netcdf" maps are produced to store information about the states and fluxes variables of the model. At each timestep, the quantity at the spatial resolution of the ~~DTMDEM~~ model is saved within the ".netcdf" stack. The required variable to be sampled should be specified in the ".INT" file under the "reporting options": for ".csv" files a ".map" file containing the location

of sample points while for “.netcdf” the name of the variable required should be specified. Using the GDAL libraries for Python (GDAL/OGR contributors, 2020), the input/output geographical data has been converted to the PCRaster standard format “.map” for raster data (Karssenberget al., 2010; Sutanudjaja et al., 2018), considering WGS84 datum as a reference system for geographical projection. In the output’s files: the lateral water fluxes  $F_{sub}(t)$ ,  $F_{GW}(t)$  and  $F_{kin-dyn}(t)$  are expressed in  $[m^3s^{-1}]$ ; the vertical water fluxes  $C_I(t)$ ,  $S_{ml}(t)$ ,  $I(t)$ ,  $ETc(t)$ ,  $R(t)$ ,  $L_{per}(t)$ ,  $Ex(t)$  and  $Ex_{GW}(t)$  are expressed in  $[mm timestep^{-1}]$ ; storage quantities  $h_{snow}(t)$ ,  $h_{soilwater}(t)$ ,  $h_{groundwater}(t)$  and  $h_{runoff}(t)$  are converted into  $[m^3]$  for volumes simply multiplying the storage height by the cell area extension of the DEM in  $[m^2]$ . Further description of the sub-modules can be found inside the CRHyME’s manual (Abbate and Mancusi, 2021a, b).

### .INI FILE EXAMPLE

```
[globalOptions] _____ (CRHYME'S GENERAL OPTIONS)
inputDir = ***\ModelCRHyME\CRHyME_Inputs_Trebbia _____ (input directory)
outputDir = ***\ModelCRHyME\CRHyME_Outputs_R _____ (output directory)
1535 cloneMap = map\clone.map _____ (clone map for delimiting domain)
landmask = None
institution = RSE_Ricerca Sistema Energetico _____ (institution name)
title = CRHyME project _____ (project title)
description = by Andrea Abbate and Leonardo Mancusi, resolution = 90 m _____ (project description)
1540 resolution = 90 _____ (spatial data resolution)
startSeries = 1985-12-31 _____ (starting data of series)1
startTime = 1986-01-01 _____ (starting data of simulation)1
endTime = 2005-12-30 _____ (ending data of simulation)1
timestep = 24 _____ (timestep resolution in hours)
1545 startingStamp = 0
stampTimestep = 1 _____ (stamp timestep in n° timestep)
Restart = 1 _____ (activate restart option after spin-up)
Restart_Snow = \restarts\mod2\Restart_Snow.map _____ (snow height state for restart)
Restart_Surface = \restarts\mod2\Restart_Surface.map _____ (runoff height state for restart)
1550 Restart_Soil = \restarts\mod2\Restart_Soil.map _____ (soil water height state for restart)
Restart_Ground = \restarts\mod2\Restart_Ground.map _____ (groundwater height state for restart)
Restart_SoilSed = \restarts\mod2\Restart_SoilSed.map _____ (sediment height state for restart)

[climaOptions] _____ (CLIMA MODULE OPTIONS)
1555 CLIMA_Switch = 1 _____ (enable reanalysis-climatic input data)
Rain_NC4 = netcdf\euCORDHI_mod2_pr_day.nc _____ (.netcdf reanalysis-climatic input data)
CorrectionFactor = 86400

[meteoOptions] _____ (METEO MODULE OPTIONS)
1560 input_tab = tab _____ (folder containing .tab (txt) datasheet)
mask = map\mask01.map _____ (0-1 mask map, equal to clone.map)
BTMDDEM = map\BTMDDEM_clip.map _____ (elevation model DEM.map [m])
z0 = tss\mod2\Z0_euCORDHI_mod2_tas_day.tss _____ (regression temp-elev: intercept)
TempRatio = tss\mod2\TCoeff_euCORDHI_mod2_tas_day.tss _____ (regression temp-elev: angular coeff.)
1565 z0MAX = tss\mod2\Z0_euCORDHI_mod2_tasmax_day.tss _____ (intercept for MAX temp.)
TempRatioMAX = tss\mod2\TCoeff_euCORDHI_mod2_tasmax_day.tss _____ (angular coeff. for MAX temp.)
z0MIN = tss\mod2\Z0_euCORDHI_mod2_tasmin_day.tss _____ (intercept for MIN temp.)
TempRatioMIN = tss\mod2\TCoeff_euCORDHI_mod2_tasmin_day.tss _____ (angular coeff for MIN temp.)
infilRain_file = tss\2011_2016\Rain_TREBBIA_Precipitazione_ALL.tss _____ (rain gauges time series .tss (txt))2
1570 mayrainstat = map\Rain_Stations_Trebbia.map _____ (rain gauges location .map)2
```

Kc\_FAO = tbl\Kc\_FAO.tbl (kc coefficient for FAO evapotras.)<sup>3</sup>  
Albedo = tbl\Albedo.tbl (albedo coefficient for FAO evapotras.)<sup>3</sup>

1575 [interceptionSnowOptions] (SNOW AND INTERCEPTION MODULE OPTIONS)  
input\_tab = tab (folder containing .tab (txt) datasheet)  
LAI\_max = tbl\LAI\_max.tbl (LAI maximum index)<sup>4</sup>  
LAI\_min = tbl\LAI\_min.tbl (LAI minimum index)<sup>4</sup>  
SNOW\_Switch = 1 (snow calc. enabled)

1580 [landSurfaceOptions] (LAND SURFACE MODULE OPTIONS)  
input\_tab = tab (folder containing .tab (txt) datasheet)  
INF\_Switch = 2 (infiltration calc. enabled)<sup>5</sup>  
sand\_sup = map\Sand\_SUP90C.map (%sand on surface soil at 10cm depth)  
1585 silt\_sup = map\Silt\_SUP90C.map (%silt on surface soil at 10cm depth)  
clay\_sup = map\Clay\_SUP90C.map (%clay on surface soil at 10cm depth)  
CoarseFrc\_SUP = map\CoarsFrg\_SUP90C.map (%coarse on surface soil at 10cm depth)  
myrivermap = map\PathRiverSM.map (river location .map)<sup>6</sup>  
Loss\_River = tbl\Loss\_RIV.tbl (reduction coeff. for river losses)<sup>6</sup>  
1590 Inf\_CLC = tbl\Infiltr\_CLC.tbl (infiltration coeff. f(soil use))  
CN\_I = map\CN\_I.map (SCS-CN method CN I .map)  
CN\_II = map\CN\_II.map (SCS-CN method CN II .map)  
CN\_III = map\CN\_III.map (SCS-CN method CN III .map)  
Initial\_SM = 0.9 (initial condition of soil moisture)  
1595 SoilDepth = map\BDRICM\_M.map (soil depth .map [cm])  
MaxWatStgTOP = map\TSH1\_clip.map (%max water storage soil 10cm depth)  
MaxWatStgBTM = map\TSH5\_clip.map (%max water storage soil 1m depth)  
sand\_btm = map\Sand\_BTM90C.map (%sand on surface soil at 1m depth)  
1600 silt\_btm = map\Silt\_BTM90C.map (%silt on surface soil at 1m depth)  
clay\_btm = map\Clay\_BTM90C.map (%clay on surface soil at 1m depth)  
CoarseFrc\_BTM = map\CoarsFrg\_BTM90C.map (%coarse on surface soil at 1m depth)

[groundwaterOptions] (GROUNDWATER MODULE OPTIONS)  
1605 input\_tab = tab (folder containing .tab (txt) datasheet)  
Sr\_Falda = 0.8 (initial condition of groundwater table)  
Idro\_Map = map\Idrogeology\_Emilias\_Trebbia.map (hydrogeological .map)<sup>7</sup>  
Ks\_GLHYMPS\_exp = map\GLHYMPS\_Emilias\_Trebbia.map (saturated permeability from GLHYMPS)<sup>7</sup>  
Permeability = tbl\IdrogeologyTabs\Permeability.tbl (saturated permeability .tbl (txt))<sup>7</sup>  
1610 Anisotropy = tbl\IdrogeologyTabs\Anisotropy.tbl (anisotropy coefficient .tbl (txt))<sup>7</sup>  
Porosity = tbl\IdrogeologyTabs\Porosity.tbl (porosity coefficient .tbl (txt))<sup>7</sup>  
Storativity = tbl\IdrogeologyTabs\Storativity.tbl (storativity coefficient .tbl (txt))<sup>7</sup>  
Type\_Depth = tbl\IdrogeologyTabs\Type.tbl (hydrogeological reclassify .tbl(txt))<sup>7</sup>

1615 [LandSlidesOptions] (LANDSLIDE MODULE OPTIONS)  
LANDSLIDE\_Switch\_1 = 2 (landslide trigger calc. enabled)<sup>8</sup>  
C\_Veg = tbl\C\_Veg.tbl (cohesion from vegetation .tbl(txt))  
Surcharge = tbl\Sur\_Veg.tbl (cohesion from vegetation .tbl(txt))  
fa\_factor = 2

1620 X\_Gavrilovic = tbl\X\_Gavrilovic.tbl (EPM X parameter .tbl(txt))<sup>9</sup>  
Y\_Gavrilovic = tbl\Y\_Gavrilovic.tbl (EPM Y parameter .tbl(txt))<sup>9</sup>  
LithoY\_Gavrilovic = map\Idrogeology\_Emilias\_Trebbia.map (EPM Y parameter Lithology .map)<sup>9</sup>  
FI\_Gavrilovic = map\Kst\_Emilias\_Trebbia.map (EPM fi parameter .map)<sup>9</sup>

1625 [routingOptions] \_\_\_\_\_ (ROUTING MODULE OPTIONS)  
ROUTING\_Switch = 1 \_\_\_\_\_ (enable calc. routing)  
lddMap = map\ldd\_clip.map \_\_\_\_\_ (ldd.map of flow directions)  
cellAreaMap = map\cellsizeArea.map \_\_\_\_\_ (map of cell area extension)  
River\_Pit = map\Pit\_Point.map \_\_\_\_\_ (basin outlet location)

1630 Strickler = tbl\Ks\_Strickler.tbl \_\_\_\_\_ (Strickler-Manning coefficient)  
SectionTable = tbl\Dynamic\Sections2.tbl \_\_\_\_\_ (section type table .map)<sup>20</sup>  
~~RiverDynPath = tbl\Dynamic\map\PathDyn.map~~  
~~RiverDynDist = tbl\Dynamic\map\DistDyn.map~~  
~~RiverDynPit = tbl\Dynamic\map\Pit\_Point.map~~

1635 ~~RiverDynPitLake = tbl\Dynamic\map\Pit\_Point\_Lakes\_IN.map~~

[reportingOptions] \_\_\_\_\_ (REPORTING MODULE OPTIONS)  
mysamples\_real = map\Idro\_Samples\_Trebbia.map \_\_\_\_\_ (real hydrometers sampling .map)  
mysamples\_fake = map\Idro\_Samples\_F.map \_\_\_\_\_ (other hydrometers sampling .map)

1640 mysamples\_solid = map\Solid\_Samples.map \_\_\_\_\_ (reservoir sampling .map)  
~~debugmode = FAST~~  
outDailyTotNC = CumFails,CumFails\_D \_\_\_\_\_ (daily counted .netcdf)<sup>11</sup>  
outMonthTotNC = P,Etc \_\_\_\_\_ (monthly counted .netcdf)  
outMonthAvgNC = T \_\_\_\_\_ (monthly averaged .netcdf)

1645 outMonthEndNC = CumFails,CumFails\_D \_\_\_\_\_ (end-monthly counting .netcdf)<sup>11</sup> \_  
outAnnualTotNC = P,Etc \_\_\_\_\_ (annual cumulated .netcdf)  
outAnnualAvgNC = T \_\_\_\_\_ (monthly averaged .netcdf)  
outAnnuaEndNC = CumFails,CumFails\_D \_\_\_\_\_ (end-annual cumulated .netcdf)<sup>11</sup>

~~#debugmode = SLOW~~

1650 ~~#outDailyTotNC = P,T,Etc,DeltaWS0,Sr3,DeltaBF0,FS,CumFails,FS\_D,CumFails\_D,FS\_ST,CumFails\_ST~~  
formatNetCDF = NETCDF4 \_\_\_\_\_ (.netcdf specified format)  
zlib = True \_\_\_\_\_ (enable .netcdf creation)

ID	Description	Module	Additional References
1	The starting point of the time series, the starting point of the simulation and the ending point are specified.	[GLOBAL OPTIONS]	-
2	To compute rain gauge simulation, a time series in .tss format and a .map of stations are required. Each station has its IDs (1,2,3,...,n) for the corresponding time series with map.	[METEO OPTIONS]	(Karssenberget al., 2010; Sutanudjaja et al., 2018)
3-4	Fao crop coefficient Kc, albedo coefficient and LAI coefficient within .tbl file (a txt table).	[METEO OPTIONS] - [INTERCEPTION SNOW OPTIONS]	(Allan et al., 1998; Nazari et al., 2019)
5	Infiltration model selector: 1) Horton, 2) SCS-SN	[LANDSURFACE OPTIONS]	(Chow et al., 1988)
6	River map derived from PCR flow accumulation and percolation reduction factor below riverbed path.	[LANDSURFACE OPTIONS]	(Chow et al., 1988)
7	Groundwater parameters (.tbl), lithology map and saturated permeability map retrieved from literature and GHYMPS database.	[GROUNDWATER OPTIONS]	(Huscroft et al., 2018; Anderson, 2005; Hayashi, 2020; de Graaf et al., 2015)
8	Landslide model selector: 1) Iverson, 2) Harp, 3) Milledge and 4) SLIP	[LANDSLIDE OPTIONS]	(Iverson, 2000; Montrasio, 2008; Harp et al., 2006; Milledge et al., 2014)
9	EPM parameters from Gavrilovic's method (.tbl and .map)	[LANDSLIDE OPTIONS]	(Milanesi et al., 2015; Panagos et al., 2015)

10	<a href="#">Section table (.tbl) requires for implementation of dynamic routing (experimental)</a>	[ROUTING OPTIONS]	(Karssenberg et al., 2010; Sutanudjaja et al., 2018)
11	Cumulated shallow landslides and debris flow fails are sampled at yearly/monthly/daily bases	[REPORTING OPTIONS]	-

1655

## Appendix B

~~Here In this section, are reported all the~~ main symbols and their measurement units included in CRHyME are reported (Abbate and Mancusi, 2021a, b).

Main symbols	Description	Units of measurement
$A$	Hydraulic section area	$m^2$
$\Delta x$ and $\Delta y$	Cell length and width	m
$B$	Width of the hydraulic section	m
$c$	Cohesion of surface soils	kPa
$C^{*}$	Concentration of debris flows	-
$C_i$	Canopy Interception	$mm\ day^{-1}$
CNI CNII CNIII	Curve Numbers SCS-CN for dry-mild-wet conditions	-
$D_{50}$	Median diameter of soil grain size	mm
$ddf_0$	Degree day factor	$mm\ ^{\circ}C^{-1}\ day^{-1}$
$E_s$ or $W_s$	Surface erosion (source parameter for EPM)	$mm\ timestep^{-1}$ or $m^3\ yr^{-1}$
$Et_0$	Potential evapotranspiration	$mm\ timestep^{-1}$
$Et_c$	Evapotranspiration	$mm\ timestep^{-1}$
$E_x$	Exfiltration	$mm\ timestep^{-1}$
$f_0$	Maximum infiltration rate of Horton	$mm\ h^{-1}$
$f_c$	Horton's minimum infiltration rate	$mm\ h^{-1}$
$F_{gw}$	Groundwater flow	$m^3\ s^{-1}$
$F_{sub}$	Subsurface flow	$m^3\ s^{-1}$
$depth_{GW}$	Groundwater depth	mm or m
$depth_{soil}$ or $Z$	Surface soil depth	mm or m
$h_{snow}$	Snow height	mm
$h_{runoff}$	Water height at <u>the</u> surface	mm
$h_{soilwater}$	Water height in surface soil	mm
$h_{groundwater}$	Water height in <u>the</u> aquifer	mm
$h_{solid}$	Sediment height at <u>the</u> surface	mm
$\alpha$ , $slope$ or $i$	Terrain slope (degrees and dimensionless)	$^{\circ}$ or %
$I_a$	Initial imbibition of the SCS-CN method	mm
$k$	Horton decay constant	$h^{-1}$
$K_c$	Crop Coefficient	-
$K_s$	Hydraulic permeability	$m\ s^{-1}$
$K_{Strickler}$	Strickler roughness coefficient	-
$LAI$	Leaf Area Index	-
$L_{per}$	Percolation	$mm\ timestep^{-1}$
$n$	Porosity	-

$n_{VG}$	Van Genuchten n parameter	-
$P$	Rainfall	mm timestep <sup>-1</sup>
$P_n$	Net Rainfall	mm timestep <sup>-1</sup>
$F_{kin\_dyn}$ or $Q_l$	Liquid Discharge	m <sup>3</sup> s <sup>-1</sup>
$Q_c$	Critical flow rate of incipient motion for solids	m <sup>3</sup> s <sup>-1</sup>
$Q_s$	Solid flow rate	m <sup>3</sup> s <sup>-1</sup>
$R$	Runoff	mm timestep <sup>-1</sup>
$R_{EPM}$	Routing coefficient for EPM	-
$S$	Snow	mm
$S_{stor}$	SCS-CN Storativity	mm
$S_{ml}$	Snowmelt	mm timestep <sup>-1</sup>
$S_m$	Soil Moisture	%
$T$	Temperature	°C
$T_{max}$ and $T_{min}$	Maximum and minimum temperature	°C
$T_s$	Solid Transport	m <sup>3</sup> s <sup>-1</sup>
$a_x$ and $b_x$	Parameters of <i>Slope</i> → $D_{50}$ equations	-
$\alpha_{liquid}$ e $\beta_{liquid}$ ⚡	Parameters of the uniform (liquid) flow rate curve	-
$\alpha_{solid}$ e $\beta_{solid}$ ⚡	Parameters of the uniform (solid) flow rate curve	-
$\varphi$	Friction angle of surface soils	°
$\theta_s$ e $\theta_r$	Maximum and minimum surface soil water content	mm or %

### Code and data availability

1660 All the data shown in this paper are freely consultable on Internet websites as reported in the references and within the links we specified through the text. Since the CRHyME code is currently ~~underdeveloped~~~~underdeveloped~~, we suggest you contact the main author at this mail [andrea.abbate@rse-web.it](mailto:andrea.abbate@rse-web.it) to receive the most updated and stable copy of the code. For functioning, the CRHyME code requires a Python environment (we suggest Python 3.78 or 3.87 version) and the installation of PCRaster libraries (see the references and links). Further details can be found in [Abbate and Mancusi \(2021a, b\)](#).

### 1665 Author contributions

AA and LM conceptualized the study. AA carried out the formal analysis and wrote the manuscript with contributions from all co-authors. FA, AF, LL and MP supervised the research, and all the authors reviewed and edited the manuscript.

### Competing interests

The authors declare that they have no conflict of interest.

### 1670 Acknowledgements

“This work has been financed by the Research Fund for the Italian Electrical System under the Three-Year Research Plan 2022-2024 (DM MITE n. 337, 15.09.2022), in compliance with the Decree of April 16th, 2018”.

## References

- 1675 Abbate, A. and Mancusi, L.: Manuale del modello CRHyME (Climate Rainfall Hydrogeological Modelling Experiment), RSE Report RdS 21012462, Milano, 2021a.
- Abbate, A. and Mancusi, L.: Strumenti per la mappatura delle minacce idrogeologiche per il sistema energetico e incidenza dei cambiamenti climatici, RSE Report RdS 21010317, Milano, 2021b.
- Abbate, A., Longoni, L., Ivanov, V. I., and Papini, M.: Wildfire impacts on slope stability triggering in mountain areas, *MDPI Geosciences*, 9, 1–15, <https://doi.org/10.3390/geosciences9100417>, 2019.
- 1680 Abbate, A., Papini, M., and Longoni, L.: Analysis of meteorological parameters triggering rainfall-induced landslide: a review of 70 years in Valtellina, *Nat. Hazards Earth Syst. Sci.*, 21, 2041–2058, <https://doi.org/10.5194/nhess-21-2041-2021>, 2021a.
- Abbate, A., Longoni, L., and Papini, M.: Extreme Rainfall over Complex Terrain: An Application of the Linear Model of Orographic Precipitation to a Case Study in the Italian Pre-Alps, 2021, *MDPI Geosciences*, 18, 2021b.
- 1685 Abeshu, G. W., Li, H.-Y., Zhu, Z., Tan, Z., and Leung, L. R.: Median bed-material sediment particle size across rivers in the contiguous U.S., *Earth Syst. Sci. Data Discuss.*, 2021, 1–22, <https://doi.org/10.5194/essd-2021-201>, 2021.
- Allan, R., Pereira, L., and Smith, M.: Crop evapotranspiration-Guidelines for computing crop water requirements-FAO Irrigation and drainage paper 56, 1998.
- 1690 Alvioli, M., Melillo, M., Guzzetti, F., Rossi, M., Palazzi, E., von Hardenberg, J., Brunetti, M. T., and Peruccacci, S.: Implications of climate change on landslide hazard in Central Italy, *Science of The Total Environment*, 630, 1528–1543, <https://doi.org/10.1016/j.scitotenv.2018.02.315>, 2018.
- Ancey, C.: Bedload transport: a walk between randomness and determinism. Part 1. The state of the art, *null*, 58, 1–17, <https://doi.org/10.1080/00221686.2019.1702594>, 2020.
- 1695 Anderson, E. I.: Modeling groundwater–surface water interactions using the Dupuit approximation, *Advances in Water Resources*, 28, 315–327, <https://doi.org/10.1016/j.advwatres.2004.11.007>, 2005.
- Angeli, M. G., Buma, J., Gasparetto, P., and Pasuto, A.: A combined hill slope hydrology/stability model for low-gradient slopes in the Italian Dolomites, *Engineering Geology*, 49, 1–13, [https://doi.org/10.1016/S0013-7952\(97\)00033-1](https://doi.org/10.1016/S0013-7952(97)00033-1), 1998.
- 1700 Rete Monitoraggio ARPA Emilia: <https://www.arpae.it/it/temi-ambientali/meteo>.
- Rete Monitoraggio ARPA Lombardia: [www.arpalombardia.it/stiti/arpalombardia/meteo](http://www.arpalombardia.it/stiti/arpalombardia/meteo).
- Autorità di Bacino Distrettuale del Fiume Po: Linee Generali di Assetto Idrogeologico e Quadro degli Interventi, 2022.
- 1705 Ballio, F., Brambilla, D., Giorgetti, E., Longoni, L., Papini, M., and Radice, A.: Evaluation of sediment yield from valley slopes: A case study, 149 pp., <https://doi.org/10.2495/DEB100131>, 2010.
- Bancheri, M., Rigon, R., and Manfreda, S.: The GEOframe-NewAge Modelling System Applied in a Data Scarce Environment, *Water*, 12, <https://doi.org/10.3390/w12010086>, 2020.
- Barnes, R.: Parallel Priority-Flood depression filling for trillion cell digital elevation models on desktops or clusters, *Computers & Geosciences*, 96, 56–68, <https://doi.org/10.1016/j.cageo.2016.07.001>, 2016.
- 1710 Barnes, R.: Parallel non-divergent flow accumulation for trillion cell digital elevation models on desktops or clusters, *Environmental Modelling & Software*, 92, 202–212, <https://doi.org/10.1016/j.envsoft.2017.02.022>, 2017.

- Bemporad, G. A., Alterach, J., Amighetti, F. F., Peviani, M., and Saccardo, I.: A distributed approach for sediment yield evaluation in Alpine regions, *Journal of Hydrology*, 197, 370–392, [https://doi.org/10.1016/0022-1694\(95\)02978-8](https://doi.org/10.1016/0022-1694(95)02978-8), 1997.
- 1715 Berg, J. H.: Prediction of Alluvial Channel Pattern of Perennial Rivers, *Geomorphology*, 12, 259–279, [https://doi.org/10.1016/0169-555X\(95\)00014-V](https://doi.org/10.1016/0169-555X(95)00014-V), 1995.
- Bonanno, R., Lacavalla, M., and Sperati, S.: A new high-resolution Meteorological Reanalysis Italian Dataset: MERIDA, *Quarterly Journal of the Royal Meteorological Society*, 145, 1756–1779, <https://doi.org/10.1002/qj.3530>, 2019.
- 1720 Bordoni, M., Meisina, C., Valentino, R., Lu, N., Bittelli, M., and Chersich, S.: Hydrological factors affecting rainfall-induced shallow landslides: From the field monitoring to a simplified slope stability analysis, *Engineering Geology*, 193, <https://doi.org/10.1016/j.enggeo.2015.04.006>, 2015.
- Bovolo, C. I. and Bathurst, J. C.: Modelling catchment-scale shallow landslide occurrence and sediment yield as a function of rainfall return period, *Hydrological Processes*, 26, 579–596, <https://doi.org/10.1002/hyp.8158>, 2012.
- 1725 Bovy, B., Braun, J., Cordonnier, G., Lange, R., and Yuan, X.: The FastScape software stack: Reusable tools for landscape evolution modelling, in: EGU General Assembly Conference Abstracts, 9474, 2020.
- Bozzolan, E., Holcombe, E., Pianosi, F., and Wagener, T.: Including informal housing in slope stability analysis – an application to a data-scarce location in the humid tropics, *Natural Hazards and Earth System Sciences*, 20, 3161–3177, <https://doi.org/10.5194/nhess-20-3161-2020>, 2020.
- 1730 Brambilla, D., Papini, M., Ivanov, V. I., Bonaventura, L., Abbate, A., and Longoni, L.: Sediment Yield in Mountain Basins, Analysis, and Management: The SMART-SED Project, in: *Applied Geology: Approaches to Future Resource Management*, edited by: De Maio, M. and Tiwari, A. K., Springer International Publishing, Cham, 43–59, [https://doi.org/10.1007/978-3-030-43953-8\\_3](https://doi.org/10.1007/978-3-030-43953-8_3), 2020.
- Bresciani, E., Davy, P., and de Dreuzy, J.-R.: Is the Dupuit assumption suitable for predicting the groundwater seepage area in hillslopes?, *Water Resources Research*, 50, 2394–2406, <https://doi.org/10.1002/2013WR014284>, 2014.
- Campforts, B., Shobe, C., Steer, P., Vanmaercke, M., LAGUE, D., and Braun, J.: HyLands 1.0: a Hybrid Landscape evolution model to simulate the impact of landslides and landslide-derived sediment on landscape evolution, *Geoscientific Model Development*, 13, 3863–3886, 2020.
- 1740 Cazorzi, F. and Dalla Fontana, G.: Snowmelt modelling by combining air temperature and a distributed radiation index, *Journal of Hydrology*, 181, 169–187, [https://doi.org/10.1016/0022-1694\(95\)02913-3](https://doi.org/10.1016/0022-1694(95)02913-3), 1996.
- Ceriani, M., Lauzi, S., and Padovan, M.: Rainfall thresholds triggering debris-flow in the alpine area of Lombardia Region, central Alps – Italy, in: *In Proceedings of the Man and Mountain’94, First International Congress for the Protection and Development of Mountain Environmen*, Ponte di Legno (BS), Italy, 1994.
- 1745 Chen, L. and Young, M. H.: Green-Ampt infiltration model for sloping surfaces, *Water Resources Research*, 42, <https://doi.org/10.1029/2005WR004468>, 2006.
- Chiarelli, D. D., Galizzi, M., Bocchiola, D., Rosso, R., and Rulli, M. C.: Modeling snowmelt influence on shallow landslides in Tartano valley, Italian Alps, *Science of The Total Environment*, 856, 158772, <https://doi.org/10.1016/j.scitotenv.2022.158772>, 2023.
- 1750 Chow, V. T., Maidment, D. R., and Mays, L. W.: *Applied hydrology*, McGraw-Hill, New York, 1988.
- Ciampalini, A., Raspini, F., Lagomarsino, D., Catani, F., and Casagli, N.: Landslide susceptibility map refinement using PSInSAR data, *Remote Sensing of Environment*, 184, 302–315, <https://doi.org/10.1016/j.rse.2016.07.018>, 2016.



- 1755 Ciccacese, G., Mulas, M., Alberoni, P. P., Truffelli, G., and Corsini, A.: Debris flows rainfall thresholds in the Apennines of Emilia-Romagna (Italy) derived by the analysis of recent severe rainstorms events and regional meteorological data, *Geomorphology*, 358, 107097, <https://doi.org/10.1016/j.geomorph.2020.107097>, 2020.
- Ciccacese, G., Mulas, M., and Alessandro, C.: Combining spatial modelling and regionalization of rainfall thresholds for debris flows hazard mapping in the Emilia-Romagna Apennines (Italy), *Landslides*, 18, <https://doi.org/10.1007/s10346-021-01739-w>, 2021.
- 1760 Cislighi, A., Chiaradia, E. A., and Bischetti, G. B.: Including root reinforcement variability in a probabilistic 3D stability model, *Earth Surface Processes and Landforms*, 42, 1789–1806, <https://doi.org/10.1002/esp.4127>, 2017.
- CNR and IRPI: Rapporto Periodico sul Rischio posto alla Popolazione italiana da Frane e Inondazioni, Anno 2020, 19 pp., <https://doi.org/10.30437/report2020>, 2021.
- 1765 Collischonn, W., Fleischmann, A., Paiva, R. C. D., and Mejia, A.: Hydraulic Causes for Basin Hydrograph Skewness, *Water Resources Research*, 53, 10603–10618, <https://doi.org/10.1002/2017WR021543>, 2017.
- Crosta, G. B. and Frattini, P.: Distributed modelling of shallow landslides triggered by intense rainfall, *Natural Hazards and Earth System Sciences*, 3, 81–93, <https://doi.org/10.5194/nhess-3-81-2003>, 2003.
- Crosta, G. B., Imposimato, S., and Roddeman, D. G.: Numerical modelling of large landslides stability and runout, *Nat. Hazards Earth Syst. Sci.*, 3, 523–538, <https://doi.org/10.5194/nhess-3-523-2003>, 2003.
- 1770 Dade, W. B. and Friend, P. F.: Grain-Size, Sediment-Transport Regime, and Channel Slope in Alluvial Rivers, *The Journal of Geology*, 106, 661–676, <https://doi.org/10.1086/516052>, 1998.
- D’Agostino, V. and Marchi, L.: Debris flow magnitude in the Eastern Italian Alps: Data collection and analysis, *Physics and Chemistry of the Earth, Part C: Solar, Terrestrial & Planetary Science*, 26, 657–663, [https://doi.org/10.1016/S1464-1917\(01\)00064-2](https://doi.org/10.1016/S1464-1917(01)00064-2), 2001.
- 1775 Daly, C., Taylor, G., and Gibson, W.: *The PRISM Approach to Mapping Precipitation and Temperature*, 1997.
- Daly, C., Slater, M. E., Roberti, J. A., Laseter, S. H., and Swift Jr, L. W.: High-resolution precipitation mapping in a mountainous watershed: ground truth for evaluating uncertainty in a national precipitation dataset, *International Journal of Climatology*, 37, 124–137, <https://doi.org/10.1002/joc.4986>, 2017.
- 1780 Davolio, S., Della Fera, S., Laviola, S., Miglietta, M. M., and Levizzani, V.: Heavy precipitation over Italy from the Mediterranean storm “Vaia” in October 2018: Assessing the role of an atmospheric river, *Monthly Weather Review*, 148, 3571–3588, 2020.
- Davy, P. and Lague, D.: Fluvial erosion/transport equation of landscape evolution models revisited, *Journal of Geophysical Research: Earth Surface*, 114, <https://doi.org/10.1029/2008JF001146>, 2009.
- 1785 De Vita, P., Fusco, F., Tufano, R., and Cusano, D.: Seasonal and Event-Based Hydrological and Slope Stability Modeling of Pyroclastic Fall Deposits Covering Slopes in Campania (Southern Italy), *Water*, 10, 1140, <https://doi.org/10.3390/w10091140>, 2018.
- Devia, G. K., Ganasri, B. P., and Dwarakish, G. S.: A Review on Hydrological Models, *Aquatic Procedia*, 4, 1001–1007, <https://doi.org/10.1016/j.aqpro.2015.02.126>, 2015.
- 1790 D’Odorico, P. and Fagherazzi, S.: A probabilistic model of rainfall-triggered shallow landslides in hollows: A long-term analysis, *Water Resources Research*, 39, <https://doi.org/10.1029/2002WR001595>, 2003.
- Erskine, R. H., Green, T. R., Ramirez, J. A., and MacDonald, L. H.: Comparison of grid-based algorithms for computing upslope contributing area, *Water Resources Research*, 42, <https://doi.org/10.1029/2005WR004648>, 2006.

- 1795 Fan, Y., Miguez-Macho, G., Weaver, C. P., Walko, R., and Robock, A.: Incorporating water table dynamics in climate modeling: 1. Water table observations and equilibrium water table simulations, *Journal of Geophysical Research: Atmospheres*, 112, <https://doi.org/10.1029/2006JD008111>, 2007.
- Fawcett, T.: An introduction to ROC analysis, *Pattern Recognition Letters*, 27, 861–874, <https://doi.org/10.1016/j.patrec.2005.10.010>, 2006.
- 1800 Formetta, G., Capparelli, G., and Versace, P.: Evaluating performance of simplified physically based models for shallow landslide susceptibility, *Hydrology and Earth System Sciences*, 20, 4585–4603, <https://doi.org/10.5194/hess-20-4585-2016>, 2016.
- Gao, L., Zhang, L. M., and Cheung, R. W. M.: Relationships between natural terrain landslide magnitudes and triggering rainfall based on a large landslide inventory in Hong Kong, *Landslides*, 15, 727–740, <https://doi.org/10.1007/s10346-017-0904-x>, 2018.
- 1805 Gariano, S. L. and Guzzetti, F.: Landslides in a changing climate, *Earth-Science Reviews*, 162, 227–252, <https://doi.org/10.1016/j.earscirev.2016.08.011>, 2016.
- GDAL/OGR contributors: GDAL/OGR Geospatial Data Abstraction software Library, Open Source Geospatial Foundation, 2020.
- 1810 Girard, M.-C., Girard, C., Dominique, C., Gilliot, J.-M., Loubersac, L., Meyer-Roux, J., Monget, J.-M., Seguin, B., and Rao, N.: Corine Land Cover, 331–344, <https://doi.org/10.1201/9780203741917-19>, 2018.
- Gleick, P. H.: Climate change, hydrology, and water resources, *Reviews of Geophysics*, 27, 329–344, <https://doi.org/10.1029/RG027i003p00329>, 1989.
- 1815 Globovnik, L., Holjevč, D., Petkovaek, G., and Rubinj, J.: 145. Applicability of the Gavrilo vic Method in Erosion Calculation Using Spatial Data Manipulation Techniques, *Tunnelling and Underground Space Technology*, 14, 2003.
- Govers, G.: Empirical relationships for the transport capacity of overland flow., 1989.
- Govers, G., Wallings, D. E., Yair, A., and Berkowicz, S.: Empirical relationships for the transport capacity of overland flow, *International Association of Hydrological Sciences*, 189, 1990.
- 1820 de Graaf, I. E. M., Sutanudjaja, E. H., van Beek, L. P. H., and Bierkens, M. F. P.: A high-resolution global-scale groundwater model, *Hydrol. Earth Syst. Sci.*, 19, 823–837, <https://doi.org/10.5194/hess-19-823-2015>, 2015.
- Groenendyk, D. G., Ferré, T. P. A., Thorp, K. R., and Rice, A. K.: Hydrologic-Process-Based Soil Texture Classifications for Improved Visualization of Landscape Function., *PLoS One*, 10, e0131299, <https://doi.org/10.1371/journal.pone.0131299>, 2015.
- 1825 Guadagno, M., IRPI CNR, P., Guzzetti, I., Reichenbach, I., and Tonelli, I.: SICI-Sistema Informativo Catastrofi Idrogeologiche-Istituto di Ricerca per la Protezione Idrogeologica (IRPI) del Consiglio Nazionale delle Ricerche e Gruppo Nazionale per la Difesa dalle Catastrofi Idrogeologiche (GNDCI) del Consiglio Nazionale delle Ricerche, 2003.
- 1830 Gudiyangada Nachappa, T., Tavakkoli Piralilou, S., Ghorbanzadeh, O., Shahabi, H., and Blaschke, T.: Landslide Susceptibility Mapping for Austria Using Geons and Optimization with the Dempster-Shafer Theory, *Applied Sciences*, 9, <https://doi.org/10.3390/app9245393>, 2019.
- Guzzetti, F. and Tonelli, G.: Information system on hydrological and geomorphological catastrophes in Italy (SICI): a tool for managing landslide and flood hazards, *Natural Hazards and Earth System Sciences*, 4, 213–232, 2004.
- 1835 Guzzetti, F., Reichenbach, P., Cardinali, M., Galli, M., and Ardizzone, F.: Probabilistic landslide hazard assessment at the basin scale, *Geomorphology*, 72, 272–299, <https://doi.org/10.1016/j.geomorph.2005.06.002>, 2005.

- Guzzetti, F., Peruccacci, S., Rossi, M., and Stark, C. P.: Rainfall thresholds for the initiation of landslides in central and southern Europe, *Meteorology and Atmospheric Physics*, 98, 239–267, <https://doi.org/10.1007/s00703-007-0262-7>, 2007.
- 1840 Harp, E. L., Michael, J. A., and Laprade, W. T.: Shallow-landslide hazard map of Seattle, Washington, Reston, VA, <https://doi.org/10.3133/ofr20061139>, 2006.
- Hayashi, M.: Alpine Hydrogeology: The Critical Role of Groundwater in Sourcing the Headwaters of the World, *Groundwater*, 58, 498–510, <https://doi.org/10.1111/gwat.12965>, 2020.
- 1845 Hengl, T., Mendes de Jesus, J., Heuvelink, G. B. M., Ruiperez Gonzalez, M., Kilibarda, M., Blagotić, A., Shangguan, W., Wright, M. N., Geng, X., Bauer-Marschallinger, B., Guevara, M. A., Vargas, R., MacMillan, R. A., Batjes, N. H., Leenaars, J. G. B., Ribeiro, E., Wheeler, I., Mantel, S., and Kempen, B.: SoilGrids250m: Global gridded soil information based on machine learning, *PLOS ONE*, 12, e0169748, <https://doi.org/10.1371/journal.pone.0169748>, 2017.
- Herrera, M.: Landslide Detection using Random Forest Classifier, <https://doi.org/10.13140/RG.2.2.31365.91369>, 2019.
- 1850 Huscroft, J., Gleeson, T., Hartmann, J., and Börker, J.: Compiling and Mapping Global Permeability of the Unconsolidated and Consolidated Earth: GLobal HYdrogeology MaPS 2.0 (GLHYMPS 2.0), *Geophysical Research Letters*, 45, <https://doi.org/10.1002/2017GL075860>, 2018.
- Iida, T.: A stochastic hydro-geomorphological model for shallow landsliding due to rainstorm, *CATENA*, 34, 293–313, [https://doi.org/10.1016/S0341-8162\(98\)00093-9](https://doi.org/10.1016/S0341-8162(98)00093-9), 1999.
- 1855 ISPRA: Dissesto idrogeologico in Italia: pericolosità e indicatori di rischio, ISPRA, Ispra, 2018.
- ITCOLD: La gestione dell'interrimento dei serbatoi artificiali italiani, Comitato Nazionale Italiano delle Grandi Dighe, 2009.
- ITCOLD: La gestione dell'interrimento dei serbatoi artificiali italiani situazione attuale e prospettive, Comitato Nazionale Italiano delle Grandi Dighe, 2016.
- 1860 Ivanov, V., Radice, A., Papini, M., and Longoni, L.: Event-scale pebble mobility observed by RFID tracking in a pre-Alpine stream: a field laboratory, *Earth Surface Processes and Landforms*, 45, 535–547, <https://doi.org/10.1002/esp.4752>, 2020a.
- Ivanov, V., Arosio, D., Tresoldi, G., Hojat, A., Zanzi, L., Papini, M., and Longoni, L.: Investigation on the Role of Water for the Stability of Shallow Landslides-Insights from Experimental Tests, *Water*, 12(4), 2020b.
- 1865 Iverson, R., Reid, M., and Lahusen, R.: Debris-flow mobilization from landslides. *Annu Rev Earth Planet Sci*, *Annu. Rev. Earth Planet. Sci*, 25, 85–138, <https://doi.org/10.1146/annurev.earth.25.1.85>, 1997.
- Iverson, R. M.: Landslide triggering by rain infiltration, *Water Resources Research*, 36, 1897–1910, <https://doi.org/10.1029/2000WR900090>, 2000.
- 1870 Jackson, C. R., Bitew, M., and Du, E.: When interflow also percolates: downslope travel distances and hillslope process zones, *Hydrological Processes*, 28, 3195–3200, <https://doi.org/10.1002/hyp.10158>, 2014.
- 1875 Jacob, D., Petersen, J., Eggert, B., Alias, A., Christensen, O. B., Bouwer, L. M., Braun, A., Colette, A., Déqué, M., Georgievski, G., Georgopoulou, E., Gobiet, A., Menut, L., Nikulin, G., Haensler, A., Hempelmann, N., Jones, C., Keuler, K., Kovats, S., Kröner, N., Kotlarski, S., Kriegsmann, A., Martin, E., van Meijgaard, E., Moseley, C., Pfeifer, S., Preuschmann, S., Radermacher, C., Radtke, K., Rechid, D., Rounsevell, M., Samuelsson, P., Somot, S., Soussana, J.-F., Teichmann, C., Valentini, R., Vautard, R., Weber, B., and Yiou, P.: EURO-CORDEX: new high-resolution climate change projections for European impact research, *Regional Environmental Change*, 14, 563–578, <https://doi.org/10.1007/s10113-013-0499-2>, 2014.
- Jakob, M. and Hungr, O.: Debris-Flow Hazards and Related Phenomena, 2005.

- 1880 Jakob, M. and Jordan, P.: Design flood estimates in mountain streams – the need for a geomorphic approach, *Can. J. Civ. Eng.*, 28, 425–439, <https://doi.org/10.1139/I01-010>, 2001.
- Jie, T., Zhang, B., He, C., and Yang, L.: Variability In Soil Hydraulic Conductivity And Soil Hydrological Response Under Different Land Covers In The Mountainous Area Of The Heihe River Watershed, Northwest China, *Land Degradation & Development*, 28, <https://doi.org/10.1002/ldr.2665>, 2016.
- 1885 Kadavi, P., Lee, C.-W., and Lee, S.: Application of Ensemble-Based Machine Learning Models to Landslide Susceptibility Mapping, *Remote Sensing*, 10, 1252, <https://doi.org/10.3390/rs10081252>, 2018.
- Karszenberg, D., Schmitz, O., Salamon, P., de Jong, K., and Bierkens, M. F. P.: A software framework for construction of process-based stochastic spatio-temporal models and data assimilation, *Environmental Modelling & Software*, 25, 489–502, <https://doi.org/10.1016/j.envsoft.2009.10.004>, 2010.
- 1890 Kim, K.-S., Kim, M.-I., Lee, M.-S., and Hwang, E.-S.: Regression Equations for Estimating Landslide-Triggering Factors Using Soil Characteristics, *Applied Sciences*, 10, <https://doi.org/10.3390/app10103560>, 2020.
- Klaus, J. and Jackson, C. R.: Interflow Is Not Binary: A Continuous Shallow Perched Layer Does Not Imply Continuous Connectivity, *Water Resources Research*, 54, 5921–5932, <https://doi.org/10.1029/2018WR022920>, 2018.
- 1895 Kobierska, F., Jonas, T., Kirchner, J. W., and Bernasconi, S. M.: Linking baseflow separation and groundwater storage dynamics in an alpine basin (Dammagletscher, Switzerland), *Hydrol. Earth Syst. Sci.*, 19, 3681–3693, <https://doi.org/10.5194/hess-19-3681-2015>, 2015.
- Kondolf, george 'mathias: Hungry Water: Effects of Dams and Gravel Mining on River Channels, *Environmental Management*, 21, 533–551, <https://doi.org/10.1007/s002679900048>, 1997.
- 1900 Lamb, M. P. and Venditti, J. G.: The grain size gap and abrupt gravel-sand transitions in rivers due to suspension fallout, *Geophysical Research Letters*, 43, 3777–3785, <https://doi.org/10.1002/2016GL068713>, 2016.
- Langland, M. J.: Bathymetry and Sediment-Storage Capacity Change in Three Reservoirs on the Lower Susquehanna River, 1996-2008, <https://doi.org/10.3133/sir20095110>, 2009.
- 1905 Lazzari, M., Piccarreta, M., and Manfreda, S.: The role of antecedent soil moisture conditions on rainfall-triggered shallow landslides, *Natural Hazards and Earth System Sciences Discussions*, 2018, 1–11, <https://doi.org/10.5194/nhess-2018-371>, 2018.
- Lee, K. and Pin Chun, H.: Evaluating the adequateness of kinematic-wave routing for flood forecasting in midstream channel reaches of Taiwan, *Journal of Hydroinformatics*, 14, 1075, <https://doi.org/10.2166/hydro.2012.093>, 2012.
- 1910 Legorreta Paulin, G., Bursik, M., Lugo-Hubp, J., and Zamorano Orozco, J. J.: Effect of pixel size on cartographic representation of shallow and deep-seated landslide, and its collateral effects on the forecasting of landslides by SINMAP and Multiple Logistic Regression landslide models, *Physics and Chemistry of the Earth, Parts A/B/C*, 35, 137–148, <https://doi.org/10.1016/j.pce.2010.04.008>, 2010.
- Lehner, B., Verdin, K., and Jarvis, A.: New Global Hydrography Derived From Spaceborne Elevation Data, *Eos, Transactions American Geophysical Union*, 89, 93–94, <https://doi.org/10.1029/2008EO100001>, 2008.
- 1915 Li, X., Xiao, Q., Niu, J., Dymond, S., McPherson, E. G., van Doorn, N., Yu, X., Xie, B., Zhang, K., and Li, J.: Rainfall interception by tree crown and leaf litter: An interactive process, *Hydrological Processes*, 31, 3533–3542, <https://doi.org/10.1002/hyp.11275>, 2017.
- 1920 Longoni, L., Ivanov, V. I., Brambilla, D., Radice, A., and Papini, M.: Analysis of the temporal and spatial scales of soil erosion and transport in a Mountain Basin, *Italian Journal of Engineering Geology and Environment*, 16, 17–30, <https://doi.org/10.4408/IJEGE.2016-02.O-02>, 2016.

- López Vicente, M., Pérez-Bielsa, C., López-Montero, T., Lambán, L. J., and Navas, A.: Runoff simulation with eight different flow accumulation algorithms: Recommendations using a spatially distributed and open-source model, *Environ. Model. Softw.*, 62, 11–21, 2014.
- Luino, F.: Sequence of instability processes triggered by heavy rainfall in the Northern Italy, *Geomorphology*, 66, 13–39, <https://doi.org/10.1016/j.geomorph.2004.09.010>, 2005.
- Ly, S., Charles, C., and Degre, A.: Different methods for spatial interpolation of rainfall data for operational hydrology and hydrological modeling at watershed scale. A review, *Biotechnology, Agronomy and Society and Environment*, 17, 392–406, 2013.
- Marnezy, A.: Alpine dams. From hydroelectric power to artificial snow, *Revue de géographie alpine*, 96, 2008.
- 1930 Meisina, C., Zizioli, D., and Zucca, F.: Methods for Shallow Landslides Susceptibility Mapping: An Example in Oltrepo Pavese, 1, 451–457, <https://doi.org/10.1007/978-3-642-31325-7-58>, 2013.
- Merritt, W. S., Letcher, R. A., and Jakeman, A. J.: A review of erosion and sediment transport models, *Environmental Modelling & Software*, 18, 761–799, [https://doi.org/10.1016/S1364-8152\(03\)00078-1](https://doi.org/10.1016/S1364-8152(03)00078-1), 2003.
- 1935 Michel, G. P., Kobiyama, M., and Goerl, R. F.: Comparative analysis of SHALSTAB and SINMAP for landslide susceptibility mapping in the Cunha River basin, southern Brazil, *Journal of Soils and Sediments*, 14, 1266–1277, <https://doi.org/10.1007/s11368-014-0886-4>, 2014.
- Milanesi, L., Pilotti, M., Clerici, A., and Gavrilovic, Z.: Application of an improved version of the Erosion Potential Method in Alpine areas, *Italian Journal of Engineering Geology and Environment*, <https://doi.org/10.4408/IJEGE.2015-01.O-02>, 2015.
- 1940 Milledge, D. G., Bellugi, D., McKean, J. A., Densmore, A. L., and Dietrich, W. E.: A multidimensional stability model for predicting shallow landslide size and shape across landscapes, *Journal of Geophysical Research: Earth Surface*, 119, 2481–2504, <https://doi.org/10.1002/2014JF003135>, 2014.
- Mishra, S. K., Tyagi, J. V., and Singh, V. P.: Comparison of infiltration models, *Hydrological Processes*, 17, 2629–2652, <https://doi.org/10.1002/hyp.1257>, 2003.
- 1945 Moges, E., Demissie, Y., Larsen, L., and Yassin, F.: Review: Sources of Hydrological Model Uncertainties and Advances in Their Analysis, *Water*, 13, <https://doi.org/10.3390/w13010028>, 2021.
- Montrasio, L.: Stability of soil-slip, *Wit Press, Risk Analysis II*, 45, 357–366, <https://doi.org/10.2495/RISK000331>, 2008.
- 1950 Montrasio, L. and Valentino, R.: Modelling Rainfall-induced Shallow Landslides at Different Scales Using SLIP - Part II, *Procedia Engineering*, 158, 482–486, <https://doi.org/10.1016/j.proeng.2016.08.476>, 2016.
- Morbidelli, R., Corradini, C., Saltalippi, C., Flammini, A., Dari, J., and Govindaraju, R. S.: Rainfall Infiltration Modeling: A Review, *Water*, 10, <https://doi.org/10.3390/w10121873>, 2018.
- Morgan, R. P. C. and Nearing, M. A.: *Handbook of erosion modelling.*, 2011.
- 1955 Munich Re: Natural disasters caused overall losses of US \$ 210bn Relevant natural catastrophe loss events worldwide 2020, 1, 2021.
- Nazari, M., Sadeghi, S. M. M., Van Stan, J., and Chaichi, M.: Rainfall interception and redistribution by maize farmland in central Iran, *Journal of Hydrology: Regional Studies*, 27, 100656, <https://doi.org/10.1016/j.ejrh.2019.100656>, 2019.
- 1960 Nino, Y.: Simple Model for Downstream Variation of Median Sediment Size in Chilean Rivers, *Journal of Hydraulic Engineering*, 128, 934–941, 2002.

- Oguz, E. A., Depina, I., and Thakur, V.: Effects of soil heterogeneity on susceptibility of shallow landslides, *Landslides*, 19, 67–83, <https://doi.org/10.1007/s10346-021-01738-x>, 2022.
- Pacina, J., Lend'áková, Z., Štojdl, J., Matys Grygar, T., and Dolejš, M.: Dynamics of Sediments in Reservoir Inflows: A Case Study of the Skalka and Nechranice Reservoirs, Czech Republic, *ISPRS International Journal of Geo-Information*, 9, <https://doi.org/10.3390/ijgi9040258>, 2020.
- Panagos, P., Borrelli, P., Poesen, J., Ballabio, C., Lugato, E., Meusburger, K., Montanarella, L., and Alewell, C.: The new assessment of soil loss by water erosion in Europe, *Environmental Science & Policy*, 54, 438–447, <https://doi.org/10.1016/j.envsci.2015.08.012>, 2015.
- Papini, M., Ivanov, V., Brambilla, D., Arosio, D., and Longoni, L.: Monitoring bedload sediment transport in a pre-Alpine river: An experimental method, *Rendiconti Online della Società Geologica Italiana*, 43, 57–63, <https://doi.org/10.3301/ROL.2017.35>, 2017.
- Parenti, C., Rossi, P., Mancini, F., Scorpio, V., Grassi, F., Ciccarese, G., Lugli, F., and Soldati, M.: Multitemporal Analysis of Slow-Moving Landslides and Channel Dynamics through Integrated Remote Sensing and In Situ Techniques, *Remote Sensing*, 15, <https://doi.org/10.3390/rs15143563>, 2023.
- Pearson, E., Smith, M. W., Klaar, M. J., and Brown, L. E.: Can high resolution 3D topographic surveys provide reliable grain size estimates in gravel bed rivers?, *Geomorphology*, 293, 143–155, <https://doi.org/10.1016/j.geomorph.2017.05.015>, 2017.
- Pebesma, E. J., de Jong, K., and Briggs, D.: Interactive visualization of uncertain spatial and spatio-temporal data under different scenarios: an air quality example, *International Journal of Geographical Information Science*, 21, 515–527, <https://doi.org/10.1080/13658810601064009>, 2007.
- Peirce, S., Ashmore, P., and Leduc, P.: Evolution of grain size distributions and bed mobility during hydrographs in gravel-bed braided rivers, *Earth Surface Processes and Landforms*, 44, 304–316, <https://doi.org/10.1002/esp.4511>, 2019.
- Pelletier, J. D., Broxton, P. D., Hazenberg, P., Zeng, X., Troch, P. A., Niu, G.-Y., Williams, Z., Brunke, M. A., and Gochis, D.: A gridded global data set of soil, intact regolith, and sedimentary deposit thicknesses for regional and global land surface modeling, *Journal of Advances in Modeling Earth Systems*, 8, 41–65, <https://doi.org/10.1002/2015MS000526>, 2016.
- Pereira, S., Garcia, R., Zêzere, J., Oliveira, S., and Silva, M.: Landslide quantitative risk analysis of buildings at the municipal scale based on a rainfall triggering scenario, *Geomatics, Natural Hazards and Risk*, 8, <https://doi.org/10.1080/19475705.2016.1250116>, 2016.
- Pérez-Peña, J. V., Azañón, J. M., and Azor, A.: CalHypso: An ArcGIS extension to calculate hypsometric curves and their statistical moments. Applications to drainage basin analysis in SE Spain, *Computers & Geosciences*, 35, 1214–1223, 2009.
- Rahardjo, H., Satyanaga, A., Leong, E. C., Santoso, V. A., and Ng, Y. S.: Performance of an instrumented slope covered with shrubs and deep-rooted grass, *Soils and Foundations*, 54, 417–425, <https://doi.org/10.1016/j.sandf.2014.04.010>, 2014.
- Raj, P. P.: Comparison of True and Residual Friction Angles, *Soils and Foundations*, 21, 99–103, [https://doi.org/10.3208/sandf1972.21.3\\_99](https://doi.org/10.3208/sandf1972.21.3_99), 1981.
- Ravi, V., Williams, J. R., and Ouyang, Y.: Estimation of infiltration rate in the vadose zone: compilation of simple mathematical models, 1998.
- Raziei, T. and Pereira, L.: Estimation of ETo with Hargreaves-Samani and FAO-PM temperature methods for a wide range of climates in Iran, *Agricultural Water Management*, 121, 1–18, <https://doi.org/10.1016/j.agwat.2012.12.019>, 2013.

- Remondo, J., Bonachea, J., and Cendrero, A.: A statistical approach to landslide risk modelling at basin scale: From landslide susceptibility to quantitative risk assessment, *Landslides*, 2, 321–328, <https://doi.org/10.1007/s10346-005-0016-x>, 2005.
- Rickenmann, D.: Empirical Relationships for Debris Flows, *Natural Hazards*, 19, 47–77, <https://doi.org/10.1023/A:1008064220727>, 1999.
- Rocha, J., Duarte, A., Silva, M., Fabres, S., Vasques, J., Revilla-Romero, B., and Quintela, A.: The Importance of High Resolution Digital Elevation Models for Improved Hydrological Simulations of a Mediterranean Forested Catchment, *Remote Sensing*, 12, <https://doi.org/10.3390/rs12203287>, 2020.
- Ronchetti, F., Borgatti, L., Cervi, F., C. G., Piccinini, L., Vincenzi, V., and Alessandro, C.: Groundwater processes in a complex landslide, northern Apennines, Italy, *Natural Hazards and Earth System Sciences*, 9, 895–904, <https://doi.org/10.5194/nhess-9-895-2009>, 2009.
- Roo, A., A.P.J, Wesseling, C. G., Jetten, V. G., and Ritsema, C.: LISEM: A physically-based hydrological and soil erosion model incorporated in a GIS, In: K. Kovar & H.P. Nachtnebel (eds.), *Application of geographic information systems in hydrology and water resources management*. Wallingford (UK), IAHS, 1996. IAHS Publ. 235, pp. 395–403, 1996.
- Ross, C. W., Prihodko, L., Anchang, J., Kumar, S., Ji, W., and Hanan, N. P.: HYSOGs250m, global gridded hydrologic soil groups for curve-number-based runoff modeling, *Sci Data*, 5, 180091–180091, <https://doi.org/10.1038/sdata.2018.91>, 2018.
- Salles, T.: eSCAPE: Regional to global scale landscape evolution model v2. 0, 2019.
- Sambrook Smith, G. H. and Ferguson, R. I.: The gravel-sand transition along river channels, *Journal of Sedimentary Research*, 65, 423–430, <https://doi.org/10.1306/D42680E0-2B26-11D7-8648000102C1865D>, 1995.
- Scheidl, C. and Rickenmann, D.: TopFlowDF - A simple gis based model to simulate debris-flow runout on the fan, <https://doi.org/10.4408/IJEGE.2011-03.B-030>, 2011.
- Schellekens, J., Verseveld, W. van, Visser, M., hewinsemius, laurenebouaziz, tanjaeuser, sandercdevries, cthiange, hboisgon, DirkEilander, DanielTollenaar, aweerts, Baart, F., Pieter9011, Pronk, M., arthur-lutz, ctenvelden, Imme1992, and Jansen, M.: *openstreams/wflow: Bug fixes and updates for release 2020.1.2*, Zenodo, <https://doi.org/10.5281/zenodo.4291730>, 2020.
- Schoener, G. and Stone, M. C.: Monitoring soil moisture at the catchment scale – A novel approach combining antecedent precipitation index and radar-derived rainfall data, *Journal of Hydrology*, 589, 125155, <https://doi.org/10.1016/j.jhydrol.2020.125155>, 2020.
- Shobe, C., Tucker, G., and Barnhart, K.: The SPACE 1.0 model: A Landlab component for 2-D calculation of sediment transport, bedrock erosion, and landscape evolution, *Geoscientific Model Development Discussions*, 1–38, <https://doi.org/10.5194/gmd-2017-175>, 2017.
- Sklar, L. S., Riebe, C. S., Marshall, J. A., Genetti, J., Leclere, S., Lukens, C. L., and Merces, V.: The problem of predicting the size distribution of sediment supplied by hillslopes to rivers, *Geomorphology*, 277, 31–49, 2017.
- Smith, R. E. and Parlange, J.-Y.: A parameter-efficient hydrologic infiltration model, *Water Resources Research*, 14, 533–538, <https://doi.org/10.1029/WR014i003p00533>, 1978.
- Strahler, A. N.: Dynamic basis of geomorphology, *Geological society of america bulletin*, 63, 923–938, 1952.
- Strauch, R., Istanbuluoglu, E., Nudurupati, S. S., Bandaragoda, C., Gasparini, N. M., and Tucker, G. E.: A hydroclimatological approach to predicting regional landslide probability using Landlab, *Earth Surf. Dynam.*, 6, 49–75, <https://doi.org/10.5194/esurf-6-49-2018>, 2018.
- Sutanudjaja, E. H., van Beek, R., Wanders, N., Wada, Y., Bosmans, J. H. C., Drost, N., van der Ent, R. J., de Graaf, I. E. M., Hoch, J. M., de Jong, K., Karssenber, D., López López, P., Peßenteiner, S., Schmitz, O., Straatsma, M.

- W., Vannamettee, E., Wisser, D., and Bierkens, M. F. P.: PCR-GLOBWB 2: a 5\arcmin global hydrological and water resources model, *Geoscientific Model Development*, 11, 2429–2453, <https://doi.org/10.5194/gmd-11-2429-2018>, 2018.
- 2050 Takahashi, T.: A Review of Japanese Debris Flow Research, *International Journal of Erosion Control Engineering*, 2, <https://doi.org/10.13101/ijece.2.1>, 2009.
- Tangi, M., Schmitt, R., Bizzi, S., and Castelletti, A.: The CASCADE toolbox for analyzing river sediment connectivity and management, *Environmental Modelling & Software*, 119, 400–406, <https://doi.org/10.1016/j.envsoft.2019.07.008>, 2019.
- 2055 Tanyaş, H., van Westen, C. J., Allstadt, K. E., and Jibson, R. W.: Factors controlling landslide frequency–area distributions, *Earth Surface Processes and Landforms*, 44, 900–917, <https://doi.org/10.1002/esp.4543>, 2019.
- Tavares da Costa, R., Mazzoli, P., and Bagli, S.: Limitations Posed by Free DEMs in Watershed Studies: The Case of River Tanaro in Italy, *Frontiers in Earth Science*, 7, 141, <https://doi.org/10.3389/feart.2019.00141>, 2019.
- 2060 Terzago, S., Palazzi, E., and von Hardenberg, J.: Stochastic downscaling of precipitation in complex orography: a simple method to reproduce a realistic fine-scale climatology, *Nat. Hazards Earth Syst. Sci.*, 18, 2825–2840, <https://doi.org/10.5194/nhess-18-2825-2018>, 2018.
- Theule, J.: Geomorphic study of sediment dynamics in active debris-flow catchments (French Alps), 2012.
- Tóth, B., Weynants, M., Pásztor, L., and Hengl, T.: 3D soil hydraulic database of Europe at 250 m resolution, *Hydrological Processes*, 31, 2662–2666, <https://doi.org/10.1002/hyp.11203>, 2017.
- 2065 Tramblay, Y., Bouvier, C., Martin, C., Didon-Lescot, J.-F., Todorovik, D., and Domergue, J.-M.: Assessment of initial soil moisture conditions for event-based rainfall–runoff modelling, *Journal of Hydrology*, 387, 176–187, <https://doi.org/10.1016/j.jhydrol.2010.04.006>, 2010.
- 2070 Uber, M., Vandervaere, J.-P., Zin, I., Braud, I., Heistermann, M., Legoût, C., Molinié, G., and Nord, G.: How does initial soil moisture influence the hydrological response? A case study from southern France, *Hydrology and Earth System Sciences*, 22, 6127–6146, <https://doi.org/10.5194/hess-22-6127-2018>, 2018.
- Vakhshoori, V. and Zare, M.: Is the ROC curve a reliable tool to compare the validity of landslide susceptibility maps?, *null*, 9, 249–266, <https://doi.org/10.1080/19475705.2018.1424043>, 2018.
- Van Der Knijff, J. M., Younis, J., and De Roo, A. P. J.: LISFLOOD: a GIS-based distributed model for river basin scale water balance and flood simulation, *null*, 24, 189–212, <https://doi.org/10.1080/13658810802549154>, 2010.
- 2075 Van Genuchten, M.: A Closed-form Equation for Predicting the Hydraulic Conductivity of Unsaturated Soils1, *Soil Science Society of America Journal*, 44, <https://doi.org/10.2136/sssaj1980.03615995004400050002x>, 1980.
- de Vente, J. and Poesen, J.: Predicting soil erosion and sediment yield at the basin scale: Scale issues and semi-quantitative models, *Earth-Science Reviews*, 71, 95–125, <https://doi.org/10.1016/j.earscirev.2005.02.002>, 2005.
- 2080 Vetsch, D., Siviglia, A., Caponi, F., Ehrbar, D., Gerke, E., Kammerer, S., Koch, A., Peter, S., Vanzo, D., Vonwiller, L., Facchini, M., Gerber, M., Volz, C., Farshi, D., Mueller, R., Roussetot, P., Veprek, R., and Faeh, R.: System Manuals of BASEMENT Version 2.8, 2018.
- Vitvar, T., Burns, D. A., Lawrence, G. B., McDonnell, J. J., and Wolock, D. M.: Estimation of baseflow residence times in watersheds from the runoff hydrograph recession: method and application in the Neversink watershed, Catskill Mountains, New York, *Hydrological Processes*, 16, 1871–1877, <https://doi.org/10.1002/hyp.5027>, 2002.
- 2085 Yu, B., Xie, C., Cai, S., Chen, Y., Lv, Y., Mo, Z., Liu, T., and Yang, Z.: Effects of Tree Root Density on Soil Total Porosity and Non-Capillary Porosity Using a Ground-Penetrating Tree Radar Unit in Shanghai, China, *Sustainability*, 10, <https://doi.org/10.3390/su10124640>, 2018.



Zhang, H., Li, Z., Saifullah, M., Li, Q., and Li, X.: Impact of DEM Resolution and Spatial Scale: Analysis of Influence Factors and Parameters on Physically Based Distributed Model, *Advances in Meteorology*, 2016, 8582041, <https://doi.org/10.1155/2016/8582041>, 2016.

Zheng, S., Zhang, G., Yuan, X., Ye, F., and Fu, W.: Failure characteristics of shallow soil slope considering surface runoff and interstitial flow, *Geomatics, Natural Hazards and Risk*, 11, 845–868, <https://doi.org/10.1080/19475705.2020.1758222>, 2020.

Zomlot, Z., Verbeiren, B., Huysmans, M., and Batelaan, O.: Spatial distribution of groundwater recharge and base flow: Assessment of controlling factors, *Journal of Hydrology: Regional Studies*, 4, 349–368, <https://doi.org/10.1016/j.ejrh.2015.07.005>, 2015.